



University of HUDDERSFIELD

University of Huddersfield Repository

Felton, Cara E.

Synthesis and Co-ordination chemistry of Allosteric systems and Sensors for Zinc Metal Ions

Original Citation

Felton, Cara E. (2009) Synthesis and Co-ordination chemistry of Allosteric systems and Sensors for Zinc Metal Ions. Doctoral thesis, University of Huddersfield.

This version is available at <http://eprints.hud.ac.uk/id/eprint/9238/>

The University Repository is a digital collection of the research output of the University, available on Open Access. Copyright and Moral Rights for the items on this site are retained by the individual author and/or other copyright owners. Users may access full items free of charge; copies of full text items generally can be reproduced, displayed or performed and given to third parties in any format or medium for personal research or study, educational or not-for-profit purposes without prior permission or charge, provided:

- The authors, title and full bibliographic details is credited in any copy;
- A hyperlink and/or URL is included for the original metadata page; and
- The content is not changed in any way.

For more information, including our policy and submission procedure, please contact the Repository Team at: E.mailbox@hud.ac.uk.

<http://eprints.hud.ac.uk/>

Synthesis and Co-ordination chemistry of Allosteric systems and Sensors for Zinc Metal Ions

Cara E. Felton MChem (Hons)



University of
HUDDERSFIELD
Inspiring tomorrow's professionals

A thesis submitted to the University of Huddersfield in partial fulfillment
of the requirements for the degree of Doctor of Philosophy

Department of Chemical and Biological Sciences
The University of Huddersfield

September 2009

Contents

List of Abbreviations	6
Acknowledgements	8
Abstract.....	9
1: Introduction	10
1.1 Supramolecular Chemistry.....	10
1.1.1 Principal research in Supramolecular Chemistry	10
1.2 Interactions in Supramolecular Chemistry.....	11
1.2.1 Ion-ion interactions	11
1.2.2 Ion-dipole interactions	12
1.2.3 Dipole-dipole interactions	12
1.2.4. Hydrogen Bonding.....	13
1.3 Host and guest chemistry.....	13
1.4 Binding domains	15
1.4.1 Crown Ethers.....	16
1.4.2 Aza Crowns	20
1.4.3 Cryptates.....	22
1.4.3.1. Functionalised Cryptates.....	23
1.4.4 Ditopic ligands.....	25
1.4.5 Allosteric effects	27
1.5 Metal ion sensors.....	29
1.5.1 Fluorescent sensors	30
1.5.2 Use of Chemical Sensors for Biology	30

1.6 Metallosupramolecular Chemistry and Transition Metal Helicates.....	32
1.6.1 Introduction to Metallosupramolecular Systems.....	32
1.6.2 Racks and Ladders.....	33
1.6.3 Grids	36
1.6.4 Cages.....	37
1.6.5 Helicates	39
1.6.5.1 Directional Helicates	40
1.6.5.2 Programmed Helicates.....	41
1.6.5.3 Reprogrammable Ligands.....	43
2: Aza crown ligands	49
2.1 Ligand Synthesis	50
2.1.1 Synthesis of L ₁	50
2.1.2 Structural elucidation	52
2.2 Results and Discussion.....	54
2.2.1. Reactivity with Cu ²⁺ ions.....	54
2.2.1.1 Reaction of CuCl ₂ ·2H ₂ O with two equivalents of L ₁	55
2.2.1.2 Reaction of CuCl ₂ ·2H ₂ O with one equivalent of L ₁	55
2.2.1.3 Reaction of two equivalents of CuCl ₂ ·2H ₂ O with L ₁	57
2.2.1.4 Higher ratios of Cu ²⁺	59
2.3 Allosteric effects.....	59
3: Diamino-functionalised Cryptate Species	62
3.1 Ligand Synthesis	63
3.1.1. Synthesis of L ₂	63
3.2 Results and discussion	76

3.2.1 – Solid State Structure of the Ammonium Iodide salt of L ₂	76
3.2.2 – Reactivity of cryptate with metal ions.....	79
3.2.3 – Cyclisation of Amino Groups	81
3.2.4 – Fixing of the Cryptate Domain	85
3.2.5 – Luminescence Studies	86
4: Luminescent Transition Metal Helicates	92
4.1 Ligand synthesis.....	93
4.1.1 Synthesis of ligand L ₃	93
4.2 Discussion and results	96
4.2.1 Solid State analysis	96
4.2.2 Luminescence Studies	101
5: Conclusions.....	105
6: Experimental	107
General details	107
6.1 - Preparation of Aza Crown L ₁	108
6.1.1. Synthesis of Acetylated-amino-chloropyridine	108
6.1.2. Synthesis of 3,3'-Diacetylamino-2,2'-bipyridine.....	108
6.1.3. Synthesis of 3,3'-Diamino-2,2'-bipyridine.....	109
6.2 – Preparation of Diamino-Cryptate, L ₂	112
6.2.1. Synthesis of 5-Acetylamino-6-chloro-2-picoline	112
6.2.2. Synthesis of 3,3'-Diacetylamino-6,6'-dimethyl-2,2'-bipyridine	112
6.2.3. Synthesis of 3,3'-Diacetylamino-6,6'-dimethyl-2,2'-bipyridine-N,N'-dioxide	113
6.2.4 Synthesis of 3,3'-Diacetylamino -2,2'-bipyridine-6,6'-diacetate	114
6.2.5 Synthesis of 3,3'-Diacetylamino-2,2'-bipyridine-6,6'-dimethanol	114

6.2.6 Synthesis of 3,3'-Diacetylamino -2,2'-bipyridine-6,6'-dimethylenechloride	115
6.2.7 Synthesis of Diacetyl-functionalised cryptate	115
6.2.8 Synthesis of Diamino-functionalised cryptate.....	116
6.2.9 Formation of Barium complex [LBa](ClO ₄) ₂	116
6.2.10 Formation of Barium cyclised complex [L ₂ Ba](ClO ₄) ₂	116
6.2.11 Formation of Zinc complex [L ₂ Zn](CF ₃ SO ₃) ₂	117
6.2.12 Formation of Zinc cyclised complex [L ₂ Zn](ClO ₄) ₂	117
6.3 – Preparation of Luminescent Transition Metal Helicate, L ₃	118
6.3.1 Synthesis of Coumarin-containing helicate, L ₃	118
6.3.2 Formation of the helicate complexes [M ₂ (L ₃) ₂](ClO ₄) ₄ (M = Zn ²⁺ , Cd ²⁺ , Hg ²⁺ and Cu ²⁺)	118
References.....	119
Copyright Declaration.....	123
Appendix 1: Crystal Data Tables	124
Table 1 – Aza crown ligand crystallographic data ^a	125
Table 2 – [Cu(L ₁)] ²⁺ Crystallographic data	126
Table 3 – [Cu ₂ (L ₁)] ⁴⁺ Crystallographic data	127
Table 4 – Diamino-functionalised cryptate crystallographic data ^a	128
Table 5 – Diamino-functionalised Barium cyclised cryptate crystallographic data ^a	129
Table 6 – Helicate crystallographic data ^a	130
Appendix 2: Publications	131

List of Abbreviations

α	Alpha
Å	Angstroms
ATP	Adenosine-5'-triphosphate
β	Beta
Bipy	Bipyridine
BuLi	Butyl Lithium
γ	Gamma
COSY	Correlation spectroscopy
δ	Delta
d	Doublet
dd	Doublet of doublets
DCM	Dichloromethane
DMF	Dimethylformamide
ESI-MS	Electrospray Ionisation Mass Spectrometry
g	Gram
^1H NMR	Proton Nuclear Magnetic Resonance
Hz	Hertz
J	Coupling constant
m	Multiplet
mCPBA	Meta-Chloroperoxybenzoic acid

ml	Milliletre
mol	Moles
mmol	Millimoles
<i>m/z</i>	Mass/charge
ppm	parts per million, δ (delta), chemical shift
Py	Pyridine
RT	Room temperature
s	Singlet
t	Triplet
TLC	Thin layer chromatography
Tz	Thiazole
THF	Tetrahydrofuran
UV/Vis	Ultraviolet/ visible spectrophotometry

Acknowledgements

I would like to thank Dr. C. R. Rice, who has been my supervisor throughout this research project, who has been an invaluable source of assistance and support both academically and emotionally. My thanks also goes to the Rice research group, in particular Martina Whitehead, all of whom have been a pleasure to work with.

The following people have assisted in certain aspects of my research and I would therefore like to thank them; Dr. T. R. Riis-Johannessen, Dr. S. J. A. Pope, Dr. M. J. Hardie, Dr. H. J. Clayton and R. Fennessey.

I would also like to thank Dr. L. P. Harding for performing numerous Mass Spectrometry experiments, and assistance in interpreting the results, and Dr. N. McLay for his help with running NMR experiments, and his patient explanations on how to use the NMR software.

I would like to thank the University of Huddersfield for providing me with the opportunity to perform this research and for providing the necessary funding. I would also like to thank the following people within the Department of Chemical and Biological Sciences for their support and help with understanding specific aspects of my research; Dr. G. Midgeley, Dr. A. Laws, Dr. L. Gillie, and Dr. P. Elliott.

Lastly, I would like to thank my parents and family, my husband Nick, and his family, and my friends, all of whom have supported me throughout my studies.

Abstract

The ditopic ligand, L_1 , contains both a bipyridine domain and a tetra-azacrown binding domain. Introduction of one equivalent of Cu^{2+} ions results in co-ordination of the ion by all four of the available N-donor atoms in the azacrown unit. However, introduction of further Cu^{2+} ions results in the formation of a variety of species depending on the ratio of Cu^{2+} ions to ditopic ligands available. The bipyridine site is capable of behaving as a bidentate chelator as co-ordination at the bipyridine unit by a further Cu^{2+} ion allosterically alters the behavior of the azacrown domain. The co-ordination of a Cu^{2+} ion at the bipyridine unit causes the unit to adopt a planar conformation, preventing all four available N-donor atoms in the tetra-azacrown from co-ordinating an encapsulated copper ion. Therefore co-ordination of the bipyridine domain changes the tetra-azacrown unit from a tetradentate to a tridentate N-donor unit.

A diamino-functionalised cryptate, L_2 , was synthesized, which is capable of reacting irreversibly with butanal in aqueous media, when in the presence of an excess of metal ions. Co-ordination of the cryptate unit is required in order for the cyclisation to occur, excess metal ions act as Lewis acids in order to promote the reaction, and also co-ordinate the cryptate ion. Co-ordination of the cryptate ion forces the bipyridine unit into a more planar position, allowing the amine groups to move into closer proximity to each other. Subsequent reaction with butanal induces the ligand to form a cyclised bis-aminal complex, as the amino groups react readily with the aldehyde to form a seven-membered bis-aminal species. The cyclised ligand was found to display metal dependent luminescent properties, with zinc ions producing the most intense increase in emissive properties by a significant margin as well as increasing the luminescent lifetime.

A potentially hexadentate ligand, L_3 , was synthesized, which upon co-ordination with dicationic metal ions forms dinuclear double stranded helicate species. The ligand partitions into two separate tridentate binding domains, consisting of two N-donor atoms from a pyridyl-triazole unit and an O-donor atom from a carbonyl oxygen group on the coumarin unit. The ligand contains two coumarin fluorophores, and the luminescent properties of the dinuclear helicate complexes were investigated. It was found that upon co-ordination of Zn^{2+} the emissive properties were enhanced in comparison with the parent ligand, however introduction of Co^{2+} , Cu^{2+} , Cd^{2+} and Hg^{2+} ions induced fluorescent quenching of varying degrees.

1: Introduction

1.1 Supramolecular Chemistry

Supramolecular chemistry is a broad subject and involves investigation of new molecular systems, the predominant feature of which is the method with which the structures are held together. These components are held together by reversible intermolecular forces, not by covalent bonds as is often the case. The structures synthesized within supramolecular chemistry are often designed for a purpose, careful planning of functional groups can allow researchers to design a ligand for a specific application. Therefore, one of the main applications of supramolecular chemistry is the development of sensors and probes.^{1,2}

Supramolecular chemistry in its current definition was established in the late 1960's, however, the principles and concepts on which it is based go back much further. Supramolecular chemistry is an area that spans many disciplines of chemical science; it encompasses aspects of physical, organic, inorganic and biochemistry. The nature of the research has fostered collaborations between a variety of specialists in a range of fields, such as crystallographers, computational chemists and biologists, in order to fully investigate the properties and utilities of a target ligand. For this reason it has been an area which is difficult to define, one description that appears to be most apt is that of Jean-Marie Lehn, which is "chemistry beyond the molecule".³ This refers to the bonding within supramolecular systems, rather than ionic or covalent bonding, supramolecular systems often form interactions and assemblies by non-covalent bonding, such as ion-dipole interactions, dipole-dipole interactions or hydrogen bonding. These associations often occur between two or more chemical species, causing organizations of ligands held together by reversible intermolecular forces.³

1.1.1 Principal research in Supramolecular Chemistry

The first modern supramolecular advance was in the field of macrocyclic ligands and was reported by the key groups of Curtis, Pederson, Jäger and Busch, with Lehn contributing later on.⁴⁻⁸ Jean-Marie Lehn prepared cryptates and went on to win the Nobel Prize for his contributions to chemistry; much of his research continues to influence supramolecular structures today.

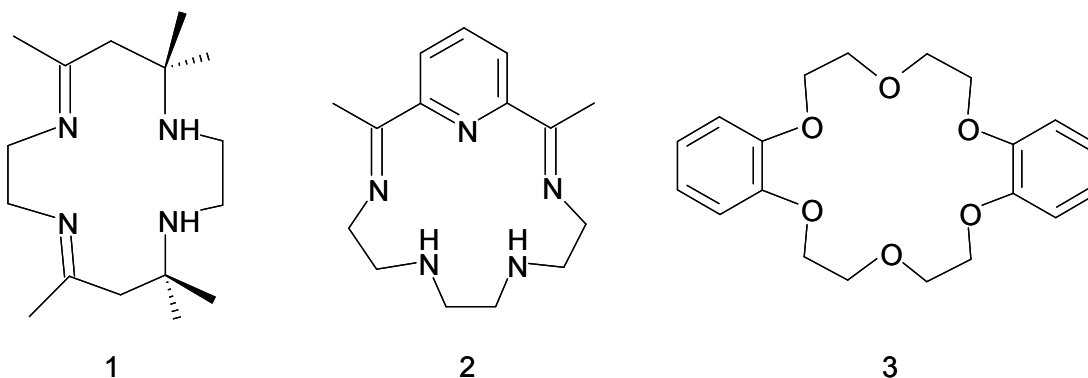


Figure 1 – Early macrocyclic ligands produced in supramolecular chemistry; 1. Curtis 1962 ⁹, 2. Busch 1964 ⁷ and 3. Pedersen 1967 ¹⁰

For example it was Lehn who first published the cryptate macrobicyclic ligand, in his paper entitled “Les Cryptates”, published in 1969. ⁸ In this paper he describes the discovery of a new type of ligand, which he terms a cryptate, from the Greek meaning hidden.

1.2 Interactions in Supramolecular Chemistry

Interactions between different components within supramolecular systems mainly occur by reversible intermolecular forces, as opposed to covalent bonds. The non-covalent interactions could be a variety of different bonds or forces and are strongest (or form the most stable complex) when the shape of the guest is complementary to the internal cavity of the host. These interactions may include; electrostatic forces, hydrophobic interactions, coordinate bonding, hydrogen bonding, ion-dipole bonding and dipole-dipole bonding.

1.2.1 Ion-ion interactions

Ionic bonding, although fairly uncommon, is possible in supramolecular interactions. The strength of the bond is similar in strength to covalent bonding, and is formed between two atoms of opposite charge, through electrostatic attraction. The most commonly cited example of ionic bonding is that of sodium chloride, where the sodium loses an electron, forming a cation, and the chlorine atom gains an electron to form an anion. The atoms are then attracted to each other by electrostatic attraction forming an ionic bond.

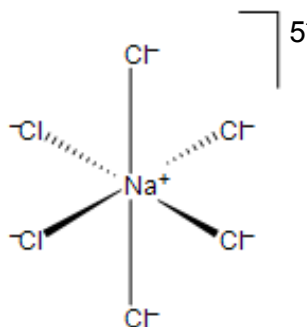


Figure 2 – Example of an ion-ion interaction.

1.2.2 Ion-dipole interactions

Ion dipole interactions are common in supramolecular chemistry where a crown ether and metal ion are involved. The polar oxygen lone pairs present in the crown ether receptor are attracted to the positive charge on the alkali metal cation forming an ion-dipole interaction. Often a crown ether will form multiple interactions with a metal ion, depending on the charge of the metal cation, allowing stable complexes to be formed.

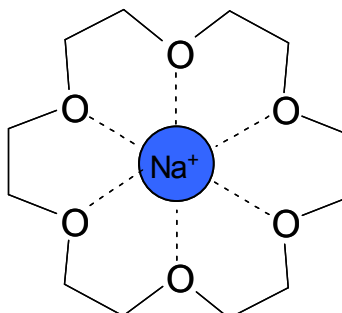


Figure 3 – Ion-dipole interaction between a metal cation and oxygen lone pairs in crown ether unit.

1.2.3 Dipole-dipole interactions

These interactions are formed when one dipole aligns with another dipole resulting in strong attractive interactions between a pair of poles on adjacent molecules, this behavior is commonly displayed in organic carbonyl compounds.

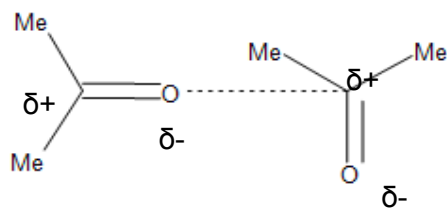


Figure 4 – Dipole-dipole interaction between two organic carbonyl compounds.

1.2.4. Hydrogen Bonding

Hydrogen bonding is a specific type of dipole-dipole interaction, in which a hydrogen atom directly attached to an electronegative atom is attracted to a dipole on an adjacent molecule or functional group. Hydrogen bonding can be important within supramolecular chemistry due to its strength and the high directional ability of the bond. Hydrogen bonds can occur in a variety of lengths and are extremely important in nature; they are responsible for the shape of many proteins, and for the double helix structure of DNA.

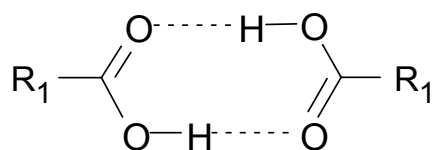


Figure 5 – Example of hydrogen bonding.

1.3 Host and guest chemistry

The simplest form of supramolecular chemistry, and arguably the most important, is host and guest chemistry. The host can be categorized into one of two distinct classes; *cavitands* and *clathrands*. *Cavitands* possess intermolecular cavities into which the guest moves and is co-ordinated inside the molecule, they usually have a large cavity capable of completely enclosing the guest, examples of these are found within solution and solid state. *Clathrands* possess extra-molecular cavities and the guest is co-ordinated outside of the molecule, usually in a cavity created between two or more host molecules, examples of these are only found within the crystalline or solid state.

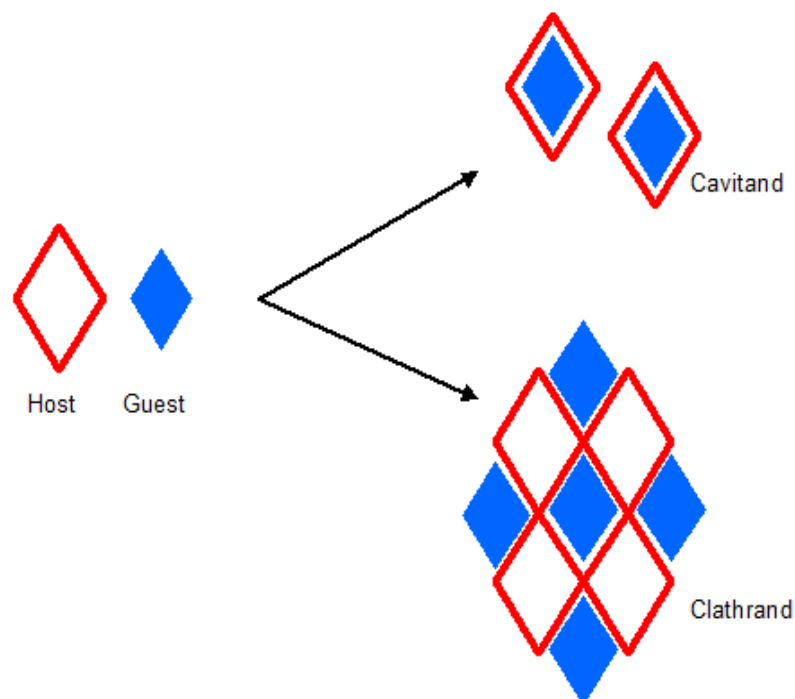


Figure 6 – Diagram illustrating the co-ordination within the intermolecular cavity in cavitands and co-ordination in the extra-molecular cavity in clathrands.

The guest can be co-ordinated within the host in a variety of spatial arrangements, such as capsular, nested, perched or wrapping. Wrapping of the host around the guest is most commonly associated with podand structures, where co-ordination sites are dotted along a chain in a similar way to pearls on a necklace.

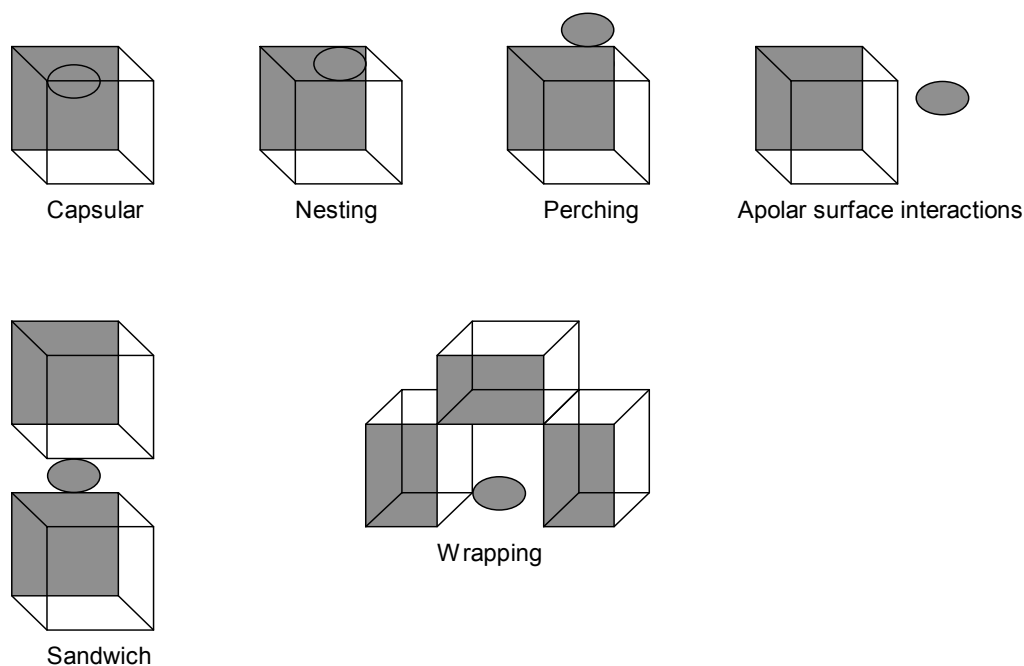


Figure 7 – Diagrams showing spatial arrangements between hosts and guests. ²

The most common type of co-ordination within crown ether structures is capsular host and guest binding. The stability of the complex and likelihood of co-ordination is greatly enhanced when the guest is complementary in shape to the host cavity. The concept of complementarity is borne from systems biological in nature, such as enzymes, these co-ordinate selectively with a guest based on their complementarity with the host's active site. The size and shape of the substrate (guest) determines whether it can co-ordinate with the host's active site, Emil Fisher described this as the "Lock and Key Principle" of enzyme reactivity. ¹¹ This principle explained the importance of geometric complementarity between a host and guest, and is the basis of molecular recognition. Combining the recognition process with reactive functions in supramolecular chemistry allows substrate or guest recognition by the host, and subsequently transformation into a product or response. ¹²

Therefore the shape and size of the host's cavity plays a key role in the selectivity and specificity of the host, the guest is complexed within the host by non-covalent forces, these could be ion-ion, ion dipole, dipole-dipole or hydrogen bonding interactions. Due to the relatively weak force of non-covalent bonding, several binding sites are often required to form a complex between the host and the guest.

1.4 Binding domains

Binding domains are important to the concept of host-guest supramolecular chemistry, different binding sites are attractive to different types of molecules and ions, and a ligand can

be tailored to a specific application by utilizing binding domains specific to an analyte of interest. Binding domains can have multiple donor atoms available for co-ordination, a simple domain such as a bipyridine unit has just two nitrogen atoms available for co-ordination, this is termed a bidentate domain. However, a large host, possessing a cavity, such as a cryptate domain may have nine available co-ordination sites. The versatility of the type of donor atom, and the number of donor atoms available, enables stable complexes to be formed, and increases the selectivity and specificity of a ligand.

1.4.1 Crown Ethers

Crown ethers are amongst the most simple macrocycles used in supramolecular chemistry, but are among the most useful domains due to their ability to act as hosts for cations and neutral molecules. Charles Pederson accidentally discovered crown ethers in 1967, while trying to synthesise a specific target ligand. Unfortunately, or fortunately due to their now widespread use, his starting material was contaminated and although it produced the desired product a small amount of unwanted by-product was present.⁵ The unknown product was found to be sparingly soluble in methanol, and when a UV spectrum was obtained the absorption curve was characteristic of a phenolic compound. When he added sodium hydroxide to the solution to alter the pH he discovered the crystals were freely soluble in methanol when in the presence of sodium ions. The elemental analysis corresponded to the structure of 2,3-benzo-1,4,7-trioxacyclonon-2-ene, but this offered no explanation for the behavior exhibited when in the presence of sodium ions.

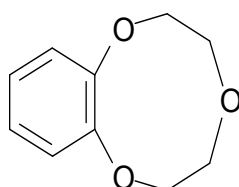


Figure 8 – Structure of 2,3-benzo-1,4,7-trioxacyclonon-2-ene.

Molecular weight analysis revealed the ligand to have a weight of exactly twice that of 2,3-benzo-1,4,7-trioxacyclonon-2-ene, which enabled Pedersen to realize the ligand structure was actually a 18-membered ring. The ring was characterized as dibenzo[18]crown-6, and was the first aromatic crown compound.

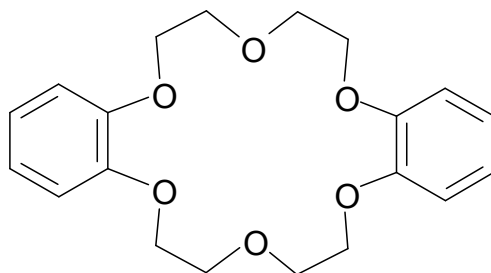


Figure 9 – Structure of dibenzo[18]crown-6.

Once the structure of the product had been characterized, Pedersen quickly interpreted that the sodium ion had moved into the centre of the donut shaped ligand. Other alkali metals and ammonium ions added to the compound also behaved in an analogous way to the sodium ions. The crown formed stable complexes with a variety of metal ions, including sodium and potassium, a feat previously unheard of. Pedersen named his new macrocyclic structures crown ethers, due to their crown like puckered shaped when free in solution, and when co-ordinated to a metal ion.¹⁰

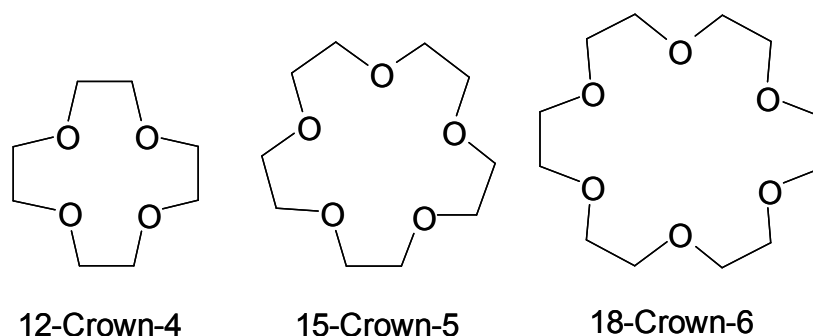


Figure 10 – Structure of the Crown Ethers.

The crown ethers consist of differing numbers of ether oxygen atoms connected by organic spacers to produce macrocyclic structures of varying sizes. The presence of multiple oxygen atoms, and therefore multiple polar oxygen lone pairs, allows crown ethers to bind selectively to alkali metal ions. The relationship between cavity size, cationic radius and stability of the resulting complex has been well established^{5, 13-15}, and further supports the idea of complementarity. A stronger complex is formed when there is a good match between the ionic size of the guest and the internal cavity volume of the host.

Crown ether	Na ⁺	K ⁺	Rb ⁺	Cs ⁺	Ca ²⁺	NH ₄ ⁺
[12]crown-4	1.70	1.30	-	-	-	-
[15]crown-5	3.24	3.43	-	2.18	2.36	3.03
[18]crown-6	4.35	6.08	5.32	4.70	3.90	4.14
[21]crown-7	2.52	2.35	-	5.02	2.80	3.27
Benzo[18]crown-6	4.30	5.30	4.62	3.66	3.50	-

Table 1.1 – Binding constants obtained for various cations and a selection of crown ethers (log *K*, methanol, 20 °C).¹⁶

Crown ether receptors have been utilized in many supramolecular arrays, and their diversity is apparent by their range of applications. In 1980, Rebek investigated whether ion transport selectivity could be controlled by allosteric effects.¹⁷

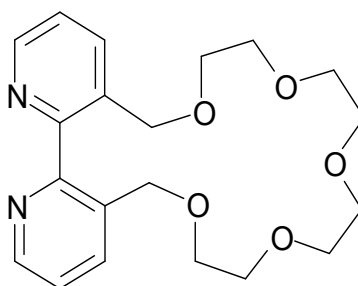


Figure 11 – Macrocyclic polyether investigated for ion transport selectivity.¹⁷

He found that when the bipyridine unit was co-ordinated with an ion, the benzylic oxygen atoms were forced into a confirmation where only one of the oxygen atoms was able to participate in co-ordinating an ion within the crown ether domain, which resulted in a preference for transporting smaller ions. However, when the bipyridine unit was not co-ordinated the ligand showed no preference.

The James research group has also utilized crown ethers in their design for a ditopic fluorescent sensor for potassium fluoride. The paper describes a boron based receptor, which is known to co-ordinate the fluoride anion strongly, connected to a crown ether domain which co-ordinates the potassium ion, an attached pyrene fluorophore is capable of fluorescent emission.^{18, 19}

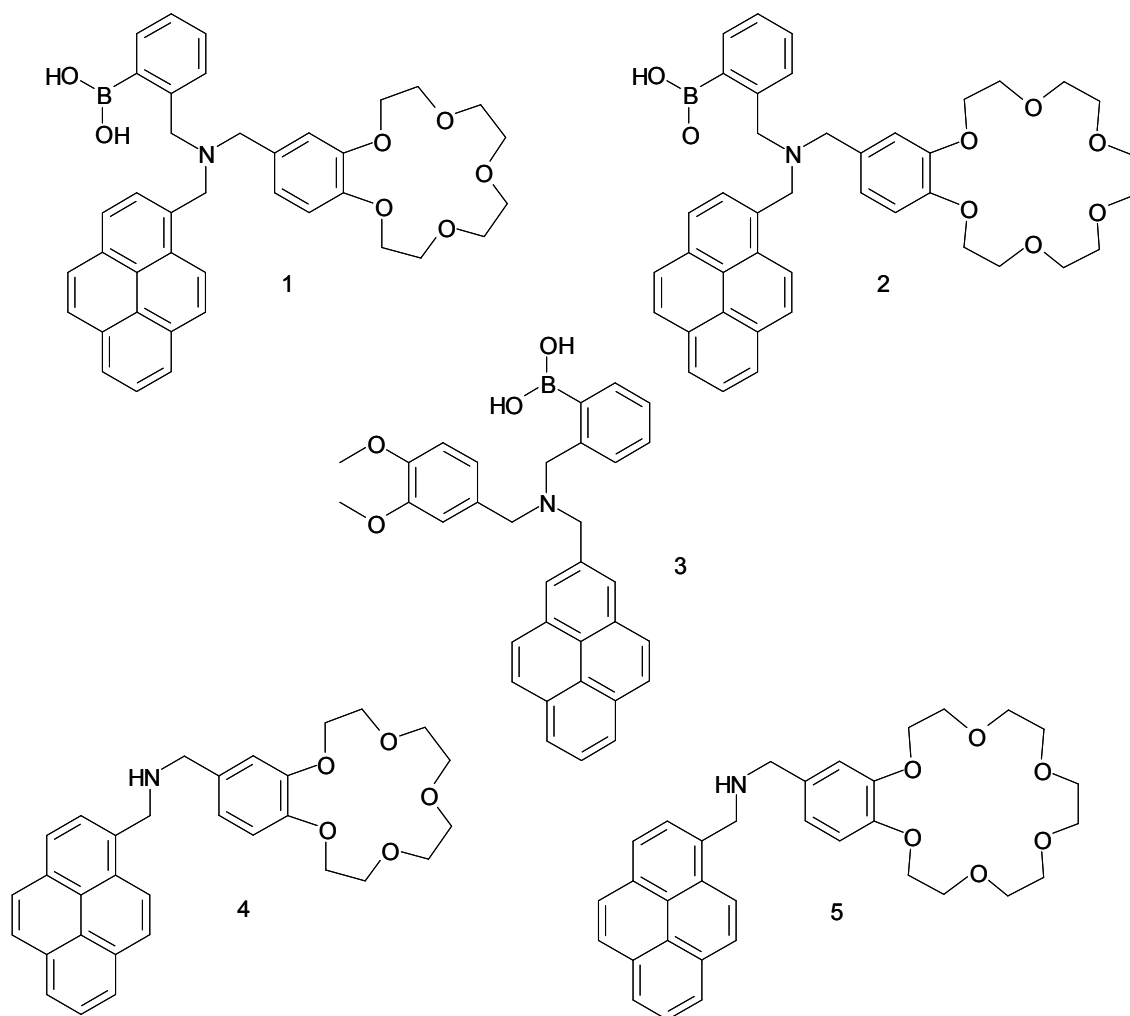


Figure 12 – Structure of the various fluorescent emission ligands investigated.¹⁹

The binding of potassium fluoride enhanced the fluorescent emission in ligands 1 and 2, coordination at both the boronic acid and the crown ether receptor occurred. The boronic acid strongly binds to the fluoride anion, causing a strong interaction. For comparison, ligands 4 and 5 were also examined for changes in fluorescent emission. However, no change in fluorescence resulted, this is due to the absence of the boronic acid chelator. A third ligand not containing a crown ether receptor was also examined, and although some fluorescent enhancement was observed it was very modest in comparison to ligands 1 and 2. Introduction of potassium chloride and potassium bromide resulted in no change in fluorescence intensity, indicating the fluoride group is required to strongly interact with the boronic acid moiety.

Further experiments were conducted where the potassium fluoride was introduced to the ligand with the addition of a cryptand species. The cryptand species had a higher binding

affinity to the potassium ion than the crown ether. Therefore the fluoride group would be available for co-ordination with the boronic acid, but the potassium ion would be encapsulated and be unable to co-ordinate with the crown ether domain. The results showed there was no enhancement in luminescence when the potassium ion was co-ordinated within the cryptate, however upon introduction of excess potassium chloride the fluorescence was restored. These results indicate that both the potassium and the fluoride group are required to switch on the fluorescent emission, and the sensor behaves like an AND logic gate.

1.4.2 Aza Crowns

Aza crowns are cyclic ligands similar in structure to the crown ethers, however they have nitrogen groups, as opposed to the oxygen donor atoms in the crown ethers. This change in donor atoms alters the co-ordination of guest ions. The crown ethers, due to their oxygen donor atoms, have a high affinity to s-block metal ions, while the aza crowns, with their nitrogen donor atoms, have a high affinity to transition metal ions. This difference in affinity allows researchers to specify ligand design, based on the specific requirements of the ligand. The development of the aza crowns has had a significant impact in the range of cryptate species available, allowing formation of cryptates with very specific binding properties. Varying the number of ethyl groups between the nitrogen donor atoms changes the properties of the aza crown; two ethyl groups between each nitrogen atom denotes a cyclen, however a crown which possesses one or more chains with 3 ethyl groups between nitrogen atoms is termed a cylam.

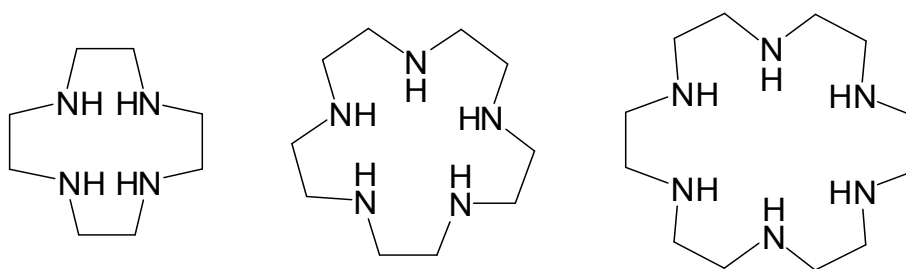


Figure 13 – Examples of cyclens of varying sizes.

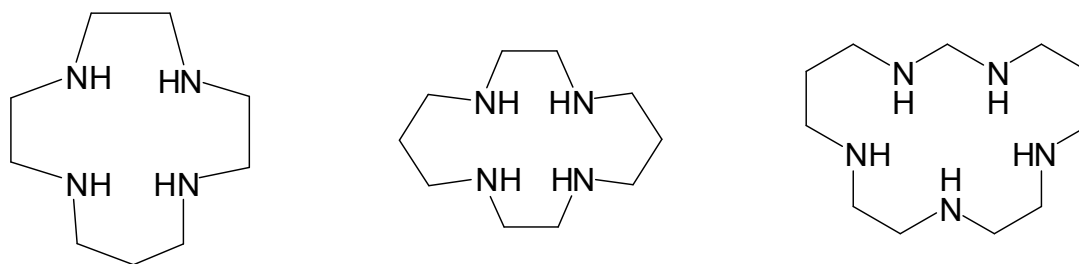


Figure 14 – Examples of cyclams of varying sizes.

Much of the primary research conducted on aza crown macrocycles was carried out by Busch and Curtis during the 1960's and 1970's. Curtis published several papers investigating the metal ion complexes of tetra-aza-cyclotridecane derivatives, examining the configurational isomers formed.^{4, 20-25} Meanwhile Busch investigated the effect of saturation on ligand field strength in tetradentate macrocyclic cyclam and cyclen ligands, and studied the electrochemical behavior of the metal complexes.²⁶ Both Curtis and Busch increased the understanding of the versatility of the aza crown macrocycles and enabled their adaptability as a binding domain to be recognized. Similarly to crown ethers, aza crown macrocycles have been utilized in supramolecular chemistry due to their ability to form complexes with high thermodynamic and kinetic stability with transition metal ions.

The Ghachtouli group published Nickel(II) complexes of cyclen and cyclam groups with attached pyridine groups. The aim of the research was to investigate the electrochemical behavior of the nickel complexes, and to demonstrate that upon application of a redox stimulus reversible rearrangements of the geometries of the complex can occur, when in solution.²⁷ The nickel complexes were synthesized and the corresponding nickel complexes were produced by introduction of stoichiometric amounts of the ligand and metal salts in methanol.

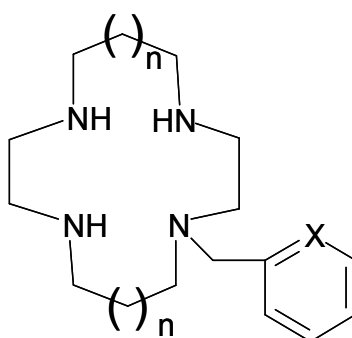


Figure 15 – General structure of the cyclen and cyclam ligands with attached pyridine groups.

The research reveals that the presence of the pyridine pendant arm on the cyclam cavity allowed isolation of two configurational isomers for the nickel complexes. X-ray crystal structures confirmed that the nickel ion adopted an octahedral orientation within the complex, with the pyridine group folding over the aza crown receptor, with an acetonitrile molecule occupying the sixth position. Electrochemical experiments established that isomerisation mechanisms existed between two configurations of the complex, and that application of a stimulus could induce a change in confirmation. The results demonstrated the importance of electron transfer in inducing geometric reorganisations.

Bencini *et al.* have reported synthesis of a variety of aza-crown macrocycles for a range of applications such as a receptor for ATP binding and hydrolysis ²⁸, ATP recognition and sensing ²⁹, cobalt and cadmium complexation in water ³⁰, co-ordination of Cu(II), Zn(II), Cd(II), Pb(II) and Hg(II) in aqueous media ³¹, encapsulation of metal cations and anions ^{32, 33} and selective binding and subsequent fluorescent signaling of uridine and uridine-containing ribodinecleotides ³⁴, to name just a few.

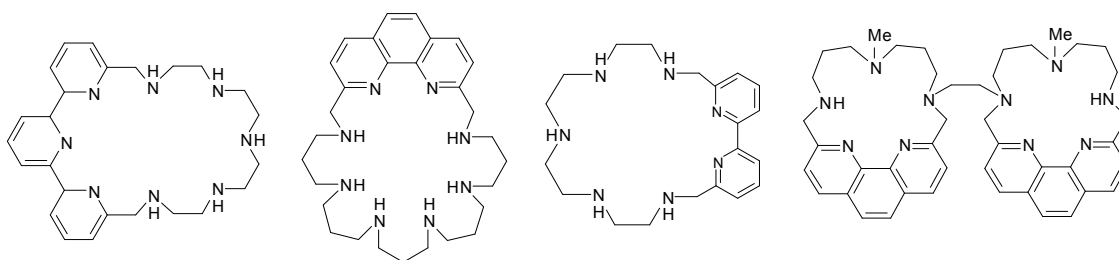


Figure 16 – Some examples of macrocyclic ligands synthesized by the Bencini group. ²⁸⁻³¹

The scope of their research highlights the versatility of these macrocyclic domains, and the diverse and specific uses to which they can be applied with careful planning of functionalisation. This calculated designing of ligands is the very essence of supramolecular chemistry, and is responsible for the growth of the subject area.

1.4.3 Cryptates

Cryptates, sometimes called cryptands, are 3-dimensional macrobicyclic ligands which are capable of spherically surrounding a guest ion. Their 3-dimensional structure is similar to a cage and it is this property that earns the name cryptate. The name cryptate comes from the Greek “Kruptos” meaning hidden, this is due to the internment of the guest within the cryptate. The cryptates were named and discovered by Jean-Marie Lehn, who found them to form very stable complexes, and have some degree of selectivity based on size exclusion.

^{3, 35} In his initial publication on the species, he described them as possibly having numerous uses, such as utilizing them in the study of anion processes, or the transport of cations. Lehn went on to win the Nobel prize for his work on Cryptates in 1987, his award was shared with Charles Pedersen and Donald Cram, and was awarded for their development and use of molecules with structure-specific interactions of high selectivity.^{5, 8, 13, 35, 36}

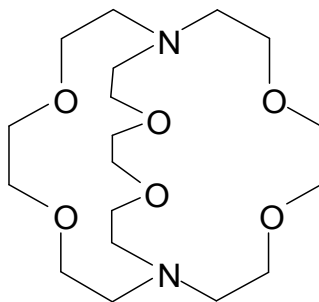


Figure 17 – Typical structure of a cryptate species.

The cryptate possesses multiple O-donor and N-donor domains, which spherically surround a guest ion forming an extremely stable complex, the ability to form such a stable complex is as a result of co-ordination occurring around the entire ion, a property called spherical recognition. Spherical recognition is the ability of the cryptate to show selectivity based on the size complementarity between the cation and the intramolecular cavity.³⁷ The metal guest ion is often co-ordinately saturated, which prevents solvating effects leading to a positive entropy effect. The complex formed is so stable that cryptates are capable of co-ordinating metal ions within aqueous media, a feature that makes them very attractive in the design of supramolecular biological metal ion sensors.

1.4.3.1. Functionalised Cryptates

Cryptands can be derivatized in order to attach functional groups and increase the specificity of the ligand. The Sadhu group has recently published data on a fluorophore derivatised cryptand which has been used in the study of fluorescence resonance energy transfer (FRET).³⁸ The ligand was sequentially derivatised with three different fluorophores and the emission intensity examined upon introduction of different transition metal ions. The system was compared with other derivatives (1-3) in order to investigate the two step FRET process.

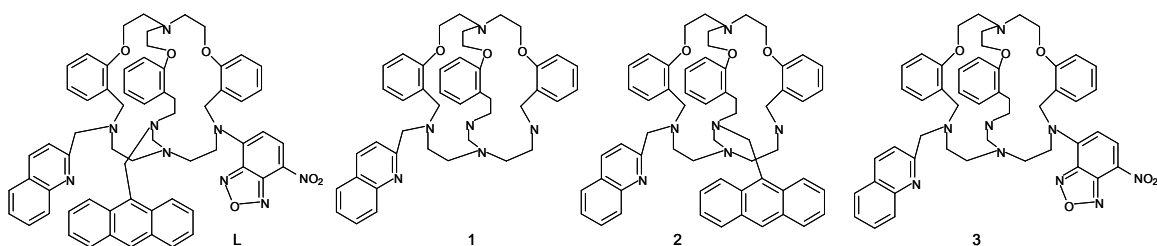


Figure 18 – Structure of the aza-oxa cryptand ligand, L, and modification of the ligand having differing fluorophores, 1-3. ³⁸

When a transition metal was introduced to the cryptand it occupied the lower end of the cryptate domain, and was co-ordinated by the amine groups. As multi-step FRET mechanisms depend on distance between fluorophores, co-ordination of a metal ion helps signal transduction between fluorophores. Therefore, the introduction of a metal ion was shown to induce fluorescent enhancement, excess of metal ions did not quench the fluorescence. The FRET signal was found to be most significant in the presence of Cu^{2+} ions, with similar behavior being observed with Zn^{2+} and Ag^+ , although to a lesser extent.

Another example of a functionalised cryptate was reported by Rice *et al.* in 2006, the article described a cryptate species connected by a bipyridine unit to a crown ether domain. ³⁹ Neodymium is capable of near infra-red emission, which enables its characteristic luminescence to be distinguished from biological auto-fluorescence, making it extremely useful in the design of biological sensors. For this reason neodymium and ytterbium, which are both capable of NIR emission, are becoming popular in the development of lanthanide based probes. ⁴⁰

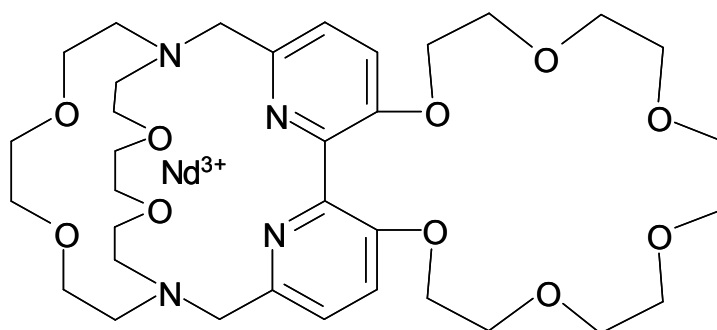


Figure 19 – Structure of the neodymium cryptate complex. ³⁹

The functionalised cryptate reported is capable of an allosteric effect, the neodymium ion is co-ordinately saturated within the cryptate domain, preventing quenching from solvent

molecules, and the event of a s-block metal ion co-ordinating within the crown ether domain induces a modulation in the NIR emission exhibited by the Nd(III) ion.

Various s-block metal ions, (Na^I , K^I , Ca^{II} and Ba^{II}) were introduced to the ligand, and the emission responses recorded. The largest change in the absorption spectrum was caused by introduction of Ba^{II} , which significantly reduced the Nd^{III} emission intensity, introduction of Na^I , K^I and Ca^{II} did not cause any significant decrease in emission. The large decrease in emission intensity exhibited upon introduction of the Ba^{II} ion is due to its large ionic size, the Ba^{II} co-ordinates within the crown ether domain with all six of the available oxygen donor atoms. Therefore, the two oxygen atoms directly bonded to the bipyridine unit are co-ordinated, in order for these two oxygen atoms to successfully bond to the barium ion the NCCN bond of the bipyridine unit must twist away from planarity. This increased torsional angle affects the binding capabilities of the cryptate domain, meaning only one of the two bipyridine nitrogen groups is available to co-ordinate the neodymium ion, this allows a solvent ion to co-ordinate the neodymium ion, and quenching of the NIR emission occurs. Thus, the event of co-ordination of the barium ion within the crown ether domain is signalled by the change in NIR emission.

1.4.4 Ditopic ligands

A ditopic ligand has two guest binding sites, there are examples of ligands with further multiple binding sites, these are called polytopic receptors. Ditopic receptors can be used to co-ordinate one specific guest which itself has two co-ordination sites, or to co-ordinate two separate guests, when two guests are co-ordinated this is often part of an allosteric effect. In the case of the ligand co-ordinating one guest with two co-ordination sites, the placement, particularly in relation to each other, of binding sites can greatly enhance the selectivity of the ligand for a specific guest. Spacer groups are often utilized in order to improve the selectivity of the ligand, these can be used to mimic the size and shape of a guest to increase the selectivity of the ligand.

In the case of co-ordinating two separate guests the likelihood of co-ordination is often increased by the first co-ordination event. The first recognition event increases the affinity of the ligand to a secondary co-ordination, compared with a monotopic ligand.⁴¹ A ditopic ligand can co-ordinate two nuclei simultaneously, or a secondary co-ordination can be made possible by the first co-ordination. Two such examples of this are the work by Kobuke *et al.* and Nabeshima *et al.* who both describe positive co-operation.^{42, 43}

The Kobuke group have designed and synthesized podand structures with β -diketone groups at both terminals of a polyethylene glycol.^{42, 44} When Zn(II) sulfate was introduced a

zinc complex was isolated, with the zinc ion co-ordinated by the two β -diketones. Similarly, upon addition of Cu(II) ions to a similar complex a copper complex was isolated, with the copper ions co-ordinated in an analogous fashion. These two complexes of Zn(II) and Cu(II) were capable of effectively extracting Na^+ and K^+ picrates into an organic phase, with the Zn(II) complex showing preference for the Na^+ ions, and the Cu(II) complex preference for the K^+ ions.

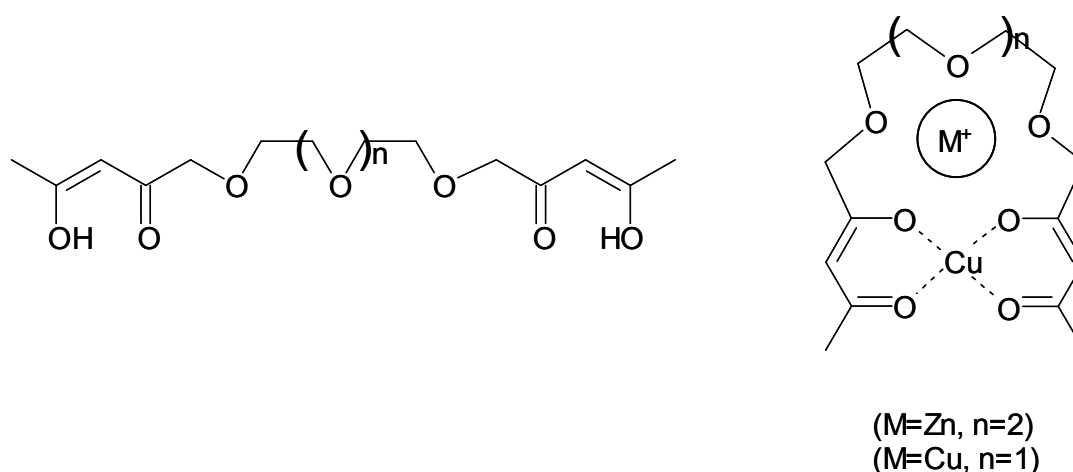


Figure 20 – Structure of unco-ordinated and co-ordinated ligand.⁴²

The co-ordination of the metal ion by the β -diketones causes direct formation of a *pseudo*-crown ether domain, which allows co-ordination of a second metal ion. The *pseudo*-crown ether exhibits selectivity for metal ions based on ionic diameter and cavity size typical of the crown ether family. The high affinity to alkali metal ions is not purely due to the formation of the *pseudo*-crown ether. However, co-ordination of the anionic diketone ligands afford reduced electrostatic repulsion to the Na^+ and K^+ ions

Thus, the length of the polyethylene chain between the two β -diketone groups allows selectivity to be tailored based on ionic radius of the target metal ion. Comparison with the free unco-ordinated ligand revealed this was unable to extract the Na^+ and K^+ picrates into an aqueous solution, as would be expected. Complexes formed with this type of metal assisted organization are interesting, as the organization occurs after synthesis, meaning the ligand could be reversible organized depending upon the specific requirements.

The Nabeshima group reported a novel ditopic ligand in 2002, which upon co-ordination of Fe(II) formed a *pseudocryptand* capable of co-ordinating s-block metal ions.⁴³ The ligand, which is initially helical in nature, forms a cavity upon co-ordination of a Fe^{2+} ion by three terminal bipyridine units. The Fe^{2+} ion is co-ordinated in an octahedral co-ordination

geometry by the three bidentate bipyridyl domains, thus creating a *pseudocryptand* cavity above with nine O-donor domains available for co-ordination.

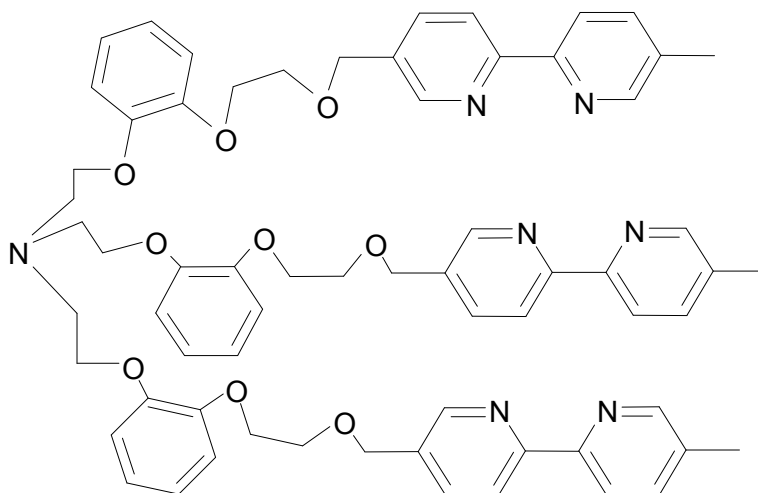


Figure 21 – Structure of the novel helical *pseudocryptand*. ⁴³

Significant changes in the ^1H NMR spectra were observed upon introduction of Cs^+ and Rb^+ , indicating co-ordination within the cryptate domain. The *pseudocryptate* exhibited complementarity behavior towards guest species, a large shift was observed in the ^1H NMR signals with the larger Cs^+ and Rb^+ ions, indicating formation of a stable complex. However, little or no change in chemical shift was observed with the smaller Na^+ and K^+ ions, indicating the radius of the ions was too small to form a stable complex, as the co-ordinated Fe^{2+} ion prevents spherical contraction. A solid state structure of the $[\text{LFeCs}]^+$ complex demonstrates the helical arms twist and lengthen to a more rigid state in order to accommodate the Cs^+ ion.

The co-ordination of the Fe^{II} ion allows metal-assisted cyclisation and effectively allows control of the guest affinity of the *pseudocryptand*. In this case the Fe^{II} ion is utilized as an effector, co-ordination of which allows encapsulation of a second metal ion.

1.4.5 Allosteric effects

Allosteric interactions involve a link between two or more co-ordination sites, a ligand is termed allosteric if the event of a interaction at one co-ordination site affects the binding or physical properties of a second connected site. This type of interaction is extremely useful in the development of sensors, as the co-ordination of a guest is signalled at the secondary connected site. Sensors often consist of a selective co-ordination site, connected by a communication bridge to a secondary site which is capable of a physical response.

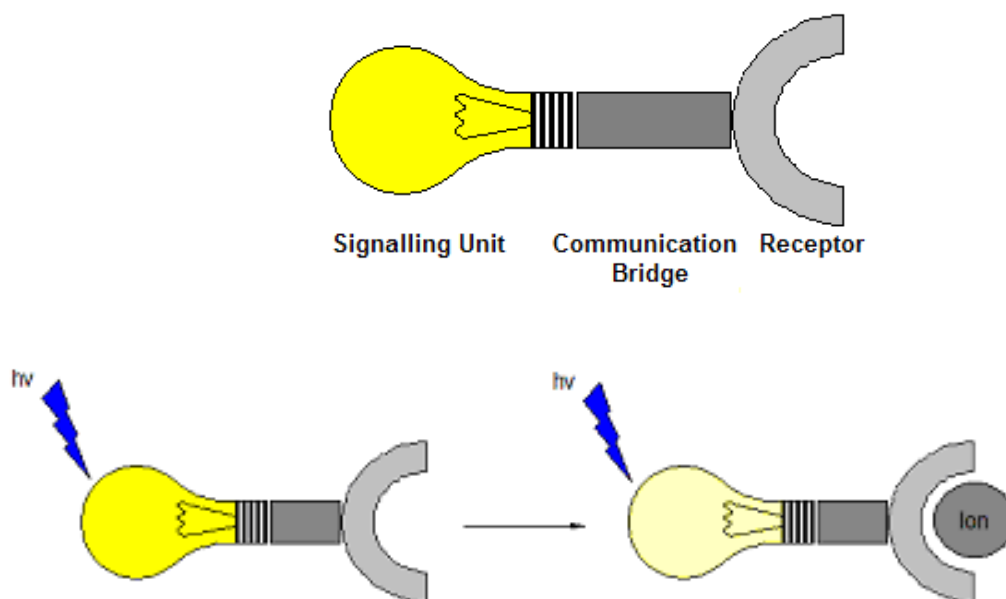


Figure 22 – Schematic diagram representing a luminescent sensor system.

Allosteric regulation is a well known mechanism in nature, direct control of protein function is achieved when effectors bind to regulatory sites which are distinct from the active site of an enzyme or protein. The binding of the effector often induces a conformational change that can profoundly influence the activity of the protein. The allosteric effectors are usually different in size and shape to the enzyme's substrate, and this helps to explain why products of metabolism can sometimes exert feedback control at the beginning of a metabolic pathway, as is often the case in the biosynthetic pathways of bacteria.⁴⁵

Intrasteric regulation is another form of allosteric control and has been observed in protein kinases and phosphatases, however it has also been observed in diverse enzyme classes and receptors. Kobe and Kemp reported in 1999 on the combination of intrasteric inhibition with allosteric control; knowing that intrasteric regulation inhibited the protein function, they investigated how the autoinhibition was reversed. It was found that the mechanism which turned the protein back on (and reversed the protein inhibition) was allosteric in nature. The combination of the intrasteric and allosteric control was found to be a powerful, flexible mechanism which controls some of the most complex cellular processes.⁴⁶

Some of the most important initial work carried out in Supramolecular chemistry utilizing allosteric effect was performed by Rebek, who became interested in utilizing these effects after studying enzymes.⁴⁷⁻⁴⁹ In enzyme behavior the activity of the enzyme is regulated by conformational changes which occur upon binding, these were termed template effects.⁵⁰

He identified the minimum requirements for an allosteric effect to occur, namely; an active site, an allosteric site, and a mechanism which connects them. In his paper published in 1979 he outlines a macrocyclic polyether, possessing two binding sites, a crown ether to co-ordinate alkali metal ions, and a 2,2'-bipyridine unit to chelate other metal ions. ⁴⁹

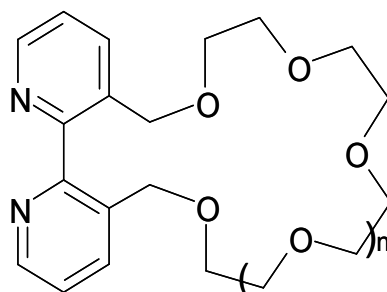


Figure 23 – Structure of the macrocycle polyether. ⁴⁹

Connection of the two sites allows an allosteric effect, chelation of metal ions at the bipyridine site forces the aromatic groups towards co-planarity restricting the conformation of the crown ether receptor. As crown ether receptors co-ordinate selectively based on size, co-ordination of the bipyridine unit dramatically effects the reactivity of the crown ether receptor. The results demonstrated that the extent of binding was largely affected by the number of oxygen donor atoms available in the crown ether domain, and that the macrocycle showed little selectivity between different ions, however an allosteric effect was achieved.

1.5 Metal ion sensors

Over recent years many types of chemical sensors have been developed. A chemical sensor is a device which responds to a specific analyte of interest by a chemical reaction, many are also capable of quantifying the amount of analyte present. There are two main parts to a chemical sensor; the receptor, where the reaction occurs, and the transducer, which reports the reaction. There are many different ways a transducer can report a reaction, and they depend upon the type of sensor being utilized. Common methods of signalling include; a change in colour, increased or decreased luminescent output, change in electrical potential or the production of heat.

Most chemical sensors can be catergorised into groups according to their signalling method, the main groups are: electrochemical sensors, optical sensors, heat sensitive sensors and mass sensitive sensors.^{51, 52} The ability of supramolecular arrays to reversibly co-ordinate ions and to be designed for specific applications mean metal ion sensors are a large area of research within supramolecular chemistry. A sensor should ideally be selective and specific

for a particular guest, reporting the presence in a clear physical way when the ion is detected from a variety of competitive ions. The most common type of sensor utilized in the field of supramolecular chemistry is the optical sensor, more specifically, the fluorescent sensor, which typically combines a binding domain with a fluorescent unit, termed a fluorophore.

1.5.1 Fluorescent sensors

An optical sensor is a sensor that reports the presence of a guest by a physical means in a visible way, such as a colour change or in the form of visible light. The most common type of optical sensor is a fluorescent sensor as it gives an easily interpretable physical output in the form of light. The benefit of the signal being visible light is that light is easily measurable even at very low concentration and the amount of light produced can indicate the quantity of guest which has co-ordinated within the host sensor. This allows physical sensors to be very sensitive and therefore suitable for use in biological systems where the concentration of the analyte of interest is often low.¹

Numerous fluorescent sensors have been produced for monitoring metal ions important in biological function. The Lippard group have produced several fluorescent sensors for the detection of Zn^{2+} ions, Smith and Pope have also produced sensors for zinc ions in recent years.⁵³⁻⁵⁷ Gunnlaugsson produced the first example of a bis-macrocyclic lanthanide based luminescent sensor which signalled the presence of sodium and potassium ions in water, and the Taki group in Japan have produced sensors for both Zn^{2+} and Cd^{2+} .⁵⁸⁻⁶⁰ The research is fuelled by a demand for greater understanding of biological functions and to understand the pathology of disease within the human body.

1.5.2 Use of Chemical Sensors for Biology

The direction and drive of the current health care system has created a demand for rapid and accurate analysis of samples within the clinical environment, this extends to require analysis at the point of care, often in clinics, wards or even patient's homes. With this in mind supramolecular sensors are becoming an interesting area of biological sensors, host and guest chemistry is ideally suited to this area, in particularly the area of optical and luminescent sensors.

An excellent example of a metal ion sensor is that devised by the research group of Qian, Zhang and Zhang, who have successfully synthesised a fluorescent sensor for Zn^{2+} . Zinc is a vital component in many cellular processes, and is the second most abundant transition metal found in the human body, 90 % of zinc found in the body is bound within proteins or playing catalytic roles in enzymes. However, pools of free zinc ions have been imaged in cells, it is these pools of zinc that scientists are currently most interested in, as they are

thought to be involved in neurophysiological and neuropathological processes.^{55, 61-63} These zinc pools have been implicated in aging, and age related disorders, such as Alzheimer's and Parkinson's disease.^{61,64}

Imaging of zinc ions has been previously achieved in living cells using diversified zinc sensors, however imaging of intact cells has not been achieved, and is in high demand due to its use in understanding the role of zinc ions within living cells.^{55, 65-67} The paper reports a novel visible light excitable Zn^{2+} fluorescent sensor based on a 4-amino-7-nitro-2,1,3-benzoxadiazole (ANBD) fluorophore.⁶⁸ ANBD was utilised due to its biocompatibility, large Stoke's shift and visible absorption band.

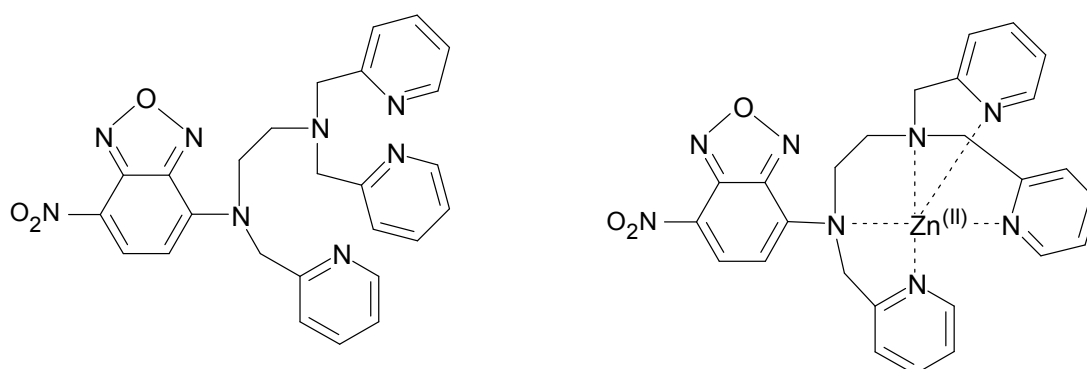


Figure 24 – Structure of the ANDB based fluorescent zinc sensor.⁶⁸

Introduction of Zn^{2+} demonstrated amplified fluorescence and induced a minor emission shift, which can be attributed to the combined effect of the Zn^{2+} ion co-ordinating the outer amine moiety and the inner amine group simultaneously. Both Zn^{2+} and Cd^{2+} induced an emission enhancement; all other metal cations tested did not induce any notable emission change. Cd^{2+} induced a less dramatic emission enhancement than the Zn^{2+} ions, but is not expected to demonstrate any competitive interference due to its relative scarcity in living cells. Introduction of common transition metals abundant in living cells (K^+ , Na^+ , Mg^{2+} and Ca^{2+}) had no effect on the Zn^{2+} response, indicating the sensor would be selective within a competitive biological media.

Intact *in-vivo* imaging of zebrafish larvae allowed observation of Zn^{2+} distribution, revealing storage areas of Zn^{2+} around the zebrafish ventricle, which could be related to development, high concentration of Zn^{2+} were also found in other areas related to development and growth. A reliable and effective Zn^{2+} sensor could become invaluable in revealing the role of zinc within biological systems.

The demand for a zinc sensor for intracellular imaging is high, therefore many research groups are currently working in this area, another example of a fluorescent sensor was published in 2003 by Taki, Wolford and O'Halloran. The paper reports the synthesis of a protein based emission ratiometric probe for imaging intracellular zinc ions, the probe is cell permeable, meaning it can access the cell without the need for microinjection.⁵⁹

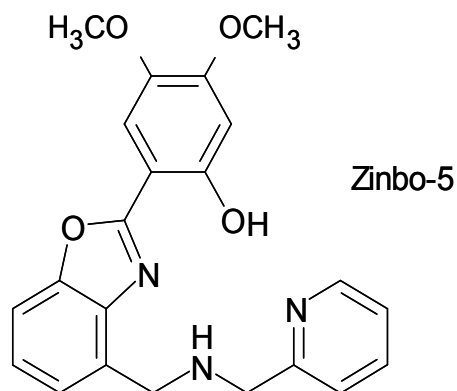


Figure 25 – Structure of Zinbo-5.⁵⁹

The probe's structure is based around a highly luminescent benzoxazole core which is substituted by various zinc chelating species, the probe was named Zinbo-5. The selectivity of the probe was examined in comparison with other heavy metal ions and revealed that only Zn^{2+} and Cd^{2+} induced an emission shift. Further analysis revealed that addition of excess metal ions to the probe did not affect the Zn^{2+} based fluorescence, suggesting the probe would be useful within a competitive biological based media. Emission ratio imaging experiments reveal Zinbo-5 to readily reveal changes in intercellular zinc availability, which may be useful in understanding many processes within the body.

1.6 Metallosupramolecular Chemistry and Transition Metal Helicates

1.6.1 Introduction to Metallosupramolecular Systems

Metallosupramolecular chemistry is a term which was introduced in 1994 by Edwin Constable to describe supramolecular assemblies that exploit the use of metal ion centres in order to self assemble structures.^{69, 70} Self organization processes are used to direct the assembly by information stored in the covalent framework, and organization occurs through specific interaction or recognition patterns.⁷¹ This means the assembly is spontaneous, but directed by pre-programming and careful design. Self assembled synthetic complexes may exhibit unexpected properties due to the binding abilities of receptor frameworks, or the physical properties of the metal ions, allowing interesting variations to be discovered.⁷² Metal to ligand dative bonds are thermodynamically strong, but can have varying degrees of

lability, meaning a range of kinetic stabilities are available. Transition metals also have very specific geometric requirements, which can be used to form structures in specific arrangements.¹ The ligands bridge one or more metal centers and construct architectures that can be one, two or three dimensional. Metal directed assembly results in formation of a wide variety of different supramolecular structures, the nature of supramolecular chemistry allows researchers to tailor and mould ligands to suit particular applications and to form specific structures. The rigidity of the ligand and the co-ordination geometry of the metal ion can dramatically affect the type of structure formed. For example, a ligand with a flexible structure and rotation around connecting bonds between rings is most likely to form a helicate structure, however a rigid structure with limited flexibility is more likely to form a ladder or grid structure.

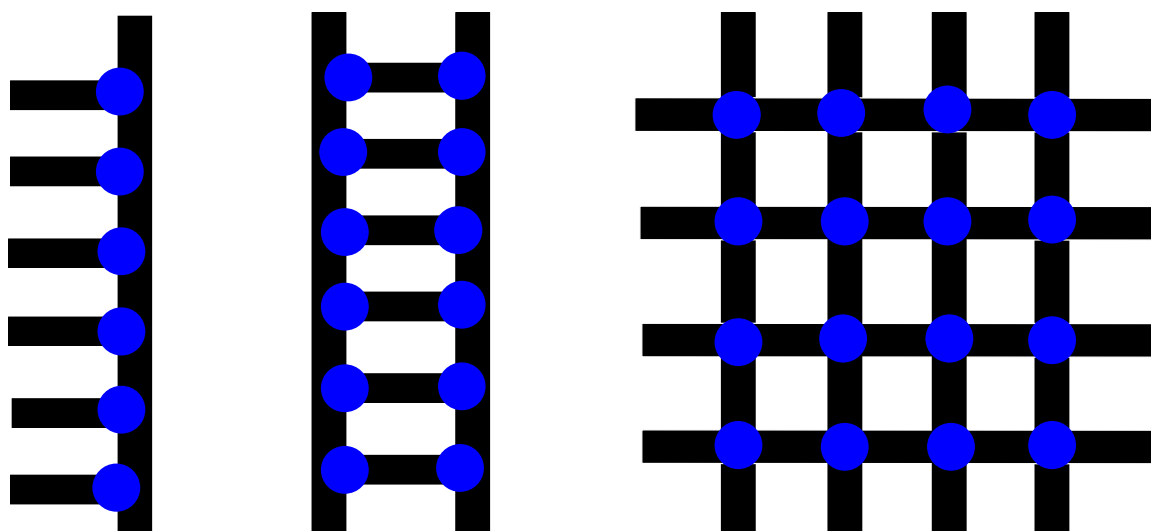


Figure 26 – Schematic representation of a rack, ladder and grid assembly.

1.6.2 Racks and Ladders

Racks and ladders are similar in structure, the number of binding domains available is the main distinguishing factor between formation of one or the other. An example of this is a tris-bipyridine strand, when mixed with three equivalents of phenanthroline and Cu^+ , a rack structure is formed, with a phenanthroline co-ordinating a Cu^+ ion at each of the bipyridine sites.

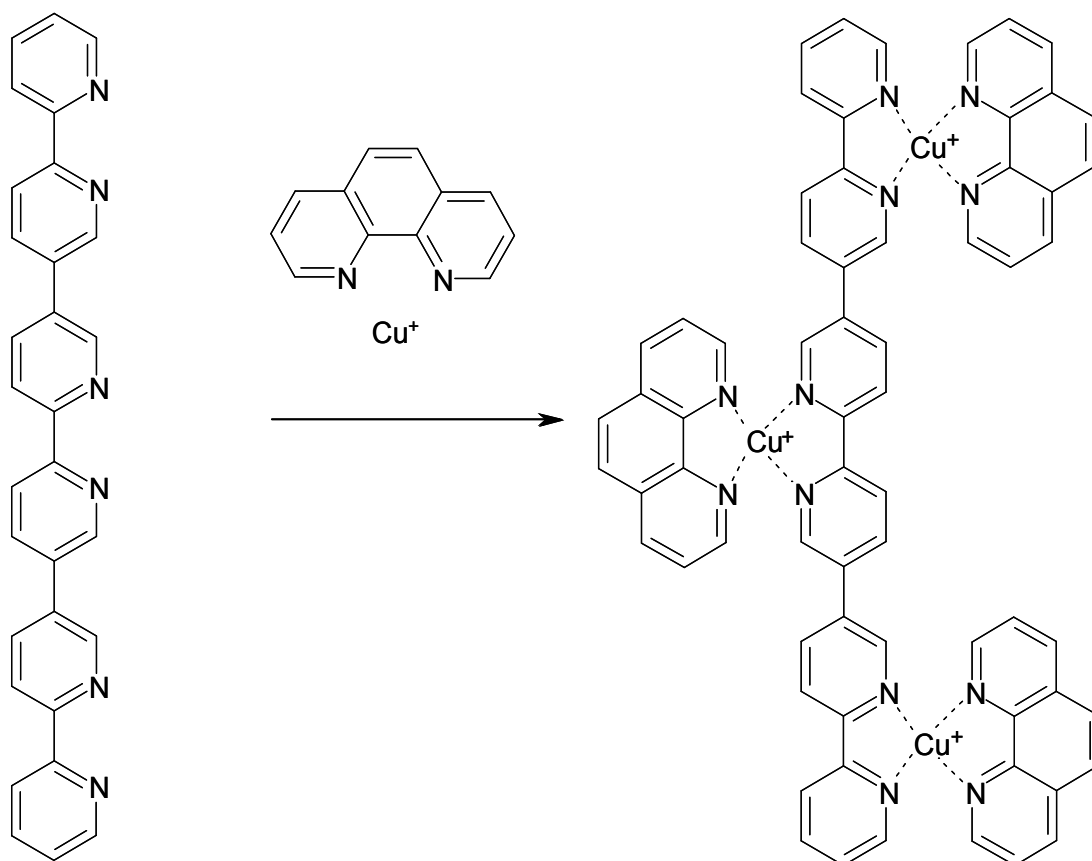


Figure 27 – Schematic diagram showing rack formation of a tris-bipyridine strand with three equivalents of phenanthroline and Cu^+ .

If the same tris-bipyridine strand is then mixed with six equivalents of Cu^+ and three equivalents of a bis-pyrimidine unit, then a ladder structure is formed, with a Cu^+ ion coordinated at each of the bipyridine sites. Each bis-pyrimidine unit co-ordinates a Cu^+ ion at either side, using all available N donor domains.

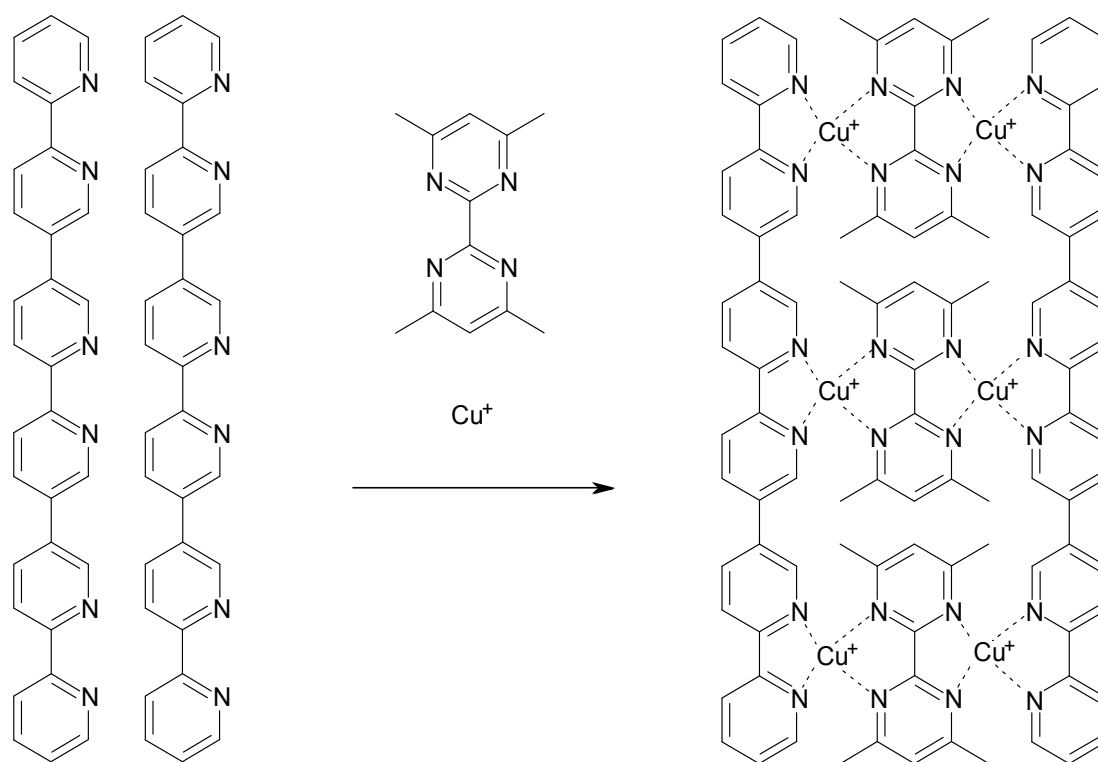


Figure 28 – Schematic diagram of ladder formation between two tris-bipyridine strands and six equivalents of Cu^+ and three equivalents of a bis-pyrimidine unit.

Remya *et al.* recently reported formation of 1-dimensional molecular ladders of terbium-4-sebacoylbis(1-phenyl-3-methyl-5-pyrazolonate) and sodium dibenzo -18-crown-6.⁷³ Three new lanthanide complexes based on a novel heterocyclic β -diketone 4-sebacoylbis(1-phenyl-3-methyl-5-pyrazolone) were synthesised and the structure characterized by single crystal X-ray diffraction. The solid state structure revealed formation of a 1-dimensional strand, with the terbium ion co-ordinated between two of the tetradentate bispyrazolone ligands, with each ligand donating four oxygen donor atoms.

The co-ordination geometry of the Tb^{3+} ion is a distorted square antiprismatic arrangement. The diaza-18-crown-6 species co-ordinates the sodium ion within its central cavity and behaves as a cationic species to the terbium complex. Therefore two ligand strands co-ordinate the terbium ion, and the diaza-18-crown-6 co-ordinates two $[\text{L}_2\text{Tb}]^{3+}$ complexes to each other, forming a chain of the order; ligand- Tb^{3+} -ligand-diazacrown-ligand- Tb^{3+} -ligand etc.

Hydrogen bonding interactions occur between two separate ligand strands, and combine to form an interesting ladder, the alternate arrangement of the $[\text{L}_2\text{Tb}]^{3+}$ and sodium co-ordinated diaza-crown form the strands, and the intermolecular hydrogen bonding connects

these two strands together, forming the steps of the ladder. This is an interesting case, demonstrating how supramolecular chains can be co-ordinated by hydrogen bonds to form a ladder complex.

1.6.3 Grids

Grid structures are formed as a result of self assembly, with rigid multidentate bridging ligands forming a grid like structure upon co-ordination with metal ions. Grid structures occur when there are multiple co-ordination sites set along a rigid chain, the chains assemble around the metal ion and form multiple co-ordinations to other ligand chains, forming a large grid. Much research has been carried out on 2 x 2 grid systems, forming tetranuclear complexes with metal ions.⁷⁴⁻⁷⁹

The Brooker group are interested in forming grid systems with metal ions which are readily available to adopt geometries which are distorted from the ideal, and in the subtle effects of secondary interactions such as steric factors. They recently reported synthesis of pyridazine-bridged Cu⁺ complexes which formed 2 x 2 grid systems.⁸⁰ The bis-bidentate ligands produced could easily be extended in order to form larger grids, however this initial research was carried out with bidentate ligands, forming 2 x 2 tetranuclear grids. The ligands were produced by reactions of 3,6-diformylpyridazine and various anilines and upon successful synthesis and characterization, complexation with Cu⁺ ions was performed.

The ligands were complexed with tetrakis(acetonitrile)copper(I)hexafluorophosphate in a 1:1 ratio, this led to the almost exclusive formation of tetranuclear grid complexes. In all of the grid complexes the Cu⁺ centres were co-ordinated in a significantly flattened tetrahedral geometry due to the positions of the ligand strands within the 2-dimensional system. Further to this, they found that addition of electron withdrawing substituents onto the phenyl rings of the bis-bidentate ligand decreased the stability of the resulting metal complexes. This is due to the decreased donating ability of the imine nitrogen atoms, preventing the formation of thermodynamically strong bonds.

Li *et al.* reported preparation of several mixed-valence Cu^ICu^{II}-terpyridyl compounds in 2005, which formed rectangular grid systems upon self assembly.⁸¹ The compounds were based on a 4'-(4-pyridyl)-2,2'-6',2''-terpyridine ligand with halogen and *pseudohalogen* (Cl, Br, I, SCN) linkers. The ligand and *pseudohalogen* (X) link two Cu^I and Cu^{II} ions resulting in the formation of a rectangular grid building block. The size of the building block can be easily influenced by modulating the length of the X linker. The mixed valence arises during the preparation, as the terpyridyl ligands partly reduce the Cu^{II} ions, however, some reduction by the halogen or *pseudohalogen* may also occur.

The ligands formed M_4L_4 or M_6L_6 grid complexes, in which the Cu^{2+} ions were co-ordinated in a distorted tetrahedral geometry, and the Cu^+ ion in a square planar geometry. The ligands formed *pseudorectangular* arrangements, with the metal ions co-ordinated in each of the corners, rather than the typical 2 x 2 grid usually associated with M_4L_4 complexes.

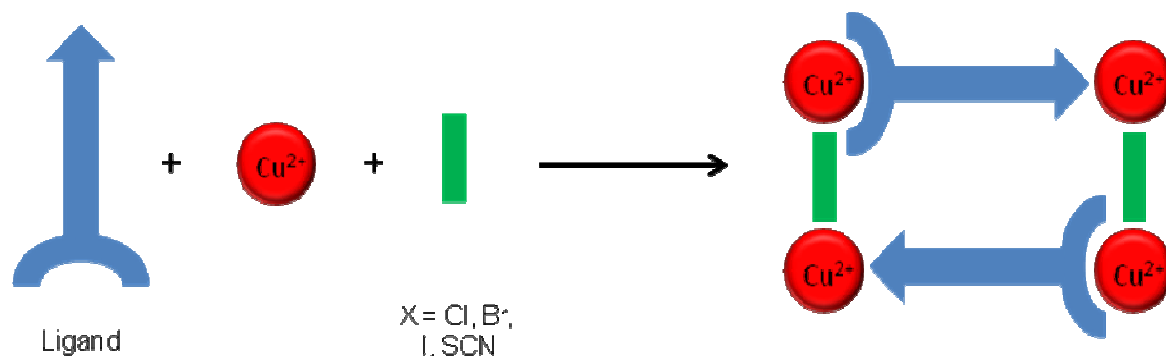


Figure 29 – Schematic cartoon demonstrating formation of the rectangular M_4L_4 grid.

The building block grid complexes can be further connected by the halogen or X linkers to create 1-dimensional chains, or 2-dimensional bilayer structures with an arrangement analogous to a brick wall. The size of the individual grid bricks can be fine-tuned by the size and length of the linker units, the number of units within a chain, or bilayer structure can be modified by the number of linkers attached.

1.6.4 Cages

Cage structures are formed by spontaneous metal directed assembly of several ligand strands to form a 3-dimensional cage structure with an internal cavity. Cages are highly symmetrical and their structure can be carefully controlled by using metal ions with specific geometric co-ordinations and rigid ligands. The cage can be designed by specific location of binding domains on a ligand chain, and the size and shape of the central cavity can be modified by this specific design. The central cavity within a cage structure is often large in size and can be used to co-ordinate multiple atoms within. The size and shape of the cages and cavities can be modified by functionalizing the ligands and using specific metal ions.⁸²

Fujita *et al.* produced a tridentate 1,3,5,-tris(4-pyridylmethyl)benzene ligand, which when treated with $(en)Pd(NO_3)_2$ and sodium 4-methoxyphenylacetate formed a single component in high yield.⁸³ Elucidation of this complex revealed a cage-like complex, the 1H NMR spectra revealed a high symmetry, and that the sodium 4-methoxyphenylacetate was co-ordinated within the cavity in the centre of the cage.

Upon complexation of the sodium ion within the cage the 1H NMR spectra show dramatic upfield shift of the signals associated with the sodium 4-methoxyphenylacetate, due to the

co-ordination within the cage. It was also noted that formation of the host in high yield was only obtained in the presence of the guest species. In the absence of a guest, co-ordination of the tridentate 1,3,5,-tris(4-pyridylmethyl)benzene ligand and (en)Pd(NO₃)₂ results in the formation of oligomeric products. However, upon addition of the sodium species these products disappear with the assembly of the cage species occurring over several hours. This research demonstrated the spontaneous metal directed assembly of a three dimensional cage complex, one which could only be directed by specific guest complexes.

Ward *et al.* have published numerous examples of co-ordination cages in recent years, however the first significant result reported in this field by the group was published in 1999.⁸⁴⁻⁸⁸ The publication describes synthesis of a hexadentate podand ligand of tris[3-(2-pyridyl)pyrazol-1-yl]hydroborate (L), which forms a mononuclear complex with Co^{II} and a tetrahedral cluster with Mn^{II} and Zn^{II}.⁸⁹ Reaction of the ligand with Co^{II} gives rise to formation of a 1:1 metal to ligand complex of [CoL][PF₆], with the Co^{II} ion co-ordinated in a trigonal prismatic geometry with the ligand relatively undistorted.

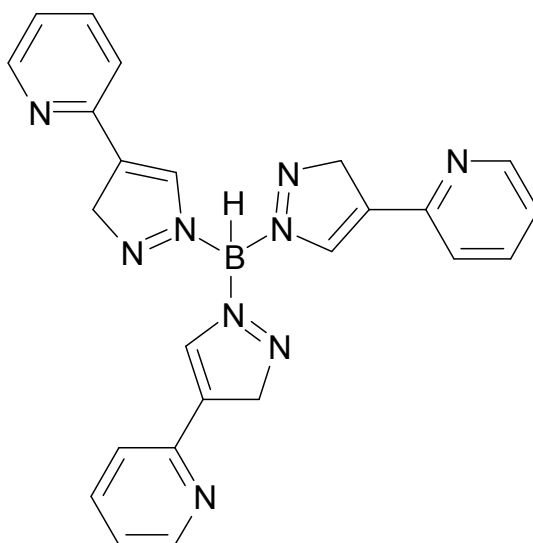


Figure 30 – Structure of the hexadentate podand ligand, L.

However, reaction of ligand with Mn^{II} or Zn^{II} initially suggested a 1:1 metal to ligand complex, but further analysis revealed a tetranuclear species of [M₄L₄(PF₆)]³⁺. The crystal structure of the complex confirmed the formation of the tetranuclear complex, and revealed that the two complexes had very similar structures. Each individual ligand within the complex spreads in order to co-ordinate each of its three bidentate arms to a separate metal ion. In order for it to achieve this the tris(pyrazolyl)borate adopts an inverted geometry so the apical hydrogen

is directed inwards. This conformation is necessary in order for the pyrazolyl donors to co-ordinate each of the separate ions, rather than co-ordinating one atom.

The group realized in hindsight that the formation of the tetrahedral cluster was the only way in which the ligand could co-ordinate the metal ion in its preferred octahedral geometry, as it is impossible for the three arms of an individual ligand to present an octahedral donor set to a single bound metal ion. It is therefore necessary to utilize three separate bidentate domains from each of the three ligands to offer an octahedral geometry to the encapsulated ion.

1.6.5 Helicates

As previously stated, transition metals can be used to direct the formation of molecular assemblies. This is beneficial as transition metals due to their varying charges have very specific geometric configurations, this allows us to program and direct the co-ordination arrangement of a complex based on different metal ions used to template the assembly. The bonds formed between metal and ligand species are dative, and are thermodynamically strong, this coupled with the varying lability of the transition metals allows us to choose our interactions specifically from a range of kinetic stabilities. These two important aspects allow chemists to design, program and direct interactions between the ligand and the metal ion, by carefully choosing which metal ion will template the reaction. For this reason helicate ligands are one of the most fascinating areas of supramolecular chemistry, and one directly inspired by nature, in the form of the DNA double helicate. Helicates can occur with a variety of ligand strands co-ordinated to two or more metal centres, however the most common helicate species are double and triple-stranded helicates.⁹⁰

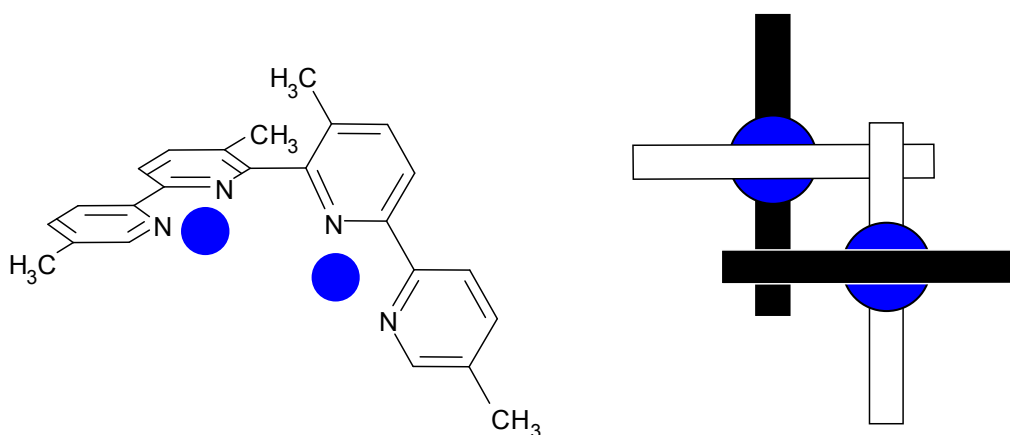


Figure 31 – Schematic representation of double helicate formation.⁹¹

1.6.5.1 Directional Helicates

A single helix may or may not be symmetrical, depending on the design. In the case of unsymmetrical helices, the concept of directional helicates is raised. One terminus of the helicate is termed the head, and the opposite terminus the tail, when self assembly occurs in the presence of a metal ion it is possible, depending upon the structure, to form different arrangements of helices. For example, a double helicate structure could form a head to head structure, or a head to tail structure, within a tri-helicate structure it is possible to form head to head to tail, or head to head to head structures. Interestingly the conformation of the helicate structure formed can be metal ion led, where certain metal ions form only the head to head species, with others preferring the head to tail conformer.

An excellent example of this was published in 2004 by Rice *et al.* which demonstrated a amide-substituted unsymmetrical ligand which formed a dinuclear triple helicate with Co^{2+} ions, which exists as an head-to-head-to-head and a head-to-head-to-tail isomer in solution.⁹² The ^1H NMR spectra confirmed the presence of both the HHH and HHT isomers upon introduction of $[\text{Co}_2(\text{L}^1)_3](\text{ClO}_4)_4$ to the ligand, with a ratio of 1:3 of HHH:HHT respectively. A total of 36 aromatic signals were observed, a clear indication that a mixture of products was present. The predominance of the HHT species is due to the reduced steric interactions in this conformer.

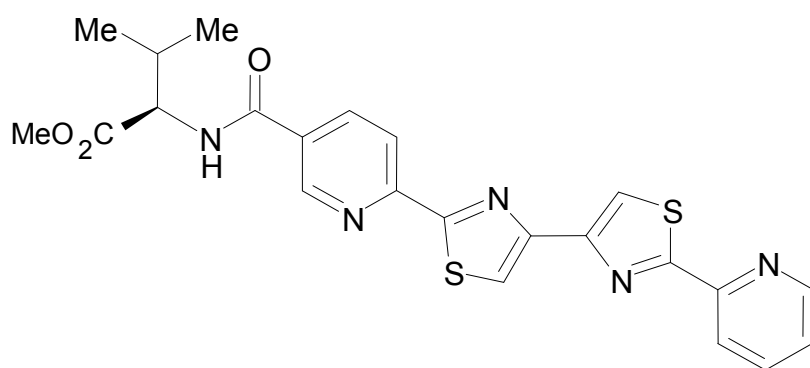


Figure 32 – Structure of the unsymmetrical ligand L_1 .⁹²

Addition of two equivalents of Bu_4NNO_3 to the complexes in solution greatly simplified the ^1H NMR spectrum, which showed only nine major signals. This reduction in the number of signals corresponds to exclusive formation of the symmetric HHH isomer. The main difference in between the structure of the two isomers is the formation of a cavity in the HHH isomer, the cavity contains three amide groups, which are capable of forming hydrogen

bonds to an anion. The cavity is not formed during the assembly of the HHT geometric isomer.

In the presence of the perchlorate anion the formation of such a cavity is not favoured, therefore addition of perchlorate results in the mixed isomers of HHT and HHH. However, the nitrate anion has a much stronger affinity for the amide cavity, making the formation of the HHH isomer more favourable. This type of preorganisation caused by a ion is termed the template effect, as the ion templates the formation of a specific arrangement. The ligand thus forms a dinuclear triple helicate in the presence of Co^{2+} ions, however the formation of isomers can be controlled by nitrate anions.

1.6.5.2 Programmed Helicates

Double helicates often contain multiple co-ordination sites, and are able to self assemble around metal ions. Depending on the size and preferred geometry of the metal ion, double helicates can often be programmed to form monotopic or ditopic species. This reprogrammable nature has attracted much interest and led to extensive research in this field. Triple helicate structures are also common, where three strands of ligand assemble around a metal ion templating species, these again can be reprogrammed depending on the geometric preferences of the co-ordinated metal ion.

The co-ordination sites within a single helicate ligand are often formed from O-donor or N-donor domains. When second, or third, ligand approaches in the presence of a metal ion they wrap themselves around the ion to form a 3-dimensional structure around the metal ion, with each ligand co-ordinating with the metal ion, to form a stable helicate structure. In order to allow multiple co-ordination sites, and to allow ditopic or even tritopic co-ordination the co-ordination sites are often spaced accordingly with spacer units, such as a bipyridine unit, to prevent steric hindrance preventing multiple co-ordination.

Some of the early research into double helicate structures was performed at Cambridge University, in a paper published in 1988 the authors present a pentadentate ligand containing quinquemy which forms complexes with transition metal complexes to give a double helicate arrangement.⁹³ The ligand formed a double helicate with Cu^{2+} and Ni^{2+} and crystal structures were obtained, each of the two ligands involved in the helicate partition and present a pseudo terpyridyl donor set to the co-ordinated metal ion.

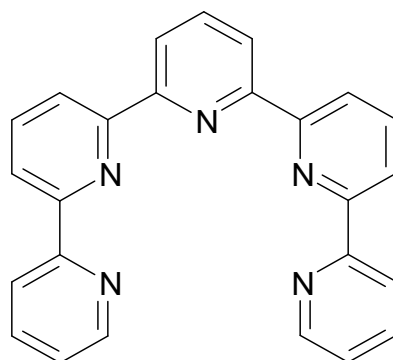


Figure 33 – Structure of the quinquepy ligand, L. ⁹³

The first Cu^{2+} ion is bonded by three nitrogen groups from each ligand, and the second Cu^{2+} ion is co-ordinated by the remaining two nitrogen groups present on the ligand. Therefore, the first copper ion is co-ordinated in a distorted octahedral manner, the second copper is co-ordinated by a weaker interaction, which reflects in its unsymmetrical arrangement and distortion of the axial interactions. The second Cu^{2+} ion is five co-ordinate, bonded by four of the remaining nitrogen groups in the ligand and the remaining site occupied by the oxygen atom of an acetate group. The ligand partitioning is responsible for the twisted arrangement which allows the double helicate structure to form.

Tsang and Yeung have recently published a new chiral pyridyl-thiazole ligand which forms a dinuclear double helicate with Cu^I ions. ⁹⁴ Pyridylthiazole ligands have previously been utilized in ligand reprogramming when binding metal ions by Rice. *et al.* and are a versatile type of helicate structure. ⁹⁵⁻⁹⁸ The ligand was synthesized from a chiral halogen functionalized pyridine group, which was cyanated and reacted with H_2S to form the thioamide. Reaction of the thioamide with 1,4-dibromo-2,3-butanedione in methanol yielded the final ligand, which was successfully characterized by ^1H NMR and ESI-MS.

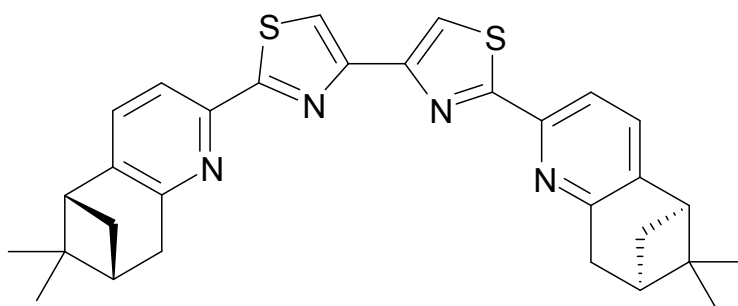


Figure 34 – Structure of the tetradentate pyridylthiazole ligand, L. ⁹⁴

Reaction of the ligand with Cu^{II} ions in methanol led to the formation of a dinuclear double helicate, however the ¹H NMR spectra showed that two species were present in solution, the diastereoisomers present were found to be in a ratio of 81:19. Isolation and recrystallisation of the major diastereoisomer allowed analysis which revealed it to be that of the P-configured helicate. Further evidence was provided by obtaining a single crystal X-ray structure of the major diastereoisomer, which clearly shows P chirality. In the complex both of the Cu^I metal centres have adopted a tetrahedral co-ordination geometry and are both co-ordinated by two pyridylthiazolyl bidentate units, one from each of the separate ligand strands. The ligand strands partition around the centre providing two separate binding domains and enabling each ligand to present a bidentate binding domain to each metal ion. To prevent steric hinderance the strand is twisted around the central carbon to carbon bond allowing the formation of the double helicate structure. The torsion angle between these two central thiazole rings is 59.95°, with additional smaller twists present between the pyridine ring and the thiazole ring.

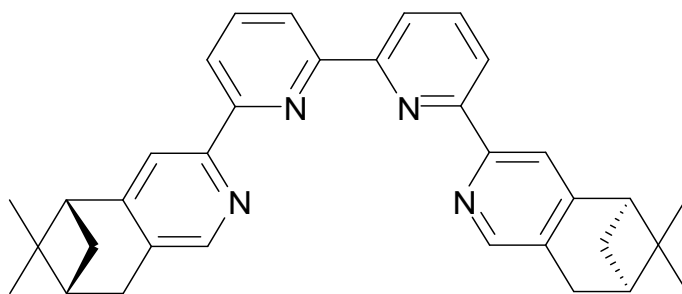


Figure 35 – Structure of the quaterpyridine equivalent of the ligand.

Comparison of the ligand with the quaterpyridine equivalent revealed that addition of Cu^I to quaterpyridine favoured the M-helicate, which was the sole diastereoisomer produced upon co-ordination. The reason for this was thought to be caused by the change in the central two rings from thiazole to pyridine, which altered the distance of the pinene group from the central bridging methylene group. This indicates that the change from five-membered to six-membered rings alters significantly affects the chirality of the product during formation of helicates, and can reverse the chirality of a copper helicate.

1.6.5.3 Reprogrammable Ligands

The first reprogrammable ligand was reported by Rice *et al.* in 2004, and described a ligand which could be allosterically and electrostatically reprogrammed.⁹⁵ A ditopic ligand was produced which contained a thiazole-pyridyl-pyridyl-thiazole chain, which could form a ditopic double helicate structure, with a crown ether domain connected to the central

complementarity between the cavity volume and the ionic radius of the Ba^{2+} ion. In the mononuclear $[\text{Hg}(\text{L}_1)\text{Ba}]^{4+}$ species the Ba^{2+} is co-ordinated by both the benzylic oxygen atoms, this restricts the mobility of the ligand, preventing it from partitioning into two binding domains as in the $[\text{Hg}_2(\text{L}_1)_2\text{Na}_2]^{6+}$ complex. This means the ligand can only act as a tetradentate donor, therefore only formation of the mononuclear species can be achieved.

The system therefore demonstrates how a ligand can be programmed by the Hg^+ ion to form a dinuclear double helicate species, but upon introduction of Ba^{2+} ions the ligand is reprogrammed and becomes a mononuclear ligand co-ordinating the Hg^+ by a tetradentate domain, and the Ba^{2+} within the crown ether.

There have been many publications concerning dinuclear helicate formation, however significantly less trinuclear helicates have been reported. An example of a trinuclear helicate was published in 2007 by Rice *et al.*, and describes an allosteric deprogramming ligand capable of trinuclear helicate formation with $\text{Cu}(\text{I})$ and $\text{Zn}(\text{II})$ ions.⁹⁹

Two multidentate ligands L_1 and L_2 were successfully synthesised by a convergent route, L_2 differs from L_1 by containing an additional bridging thiazole unit after the central bipyridine domain. Upon reaction with $\text{Zn}(\text{CF}_3\text{SO}_3)_2$ and $[\text{Cu}(\text{NCMe})_4]\text{PF}_6$ in acetonitrile, L_1 formed a heterometallic trinuclear double helicate of $[\text{Zn}_2\text{Cu}(\text{L}_1)_2]^{5+}$, confirmation of the structure was obtained by ESI-MS and single crystal X-ray crystallography. The crystal structure clearly demonstrates that the ligand partitions into three binding domains, each domain separated by a bridging $-\text{CH}_2\text{OCH}_2-$ linker unit. The two zinc ions are co-ordinated by the terminal thiazole-pyridine units, and the copper ion is co-ordinated by the bipyridine domains in the centre of the ligand. The Zn^{2+} ion adopts a pseudo-octahedral co-ordination geometry, and the Cu^+ ion has a distorted tetrahedral co-ordination geometry. The distorted geometry of the central copper ion is caused by steric interactions in the bridging ether linking units, these prevent the bipyridine unit from becoming a planar bidentate chelating group.

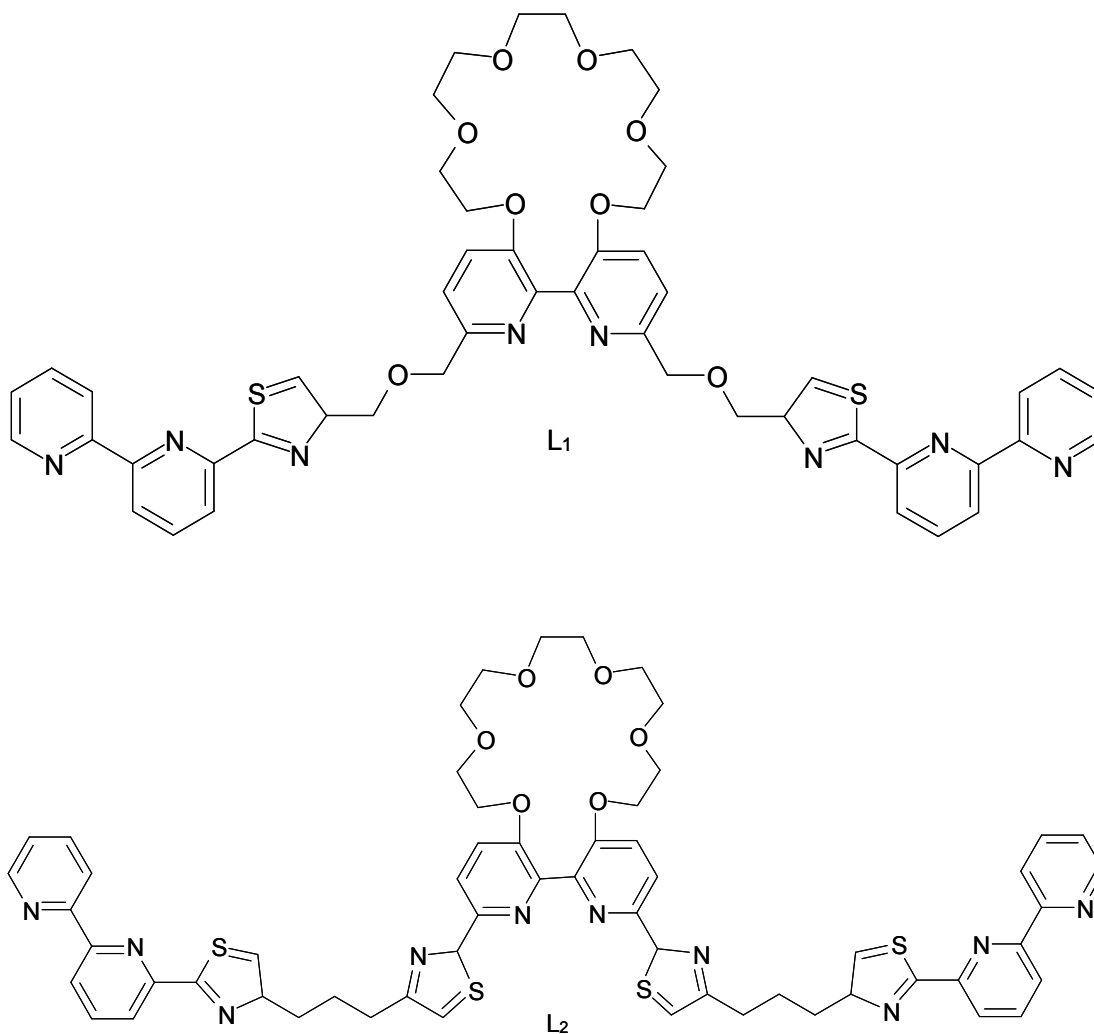


Figure 37 – Structure of ligands L₁ and L₂.⁹⁹

Reaction of L₂ with Zn(CF₃SO₃)₂ and [Cu(NCMe)₄]PF₆ in acetonitrile formed a heterometallic tetranuclear double helicate species of [Zn₂Cu₂(L₂)₂]⁶⁺, confirmed by ESI-MS and single crystal X-ray crystallography. In the solid state the ligand is seen to partition into four binding domains, which co-ordinate two Zn(II) and two Cu(I) ions between two ligand strands. The Zn²⁺ ions are again co-ordinated by the terminal thiazole-pyridine units in a pseudo-octahedral co-ordination geometry, as seen in L₁. However, the two Cu²⁺ ions are co-ordinated by the two central thiazole-pyridine units, which although it could act as a tetradentate domain, partitions along the centre, splitting into two bidentate domains. These two bidentate domains are again a consequence of the two oxygen atoms present in the ether linking units, whose unfavourable steric interactions prevent the central bipyridine unit from adopting a planar position. Instead the potentially tetradentate thiazole-bipyridine-thiazole unit separates along the central core in order to minimise steric interaction.

Although these results were very interesting in their own right, both the L_1 and L_2 ligands possess crown ether domains, therefore reaction of the complexes of $[Zn_2Cu(L_1)_2]^{5+}$ and $[Zn_2Cu_2(L_2)_2]^{6+}$ with Ba^{2+} and Na^+ was attempted. As barium and sodium are both s-block metal ions, they should move into the crown ether domain, which is both selective and specific for s-block metal ions. Addition of an excess of Ba^{2+} to $[Zn_2Cu(L_1)_2]^{5+}$ resulted in a large number of additional peaks appearing in the 1H NMR spectra of the sample, this indicates a variety of different complexes have formed. It has been previously demonstrated that upon co-ordination of barium within a crown ether directly attached to a bipyridine unit the bipyridine unit must become twisted in order to facilitate better overlap of the crown aryl oxygen atoms and the barium ion.^{95, 100} Therefore it can be assumed that upon addition of a large excess of barium ions the ligand L_1 will co-ordinate Ba^{2+} within the crown ether domain. The co-ordination of the Ba^{2+} ion within the crown ether domain will result in a significant increase in the torsion angle of the bipyridine unit, preventing the unit from acting as a bidentate binding domain to the Cu^+ ion. Therefore, upon addition of Ba^{2+} to $[Zn_2Cu(L_1)_2]^{5+}$, the ligand is reprogrammed and is no longer capable of co-ordinating a Cu^{2+} by the central bipyridine units. The terminal thiazole-pyridine units are unaffected, and can continue to co-ordinate the Zn^{2+} ions. This theory is further supported by reaction of $[Zn_2Cu(L_1)_2]^{5+}$ with an excess of Na^+ ions, which results in a slight shift in the peaks present in the 1H NMR spectra, indicating the sodium ion has moved into the crown ether domain. However, sodium has a small ionic radius, and sodium ions do not co-ordinate all the available donor units within a crown ether domain, therefore the sodium ion does not co-ordinate the oxygen donor atoms directly connected to the bipyridine unit. As the torsion angle of the bipyridine unit is unaffected by the co-ordination of the Na^+ ion the bipyridine unit is still capable of acting as a bidentate domain and chelating a Cu^+ ion.⁹⁹

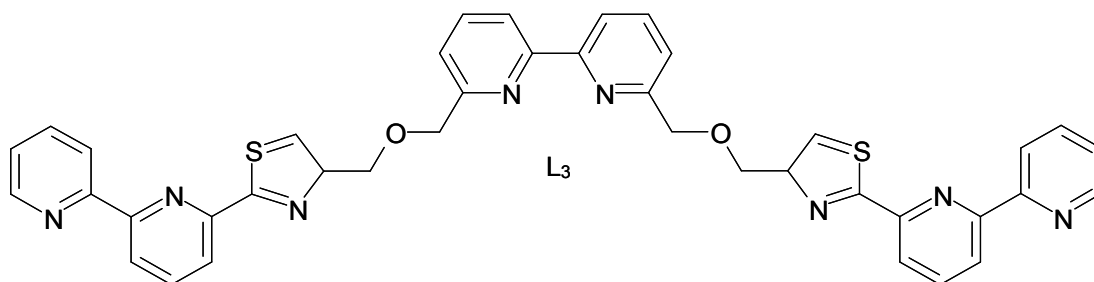


Figure 38 – Structure of ligand L_3 .⁹⁹

A third ligand L_3 was synthesised, the structure of which is identical to that of L_1 , with the exception of the absence of crown ether domain. Reaction of this ligand with Cu^+ and Zn^{2+} ions resulted in the expected heterometallic trinuclear double helicate of

$[\{Zn_2Cu(L_3)_2\}(ClO_4)^{4+}]$, addition of an excess of barium ions to the complex resulted in no change in the 1H NMR spectra, demonstrating the crown ether unit is instrumental in the changes observed in the L_1 complex.

Finally, excess barium ions were added to $[Zn_2Cu_2(L_2)_2]^{6+}$ and showed little change in the 1H NMR spectra, this result is due to the partitioning of the central tetradentate domain. The coordination of the crown ether domain has little effect on the overall structure of the complex as the central bipyridine unit already possesses a large torsional twist. The large torsional twist is present in order to partition the potentially tetradentate domain into two bidentate thiazole-pyridine units. Therefore, the helicate species is still capable of co-ordinating the two copper ions, meaning no deprogramming of the ligand occurs.

2: Aza crown ligands

Described in this chapter is the synthesis and characterization of an aza crown ditopic ligand. The aza crown ligand possesses both a bipyridine domain and a tetra-aza crown domain, and is capable of co-ordinating a Cu^{2+} ion in either or both domains, dependent upon the stoichiometry. At a ratio of 1:2 Cu^{2+} to ligand, two ligands co-ordinate one copper ion via the bipyridine domains, whereas at a ratio of 1:1 the copper is bound by the aza-crown unit. Increasing the Cu^{2+} ratio results in co-ordination of both the aza-crown and bipyridine domains. There is also evidence at high Cu^{2+} ratios that a trinuclear species results, $[\text{Cu}_3\text{L}_2]^{6+}$, where one copper ion is co-ordinated by two ligands via the bipyridine unit and the aza-crown in each ligand is also co-ordinated. At a ratio of 1:1 the ligand co-ordinates Cu^{2+} ions preferentially in the aza-crown domain; which interacts with the metal ion via all four of the N-donor atoms. Further co-ordination of Cu^{2+} via the bipyridine unit results in an interesting allosteric effect. This is a negative co-operative binding as co-ordination of the second Cu^{2+} ion changes the binding capability of the aza-crown domain. As a result the tetra aza-crown is only able to co-ordinate the Cu^{2+} ion by three of its four N-donors due to a change in torsion angle of the bipyridine unit.

2.1 Ligand Synthesis

2.1.1 Synthesis of L₁

The aim of this chapter was to synthesise a aza crown macrocyclic ligand with two specific and separate binding domains. The first binding domain consists of a bipyridine unit, the second an aza crown. Both domains are capable of co-ordinating a Cu²⁺ ion, and the event of co-ordination at one site should enable an allosteric effect in the second connect site.

The aza crowns are similar in structure to crown ethers, possessing nitrogen groups instead of the oxygen groups present in crown ethers. They are capable of co-ordinating metal ions selectively as are crown ethers, making them an interesting and selective domain to utilize in supramolecular systems.

The synthesis of the ligand was non-trivial and was performed using a 3 step linear synthesis, once the starting materials had been produced. The 3,3-diamino-2,2'-bipyridine is a common starting material for systems containing bipyridine units, and was synthesized using a 3 step process in reasonable yield. Surprisingly, even though there is literature precedent, the tetra-tosylate unit (**6**) was fairly difficult to synthesize. A number of previously reported procedures were attempted but this led to very low yields, eventually modification allowed decent yields to be achieved.

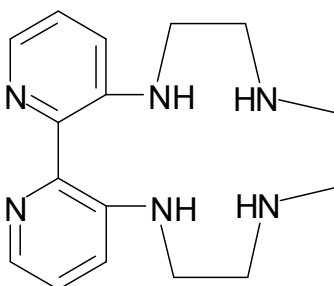
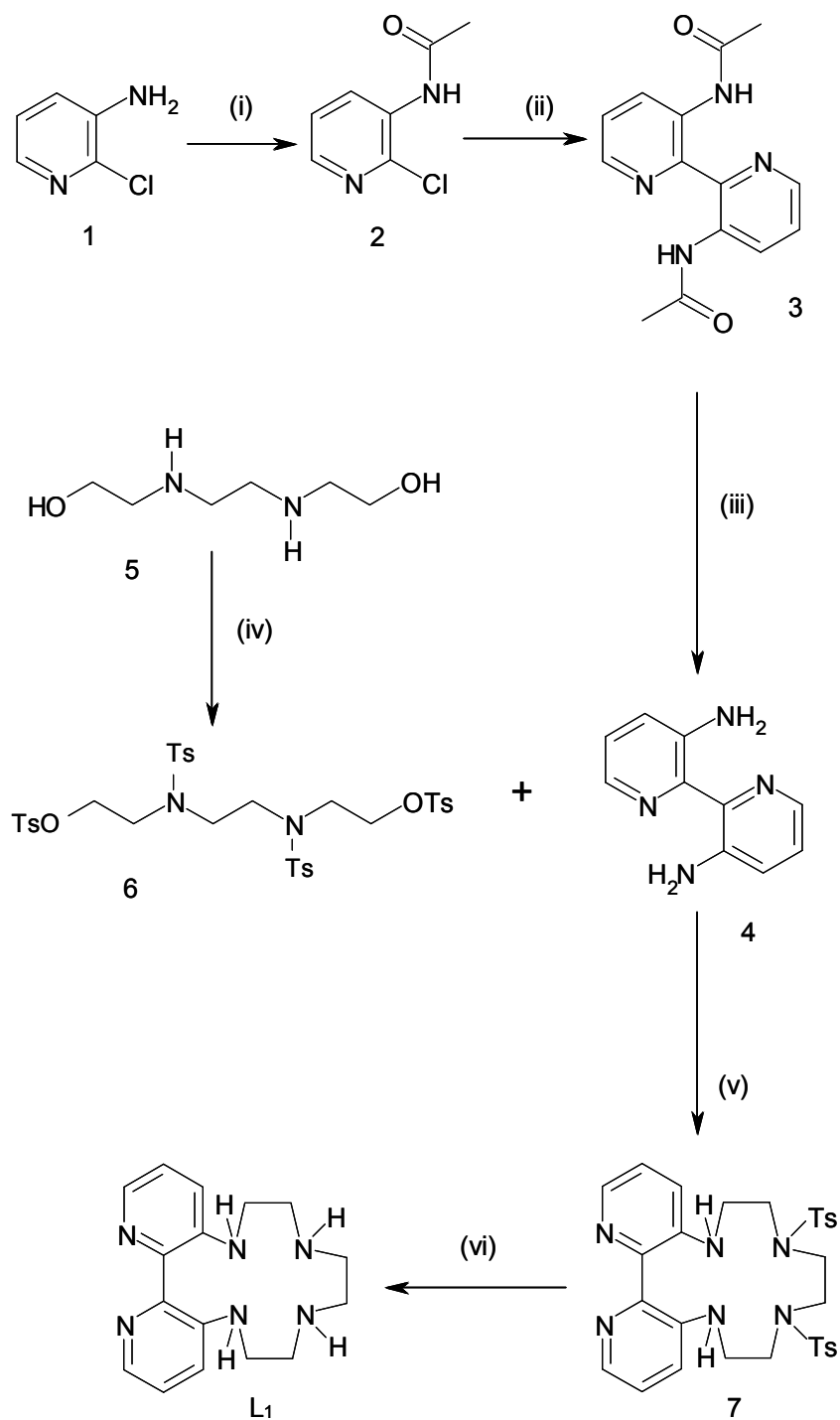


Figure 2.1 – Structure of the aza crown ligand L₁



Scheme 1 – synthesis of L₁ from 3,3-diamino-2,2'-bipyridine (1) and tetra-tosylate (6). Reagents and conditions; (i) acetic anhydride, RT, 12 hrs, (ii) Cu bronze, DMF, 80°C, 12 hrs, (iii) 1.0 M HCl, reflux, 2 hrs, (iv) TosCl, pyridine (solvent), 0°C → RT, (v) 2.2 equivs BuLi, THF, 80°C, (vi) Con^c H₂SO₄, 100°C 48 hrs.

Numerous techniques to react the 3,3'-diamino-2,2'-bipyridine with the tetratosylate chain (**6**) to create an aza-crown species were attempted. However, it was found that the most successful method was the simplest *i.e.* reaction of 3,3'-diamino-2,2'-bipyridine with BuLi to form the dianion and subsequent reaction with the tetra-tosylate. This gave the ditosylated bipyridine aza-crown species, although the yields were small (<10%). To remove the tosyl units, the tosylated species, **7**, was treated with concentrated H₂SO₄ at 100°C for 48 hrs, less forcing conditions (lower pH, temperature and reaction time) resulted in a mixture of the di- and monotosylated species. Regardless, yields for this step were tolerable (~ 50%).

2.1.2 Structural elucidation

Crystals of the ligand L₁ were formed from slow evaporation of toluene and analysis of the single crystal X-ray crystallographic data confirmed the formation of the bipyridine aza-crown ligand L₁.

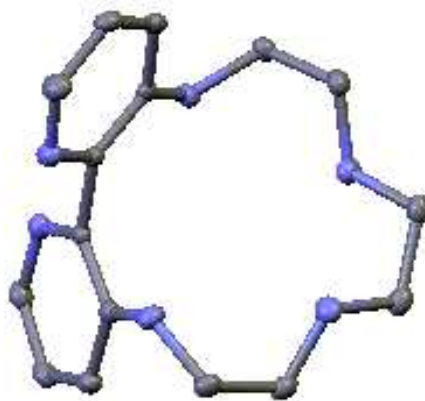


Figure 2.2 - Single crystal X-ray structure of L₁.

The crystal structure, apart from conformation of the gross molecular structure is unremarkable. However, it is noted that the two bipyridine rings are twisted, with a NCCN torsion angle of 110(1)°. Steric restraints within the aza-macrocyclic prevent the rings adopting a coplanar transoid geometry which is favoured by bipyridine systems with hydrogen bond donors in the 3,3'-position.

Bond distances (Å)

N1-C4	1.377(2)	C7-C8	1.519(3)
N1-C5	1.462(2)	C16-C15	1.381(2)
N4-C11	1.337(2)	C6-C5	1.523(2)
N4-C1	1.341(2)	C3-C4	1.403(2)
N6-C14	1.371(2)	C12-C13	1.525(2)
N6-C13	1.461(2)	C15-C14	1.408(2)
C9-C16	1.387(3)	C4-C11	1.421(2)
C2-C3	1.381(2)	C10-C14	1.422(2)
C2-C1	1.388(3)	C10-C11	1.500(2)

Bond angles (°)

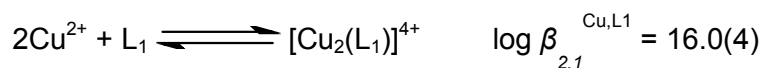
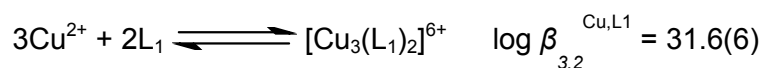
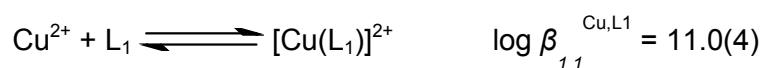
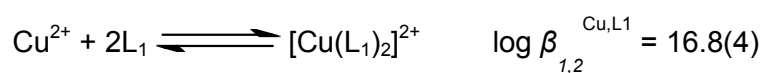
C10-N3-C9	118.7(2)	N5-C12-C13	109.3(1)
C6-N2-C7	115.7(1)	N6-C13-C12	112.8(1)
C12-N5-C8	114.1(1)	C16-C15-C14	120.0(2)
C4-N1-C5	121.3(1)	N1-C4-C3	122.2(2)
C11-N4-C1	118.5(1)	N1-C4-C11	121.3(2)
C14-N6-C13	122.4(1)	C3-C4-C11	116.5(2)
N3-C9-C16	122.3(1)	N3-C10-C14	123.3(2)
C3-C2-C1	119.2(2)	N3-C10-C11	114.2(1)
N2-C7-C8	108.5(1)	C14-C10-C11	122.5(1)
N5-C8-C7	108.6(1)	N4-C11-C4	123.3(2)
N4-C1-C2	122.5(2)	N4-C11-C10	116.2(1)
C15-C16-C9	119.4(2)	C4-C11-C10	120.4(2)
N2-C6-C5	110.2(1)	N6-C14-C15	122.4(2)
N1-C5-C6	113.5(1)	N6-C14-C10	121.4(2)
C2-C3-C4	119.9(2)	C15-C14-C10	116.2(2)

Figure 2.3 – Selected bond lengths for L₁ free ligand

2.2 Results and Discussion

2.2.1. Reactivity with Cu^{2+} ions

Upon reaction of Cu^{2+} ions with the ligand L_1 a number of different complexes are formed, depending on the ratio of Cu^{2+} ions to L_1 . Spectrophotometric titrations of $\text{CuCl}_2 \cdot 2\text{H}_2\text{O}$ in a solution of the ligand ($[\text{L}_1]_{\text{tot}} = 10^{-4}$ M, MeCN) caused complex variations in the UV-Vis spectra. The UV-Vis spectra were successfully modeled by six absorbing species; these were Cu^{2+} , L_1 , and four complexes in equilibria. UV-Vis titrations have revealed four species can be formed upon introduction of Cu^{2+} ions to L_1 , these are; $[\text{Cu}(\text{L}_1)_2]^{2+}$, $[\text{Cu}(\text{L}_1)]^{2+}$, $[\text{Cu}_2(\text{L}_1)]^{4+}$ and $[\text{Cu}_3(\text{L}_1)_2]^{6+}$.



Chloride adducts for all the species were observed in the gas phase during analogous ESI-MS titrations. The observation of the four different complexes was at first surprising; however, in hindsight it is not unexpected given the diverse co-ordination modes the ligand L_1 is capable of, and the co-ordinating ability of the MeCN solvent and Cl^- counter ion.

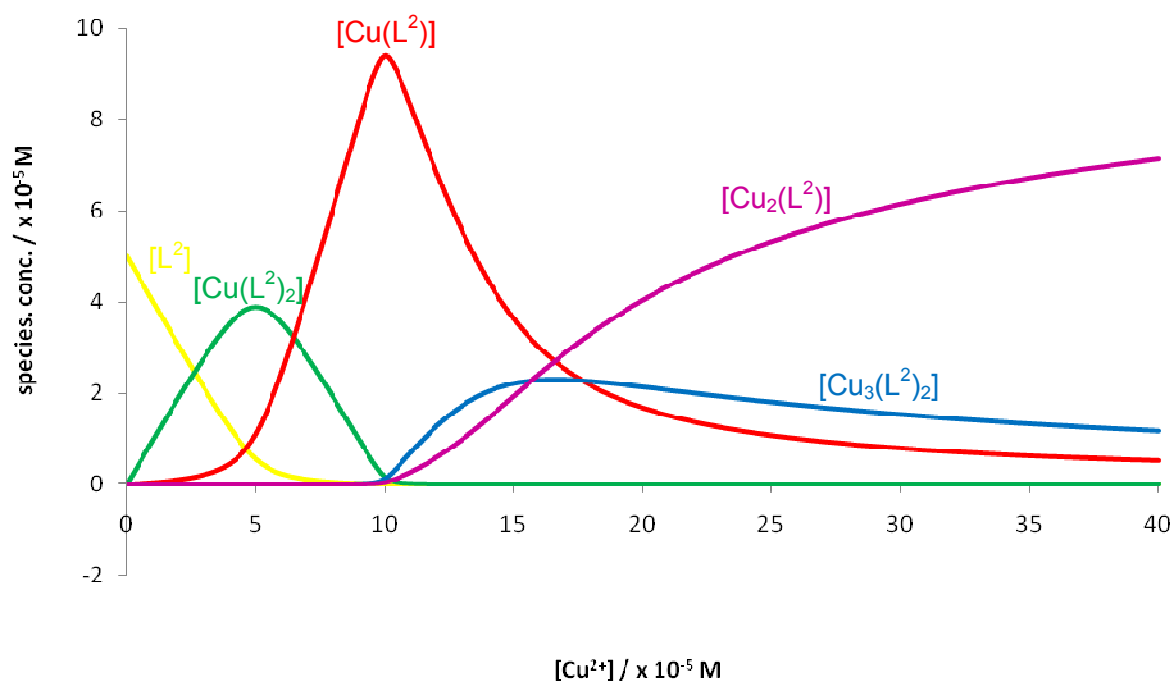


Figure 2.4 – Calculated speciation diagram for complexes of L_1 with Cu^{2+} ($[L_1]_{tot} = 10^{-4}$ M).

2.2.1.1 Reaction of $CuCl_2 \cdot 2H_2O$ with two equivalents of L_1

The complexes formed between $CuCl_2 \cdot 2H_2O$ and the ligand L_1 vary considerably depending upon the metal:ligand stoichiometry. At ratio of 2:1 (metal to ligand) the complex $[Cu(L_1)_2]^{2+}$ is the most predominant species. The proposed structure of this complex is a Cu^{2+} ion coordinated by two ligands via the bidentate imine unit (the bipyridine can act as a bidentate unit, described later). The formation of this species is supported by ESI-MS as a sample obtained at the ratio 1:2 metal to ligand shows an ion at m/z 694 corresponding to $\{[CuCl(L_1)_2]^+\}$.

2.2.1.2 Reaction of $CuCl_2 \cdot 2H_2O$ with one equivalent of L_1

When the ratio of metal to ligand is 1:1, the spectrometric titration suggest that the main species is $[CuL]^{2+}$, and it is reasonable to assume that the Cu^{2+} ions are co-ordinated by the aza crown domain. The formation of $[CuL_1Cl]Cl$ is also observed in solution as ESI-MS shows an ion at m/z 396 corresponding to $\{[CuL_1Cl]^+\}$. Crystals of this 1:1 species were grown from slow diffusion of diethyl ether into a solution of MeOH containing one equivalent of $CuCl_2 \cdot 2H_2O$ and L_1 and single crystal X-ray analysis confirmed the formation of a 1:1 species (figure 2.5). In the crystal the Cu^{2+} is co-ordinated by the four nitrogen groups of the aza crown macrocycle, forming a tetra-dentate domain. An axial chloride is available to

complete the co-ordination sphere of the Cu^{2+} bound within the aza-crown giving the ion a five-co-ordinate distorted square pyramidal geometry. The Cu-N_{aza} bond lengths range from 2.008(2)-2.083(2) Å and the Cu-Cl_{ax} distance is 2.4026(6) Å. Interestingly, the bipyridine NCCN torsion angle decreases from $110(1)^\circ$ in the free ligand to $62(1)^\circ$ upon co-ordination of the aza-crown domain. The reduction occurs in order to align the amine substituents on the 3,3'-positions for optimal binding of the complexed metal ion.

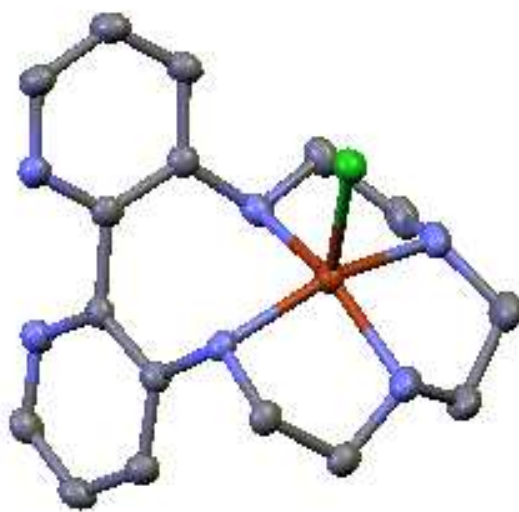


Figure 2.5 - Solid state structure of $[\text{CuL}_1\text{Cl}]^+$

Bond distances (Å)			
Cu1-N2	2.009(2)	Cu1-N1	2.083(2)
Cu1-N3	2.009(2)	Cu1-Cl3	2.4026(6)
Cu1-N4	2.049(2)		

Bond angles (°)			
N2-Cu1-N3	84.9(9)	C10-N3-Cu1	107.9(2)
N2-Cu1-N4	149.9(9)	C16-N3-Cu1	110.1(2)
N3-Cu1-N4	85.2(8)	N2-Cu1-Cl3	104.9(7)
N2-Cu1-N1	87.6(8)	N3-Cu1-Cl3	97.0(6)
N3-Cu1-N1	164.2(8)	N4-Cu1-Cl3	104.5(6)
N4-Cu1-N1	94.7(7)	N1-Cu1-Cl3	97.9(6)
C1-N1-Cu1	116.2(2)	C11-N4-Cu1	112.2(1)
C15-N1-Cu1	102.2(1)	C4-N4-Cu1	106.1(2)
C6-N2-Cu1	104.9(2)	C3-N2-Cu1	106.8(2)

Figure 2.6 – Selected bond lengths for $[\text{CuL}_1\text{Cl}]^+$ ligand.

2.2.1.3 Reaction of two equivalents of $\text{CuCl}_2 \cdot 2\text{H}_2\text{O}$ with L_1

Reaction of the $[\text{CuL}_1\text{Cl}]\text{Cl}$ complex with a further equivalent of $\text{CuCl}_2 \cdot 2\text{H}_2\text{O}$ in MeOH resulted in, upon slow evaporation, a green crystalline solid. ESI-MS studies show an ion at m/z 531 corresponding to the formation of the dicopper species $\{[\text{Cu}_2\text{Cl}_3(\text{L}_1)]^+\}$. Analysis of these crystals by single crystal X-ray diffraction revealed the dicopper complex of $[\text{Cu}_2\text{L}_1\text{Cl}_4]_2$ (figure 2.7). In the solid state one Cu^{2+} ion is co-ordinated within the aza-crown domain, and a second Cu^{2+} ion is co-ordinated by the two imine nitrogens of the bipyridine unit. The remaining co-ordination sites on the Cu^{2+} ion are occupied by chloride ions, one of which is a bridging chloride to another $[\text{Cu}_2\text{L}_1\text{Cl}_4]$ molecule, giving rise to a chloro-bridged dimer in the solid state. This structure also supports the proposed structure of $[\text{Cu}(\text{L}_1)_2]^{2+}$, where instead of having a $[\text{Cu}_2\text{Cl}_4]$ unit co-ordinating the two bipyridine ligands a single Cu^{2+} would be co-ordinated by these ligand units.

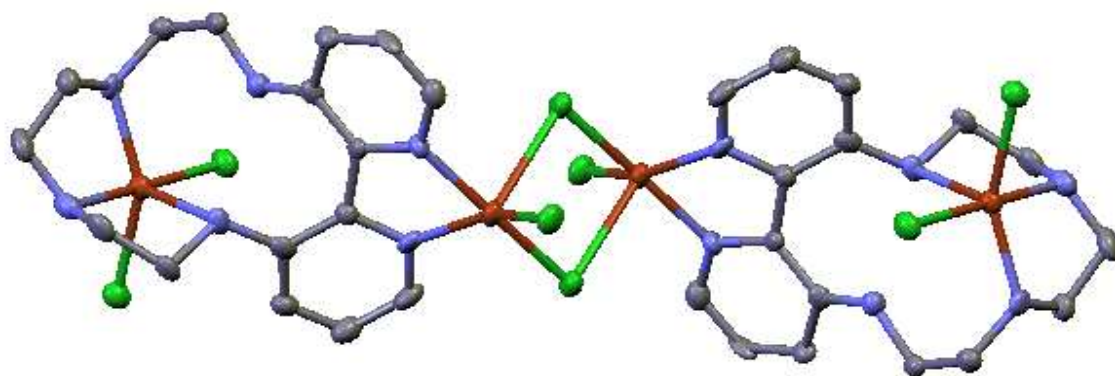


Figure 2.7 - Single crystal X ray structure of $[\text{Cu}_2\text{L}_1\text{Cl}_4]_2$

Bond distances (Å)

Cu1-N2	2.050(9)	Cu2-N5	2.093(9)
Cu1-N1	2.059(9)	Cu2-Cl4	2.286(3)
Cu1-Cl1	2.299(3)	Cu2-Cl3	2.357(3)
Cu1-Cl2	2.312(3)	Cu2-N3	2.477(8)
Cu1-Cl2	2.747(3)	Cu2-N4	2.036(9)

Bond angles (°)

N2-Cu1-N1	81.0(3)	N5-Cu2-Cl3	150.2(2)
N2-Cu1-Cl1	94.1(3)	Cl4-Cu2-Cl3	94.5(1)
N1-Cu1-Cl1	149.9(3)	N4-Cu2-N3	80.7(3)
N2-Cu1-Cl2	173.0(3)	N5-Cu2-N3	108.4(3)
N1-Cu1-Cl2	94.9(3)	Cl4-Cu2-N3	97.2(2)
Cl1-Cu1-Cl2	92.3(1)	Cl3-Cu2-N3	98.6(2)
N2-Cu1-Cl2	87.8(2)	Cu1-Cl2-Cu1	91.6(1)
N1-Cu1-Cl2	110.6(3)	C10-N2-Cu1	124.2(7)
Cl1-Cu1-Cl2	98.8(1)	C6-N2-Cu1	113.4(6)
Cl2-Cu1-Cl2	88.4(1)	C4-N3-Cu2	112.0(6)
C1-N1-Cu1	124.8(7)	C11-N3-Cu2	94.3(6)
C5-N1-Cu1	113.4(7)	C13-N4-Cu2	106.7(7)
N4-Cu2-N5	84.6(4)	C12-N4-Cu2	112.2(7)
N4-Cu2-Cl4	177.3(3)	C14-N5-Cu2	108.1(7)
N5-Cu2-Cl4	94.4(3)	C15-N5-Cu2	123.0(7)
N4-Cu2-Cl3	87.6(3)		

Figure 2.8 – Selected bond lengths for $[\text{Cu}_2\text{L}_1\text{Cl}_4]_2$ ligand.

The structure of $[\text{Cu}_2\text{L}_1\text{Cl}_5]^-$ with the second molecule removed is shown in figure 2.9, enabling us to see clearly the allosteric effect demonstrated by the ligand L_1 .

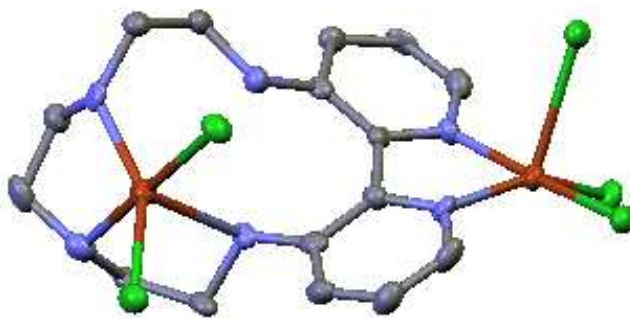


Figure 2.9 - Solid state structure of $[\text{Cu}_2\text{L}_1\text{Cl}_5]^+$

2.2.1.4 Higher ratios of Cu^{2+}

From the spectrophotometric titrations at higher ratios of Cu^{2+} another species is present and this was successfully modeled as $[\text{Cu}_3(\text{L}_1)_3]^{6+}$. It is suspected that the complex is structurally related to the $[\text{Cu}_2\text{L}_1\text{Cl}_5]^+$ complex, with two $[\text{CuL}_1\text{Cl}]^+$ complexes held together with a bridging Cu^{2+} ion. It is presumed the copper ion is bonded to the aza-crown via three nitrogen atoms (as the bipyridine unit is also bound). The remaining copper ion is co-ordinated by the bipyridine unit from *two* ligands giving the complex $\{\text{Cu}(\text{L}_1)\text{Cu}(\text{L}_1)\text{Cu}\}$ and is four-co-ordinate (perhaps five co-ordinate as a chloride ligand interacts with the central copper ion). The formation of this trimetallic species is further supported by ESI-MS with a peak at m/z 964 is observed corresponding to $[\text{Cu}_3(\text{L}_1)_2\text{Cl}_5]^+$.

2.3 Allosteric effects

In the solid state the aza-crown no longer co-ordinates via all four nitrogen atoms but only three, when the bipyridine unit is also co-ordinated. The two aza nitrogen atoms furthest from the bipyridine unit and two chloride ions lie roughly within the equatorial plane ($\text{Cu}-\text{N}_{\text{aza}}$: 2.021(3) and 2.88(3) Å; $\text{Cu}-\text{Cl}_{\text{eq}}$: 2.281(1) and 2.359(1) Å). One of the “inner” aza nitrogen atoms lies in the elongated axial position ($\text{Cu}-\text{N}_{\text{aza}}$: 2.464(3) Å), whilst, at 3.355(3) Å, the remaining inner nitrogen is too distant to bond to the Cu^{2+} centre. The bipyridine torsion angle is also greatly reduced from that observed in both the free ligand and the mononuclear species $[\text{Cu}(\text{L}_1)\text{Cl}]^+$, and is now just 31(1)°. The reduction in the torsion angle is a direct result of the co-planarity required for the bipyridine unit to complex the Cu^{2+} ion within the bipyridine unit. This reduction in torsion angle results in a change in the co-ordination ability of the two amine units directly bonded to the bipyridine unit. At least one of the inner nitrogen groups is forced into a position where the hydrogen group is pointing towards the

metal ion, preventing any interaction between the nitrogen group and the copper ion. As a result co-ordination of the bipyridine unit changes, by an allosteric interaction, the denticity of the aza-crown from a tetradentate donor (when the bipyridine unit is unco-ordinated) to a tridentate donor when the bipyridine unit is bound to a metal ion.

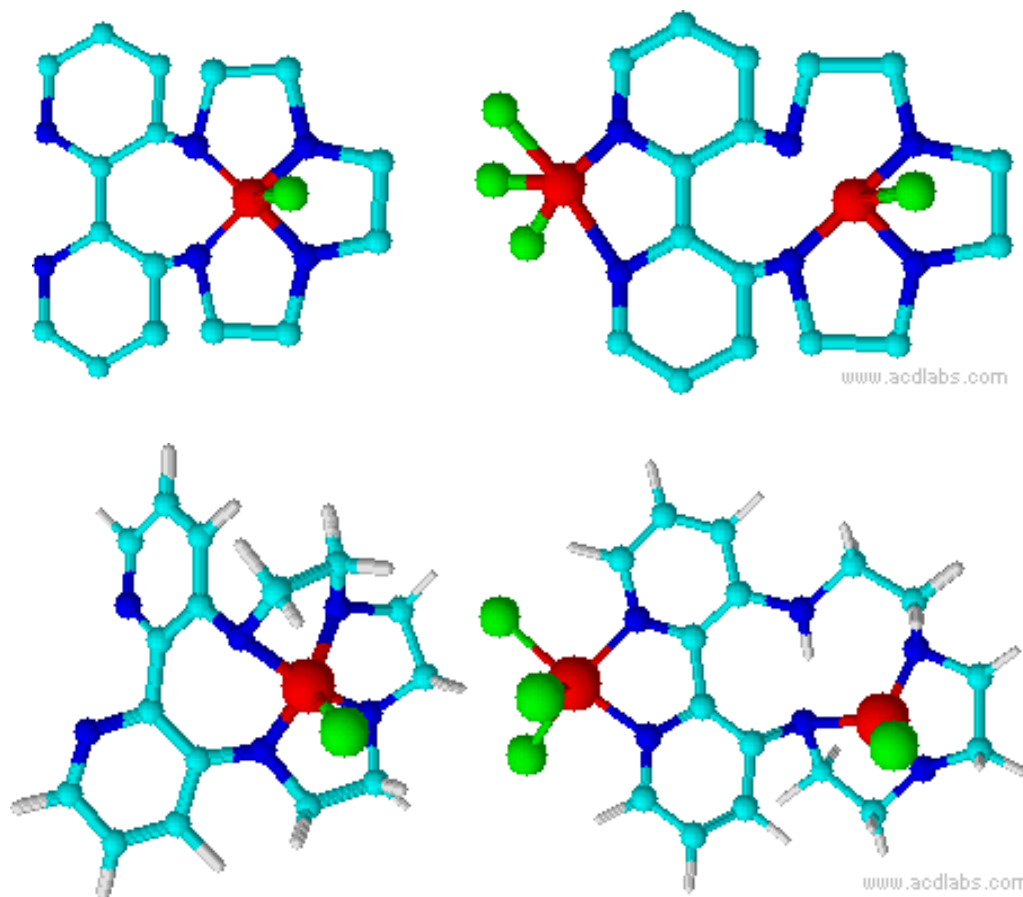


Figure 2.10 – Schematic diagram showing the ligand L_1 , with the aza crown domain behaving as a tetradentate donor (left) and as a tridentate donor when the bipyridine unit is also co-ordinated (right). In the upper structure the hydrogen atoms have been omitted for clarity, and the structure is 2-dimensional, the lower structures include the hydrogen atoms and are 3-dimensional in order to demonstrate the change in torsional angle of the bipyridine unit.

This can be described as a negative allosteric system as the co-ordination behaviour of the aza crown changes from a tetradentate donor to a tridentate donor upon co-ordination of the bipyridine unit. Ideally to fully ascertain the allosteric behavior, binding constants of the aza-crown in the ligand L_1 and the complex of L_1 bound to a metal ion via the bipyridine unit would be obtained and compared. However, formation of a complex where only the

bipyridine unit was co-ordinated proved fruitless, as reaction with metal ions such as $\text{ReCl}(\text{CO})_5$ and $(\text{MeCN})_2\text{PdCl}_2$ gave rise to a number of species which could not be isolated. It is thought that reaction of these metal ions with L_1 results in co-ordination of either the bipyridine and/or two nitrogen atoms from the aza-crown domain.

3: Diamino-functionalised Cryptate Species

Described in this chapter is the synthesis and characterization of a diamino-functionalised cryptate L_2 , (figure 3.1). The ligand contains a bipyridine unit functionalized by two amino groups and a cryptate binding domain with multiple co-ordination sites capable of co-ordinating a metal ion. Due to the number of donor atoms within the cryptate unit, and due to the 3-dimensional shape, cryptates bind metal ions very strongly. This allows co-ordination in competitive media such as water, the ability of cryptates to co-ordinate ions within aqueous media has enabled them to be extremely useful as a component of biological sensors. The luminescent properties displayed when the ligand is reacted with an aldehyde in the presence of an excess of a variety of metal ions is reported.

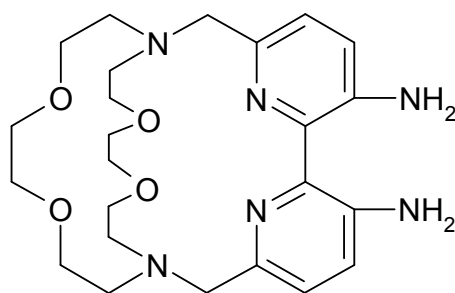


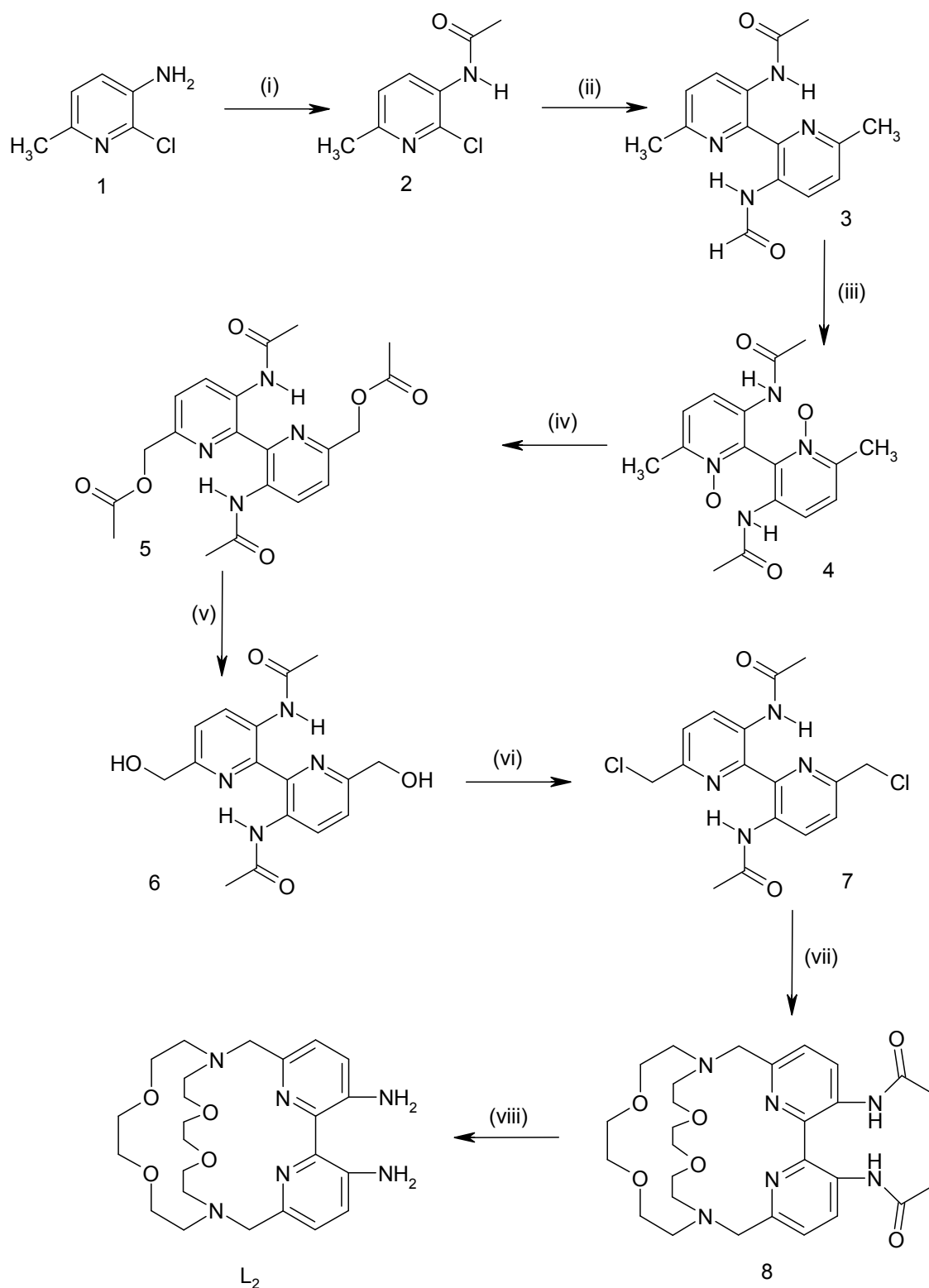
Figure 3.1 – Structure of L_2

3.1 Ligand Synthesis

3.1.1. Synthesis of L_2

The aim of the synthesis was to produce a ligand which possessed amine groups and a cryptate domain. The cryptate domain is capable of co-ordinating a metal ion within, and the amine groups are available to react with an aldehyde. It is envisaged that co-ordination of both domain will elicit a modulation in luminescent response.

The ligand L_2 was synthesised using a non-trivial eight step linear process. Structural elucidation was performed at each step of the synthesis using ^1H NMR and mass spectrometry. The linear nature of the process caused initial difficulty in obtaining high yields of the target ligand, however modification of several key steps allowed a workable amount to be achieved.



Scheme 1. Synthesis of L₂ from 5-amino-6-chloro-2-picoline (**1**). Reagents and conditions: (i) acetic anhydride, RT (ii) Et₄Nl, zinc dust, and [NiCl₂(PPh₃)₂], anhydrous DMF, N₂, 80°C, (iii) *m*CPBA, DCM, RT, (iv) acetic anhydride, 120°C, (v) Na₂CO₃, MeOH, RT, (vi) Na₂CO₃, SOCl₂, DCM, reflux, (vii) diaza-18-crown-6, NaI, Na₂HCO₃, (at reflux in MeCN), (viii) 3M HCl, RT.

The starting precursor for this synthesis is 5-amino-6-chloro-2-picoline which is acetylated in order to protect the amine groups, this was achieved by reaction with acetic anhydride at room temperature; the excess solvent was removed leaving a pale brown crystalline solid **(2)**.

The acetylated amine was then coupled using tetraethyl ammonium iodide, $[\text{NiCl}_2(\text{PPh}_3)_2]$ and zinc dust in absolute DMF at 80°C , the solution was evaporated and the product extracted into DCM. The highly luminescent crystalline solid **(3)** was recrystallised in toluene from the dried residues. The ^1H NMR spectrum is shown in figure 3.3, the structure of the ligand is symmetrical; therefore there are only 5 different hydrogen environments. The spectrum reveals two doublet aromatic signals at δ 9.0 and 7.2 respectively, these peaks represent the single hydrogens in position 4,4' and 5,5' on the bipyridine ring, as shown in figure 3.2.

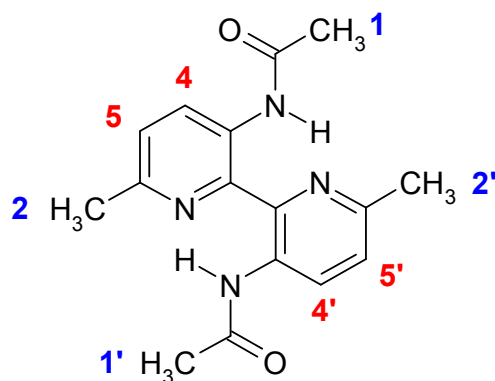


Figure 3.2 - Expected structure of product 3 showing hydrogen positioning.

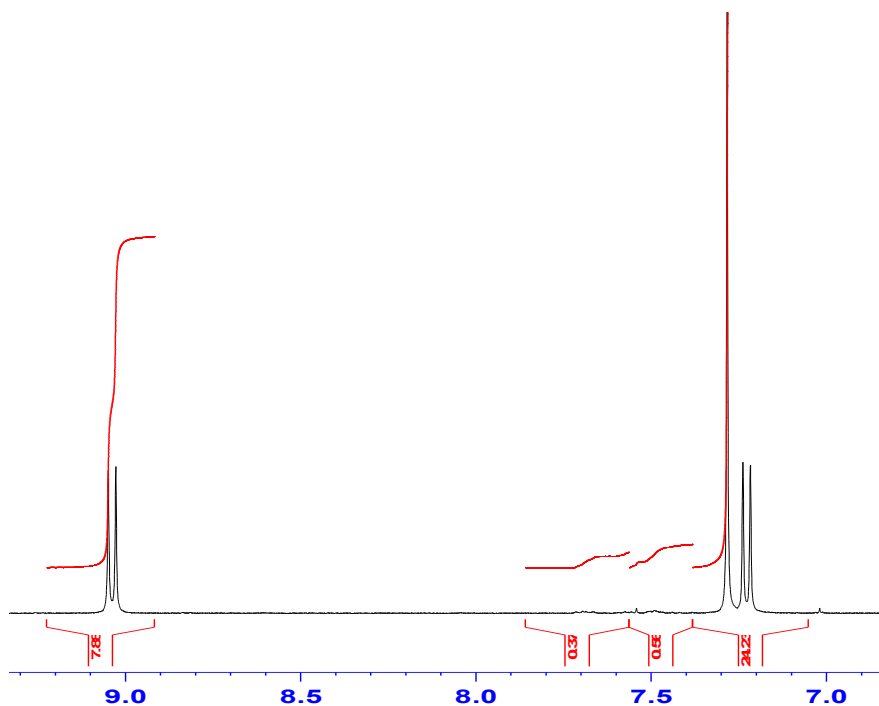


Figure 3.3 – Aromatic region of the ^1H NMR (CDCl_3) spectra of 3.

In the ^1H NMR spectrum a peak is present at $>12\text{ppm}$ and this is attributed to the amide hydrogen. This downfield shift is in part due to the hydrogen bond formed between the $-\text{NH}$ and the pyridyl hydrogen as shown in figure 3.4.

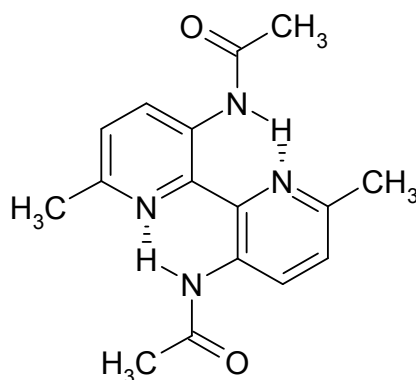


Figure 3.4 – Structure of 2,2'-Bipy-3,3'-diol showing hydrogen bonding.

This is typical of a 2,2'-bipyridine bearing acidic protons in the 3,3' position and gives rise to the highly luminescent behavior. A typical example of this is 2,2'-bipyridine-3,3'-diol which bears $-\text{OH}$ groups in the 3,3'- position and is a highly luminescent compound.

The coupled acetylated diamine was then allowed to stand in DCM with an excess of *m*CPBA for several days to allow N-oxidation of the bipyridine rings. Once bis-N-oxidation had occurred the product was purified by column chromatography to give a fine white powder (**4**).

Structural elucidation was performed using ^1H NMR and the spectrum in figure 3.5 shows two aromatic doublets with coupling constants consistent with adjacent aromatic hydrogen atoms, these have shifted considerably due to the presence of the N-oxidised nitrogen and can now be seen at δ 7.9 and 7.4, in contrast to the previous product at δ 9.0 and 7.2 (figure 3.3). The spectrum also display two singlet peaks in the aliphatic region corresponding to the two methyl groups present in the product.

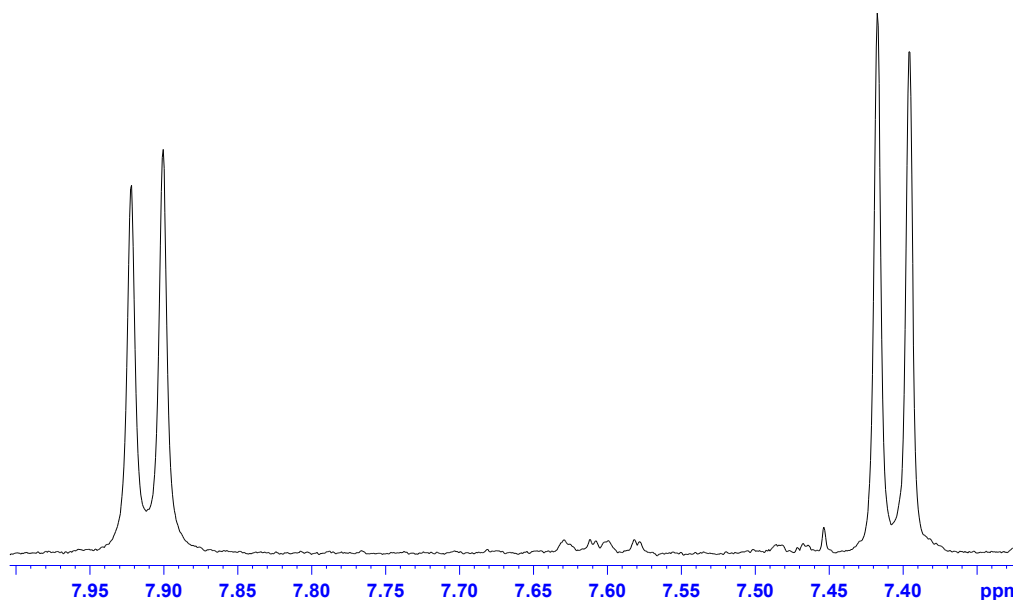


Figure 3.5 – Aromatic region of the ^1H NMR (CDCl_3) spectrum of **4.**

The bis-N,N'-oxide was then acetylated by heating in acetic anhydride at 120°C , the reaction was monitored by TLC and purified by column chromatography, once the solvent had been removed, to afford a moderate yield of (**5**). The reaction allowed the acetylation of the methyl groups situated in positions 6,6' of the bipyridine ring forming Py- CH_2OCOMe .

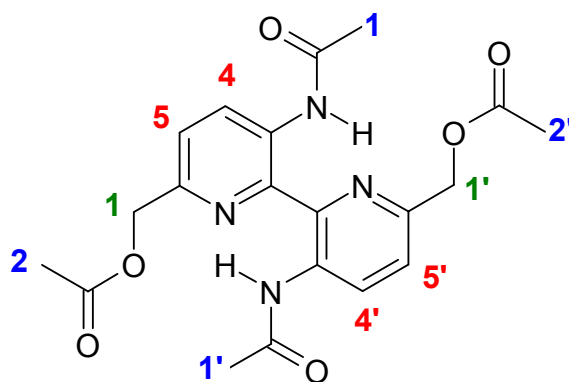


Figure 3.6 - Expected structure of product 5 showing hydrogen positioning.

^1H NMR showed 5 peaks due to the symmetry of the ligand, with two doublets present in the aromatic region. The spectrum is shown below in figure 3.7.

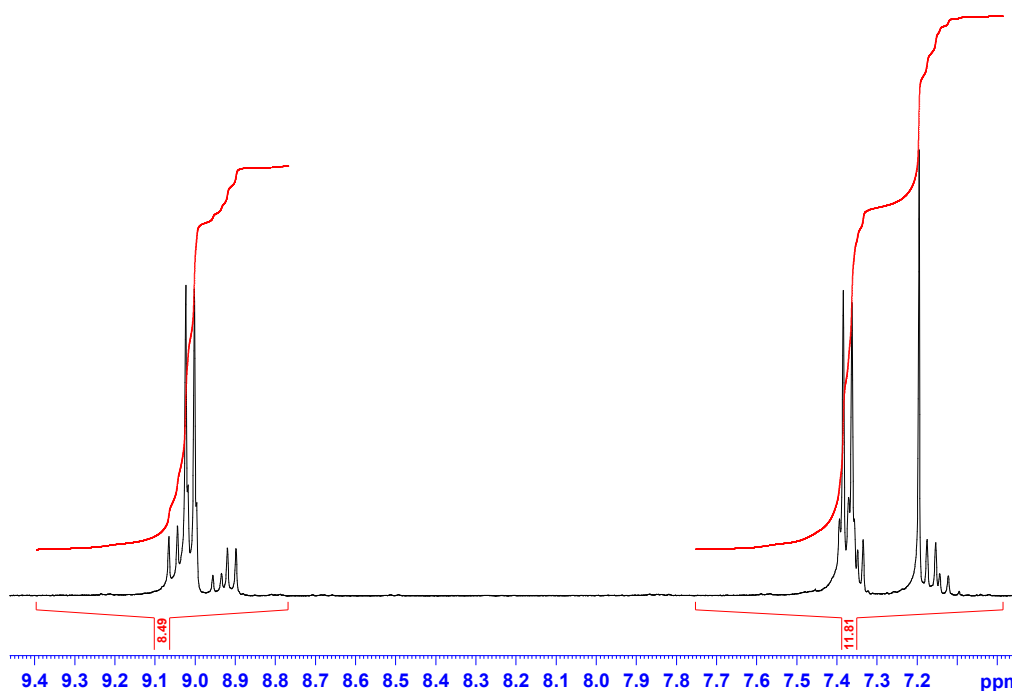


Figure 3.7 – Aromatic region of the ^1H NMR (CDCl_3) spectra of 5.

The peaks in the aromatic regions are attributed to the aromatic hydrogen atoms in positions 4,4' and 5,5' of the bipyridine ring. These signals have again shifted downfield due to the presence of the acetylated methyl group. The spectrum obtained for this product contains some impurities; this is due to hydrolysis which occurs readily within this particular product, making purification difficult. A peak at δ 5.3 is present and this corresponds to the methylene group labeled 1 in the figure 3.6 and signifies that the expected structure has

been obtained. This is further supported by the integration which shows this signal corresponds to 4 hydrogens. There are two signals in the aliphatic region, these represent the two methyl groups labeled 1 and 2 in figure 3.6, one signal represents the amide and the other the ester, the amide peak has shifted in comparison to the previous product.

The acetylated methyl group was hydrolysed using Na_2CO_3 at room temperature in MeOH, the product formed a creamy white precipitate which was filtered off at the pump to give **(6)**.

The ^1H NMR spectra shows only four signals as one of the methyl groups has been removed. The two signals in the aromatic region again correspond to the two aromatic hydrogens and a small shift has occurred in comparison with the previous spectra. A peak is visible at δ 5.7, this triplet represents the OH group now present adjacent to the methylene group. The methylene group attached to the alcohol has formed a doublet which is visible at δ 4.7, this has shifted up field due to the change in the environment which it is situated in. The most conclusive structural information to confirm the reaction has proceeded as expected is the absence of the methyl group at δ 2.3, this has now been hydrolysed to an alcohol. The remaining methyl signal represents the acetylated amine functional group.

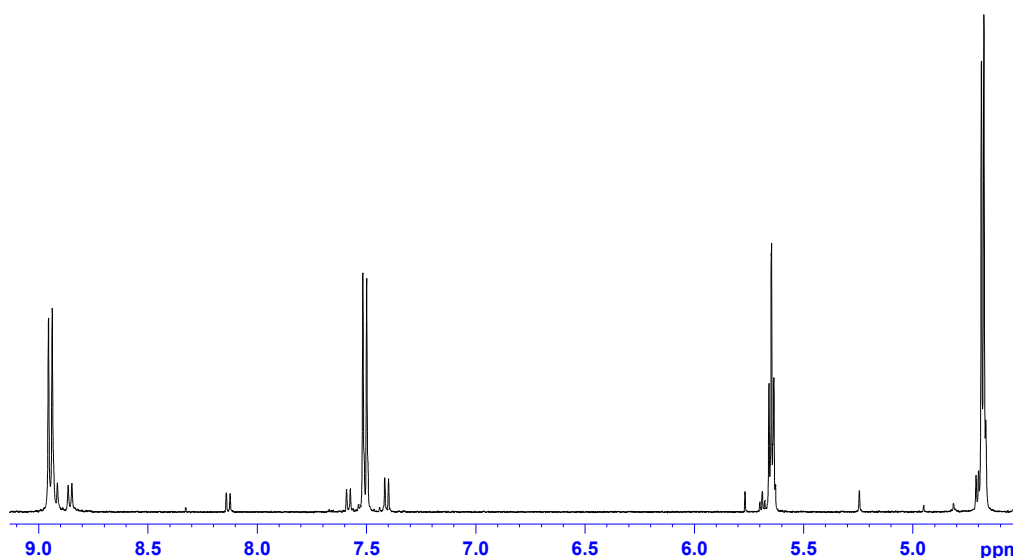


Figure 3.8 – Aromatic region of the ^1H NMR (DMSO) spectra of 6.

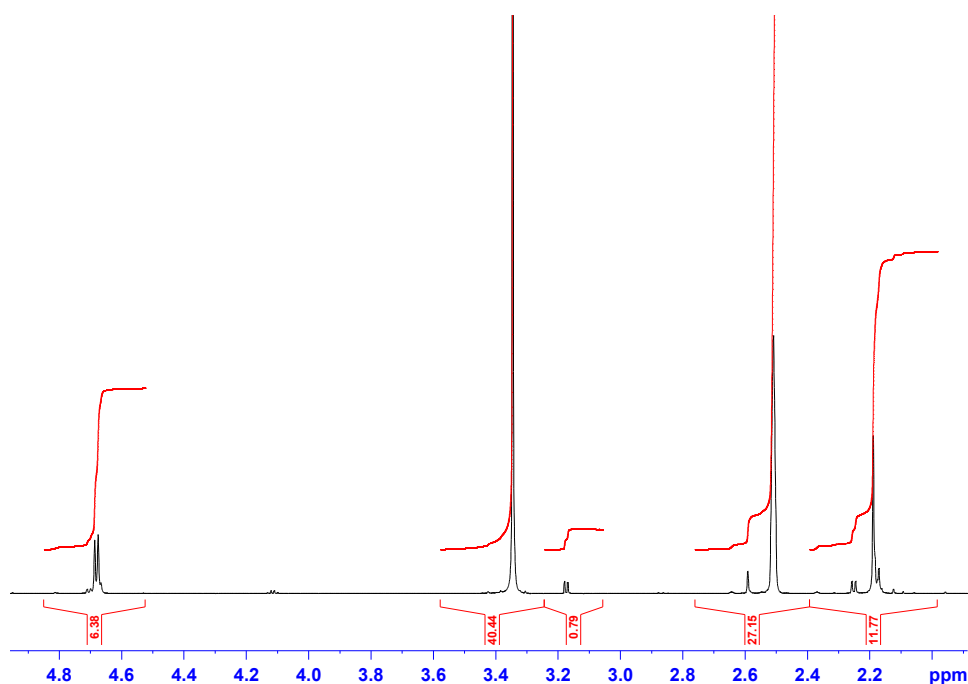


Figure 3.9 – Aliphatic region of the ^1H NMR (DMSO) spectra of 6.

Chlorination of the alcohol groups gave (**7**), and was achieved using thionyl chloride in DCM. Initially the dimethanol derivative was chlorinated by reaction with thionyl chloride in refluxing DCM. However, despite the TLC indicating that all the starting material had been consumed, very little product was isolated. It is possible that as the reaction produces HCl the amide functional groups are hydrolysed and the resulting amines react with thionyl chloride. Addition of NaHCO_3 to the chlorination reaction improves matters and as a result the chlorinated product could be isolated in fairly reasonable yield. The product was extracted into DCM with aqueous sodium hydrogen carbonate and the solvent removed.

The ^1H NMR shows little change compared with the spectrum of product 6, this is mainly because the chlorination of the alcohol group has produced little change within the environments of the hydrogen signals observed. There is a slight shift of both the methyl and ethyl group, but otherwise the spectrum (shown in figures 3.10 and 3.11) are very similar, however, this is expected as little change has occurred within the structure.

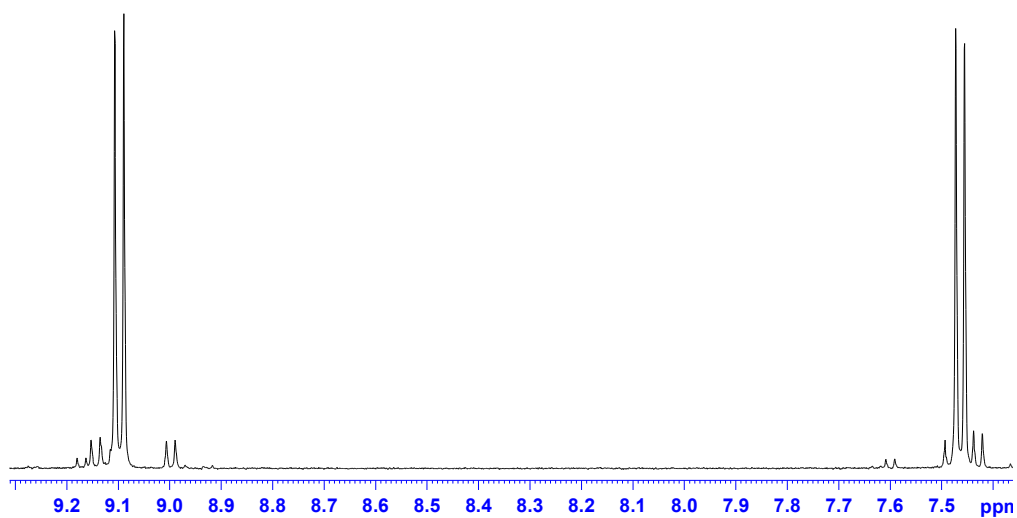


Figure 3.10 – Aromatic region of the ^1H NMR (CDCl_3) spectra of 7.

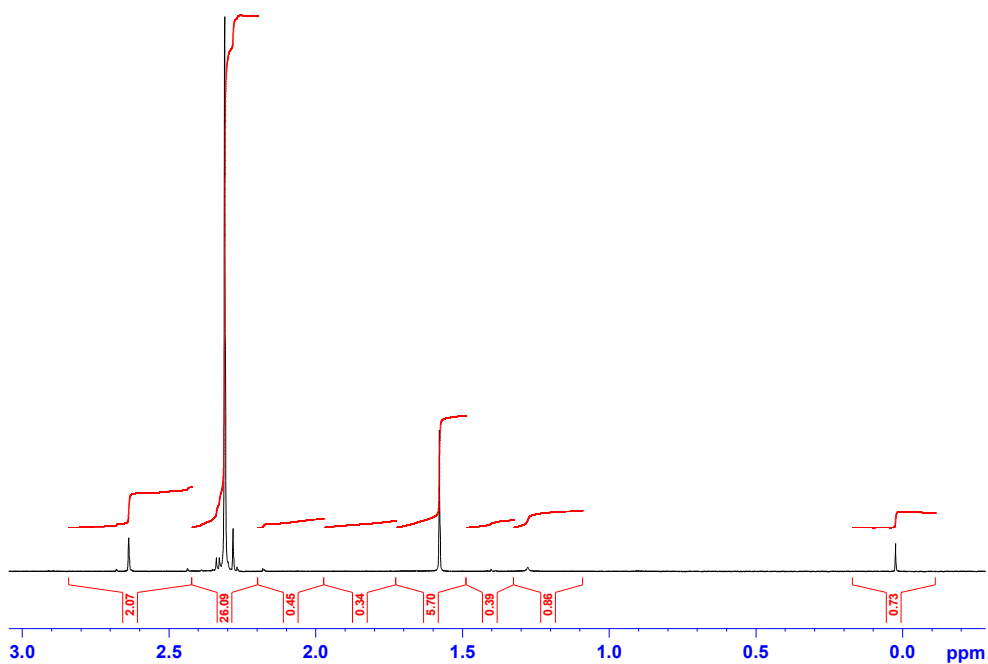


Figure 3.11 – Aliphatic region of the ^1H NMR (CDCl_3) spectra of 7.

Formation of the cryptate was achieved by reaction of the dichloro derivative (**7**) with diaza-18-crown-6 in refluxing MeCN with NaHCO_3 and NaI. The sodium ion is required to

template the addition reaction as is common in cryptate synthesis. Furthermore, iodide is also required as without the addition of this anion no reaction is observed. This is due to the relatively unreactive nature of the $-\text{CH}_2\text{Cl}$ units which will not be displaced by the R_2NH of the aza-crown. However, the nucleophilic iodide reacts with the chloromethane unit giving $-\text{CH}_2\text{I}$ which is much more reactive than the chloro derivative and reacts cleanly with the aza-crown.

The ^1H NMR spectrum shown in figure 3.12 shows a large shift in the aromatic hydrogen signals. A number of highly coupled signals are present from δ 4.0 to 2.1 which represent the 24 aliphatic hydrogens within the cryptate, interpretation and assignment of the individual peaks is impossible due to overlap of signals, but this type of multiplet is characteristic of a cryptate domain and would be expected.

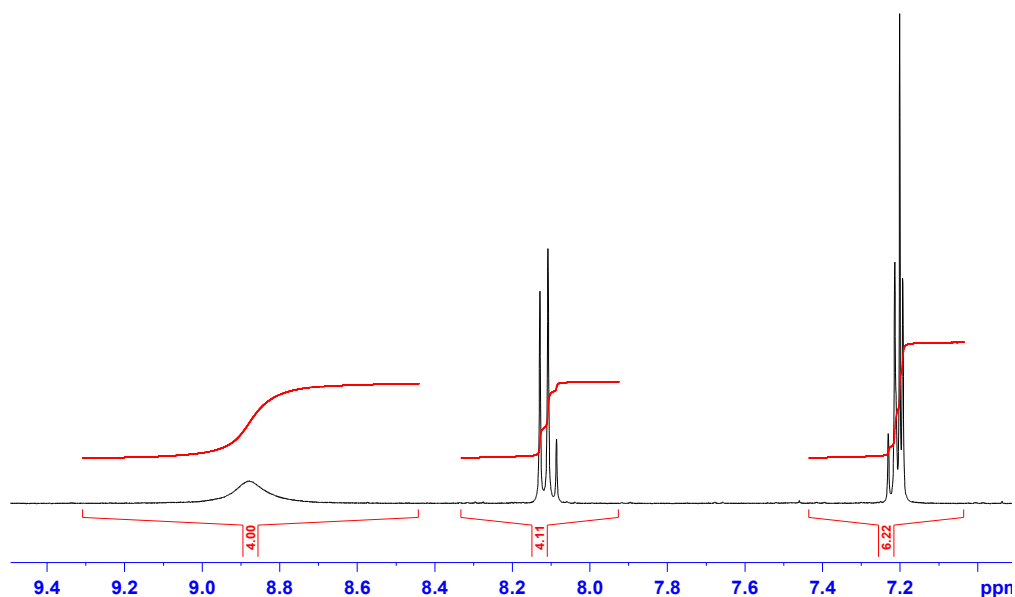


Figure 3.12 – Aromatic region of the ^1H NMR (CD_3CN) spectrum of **8**.

The protecting acetylate groups were removed from (**8**) to give the final ligand L_2 using 3M HCl solution. The acid hydrolysis occurred at room temperature over several days, upon completion the solution was neutralized with concentrated ammonia solution and immediately extracted into DCM. An analytically pure solid of L_2 was recrystallised from chloroform.

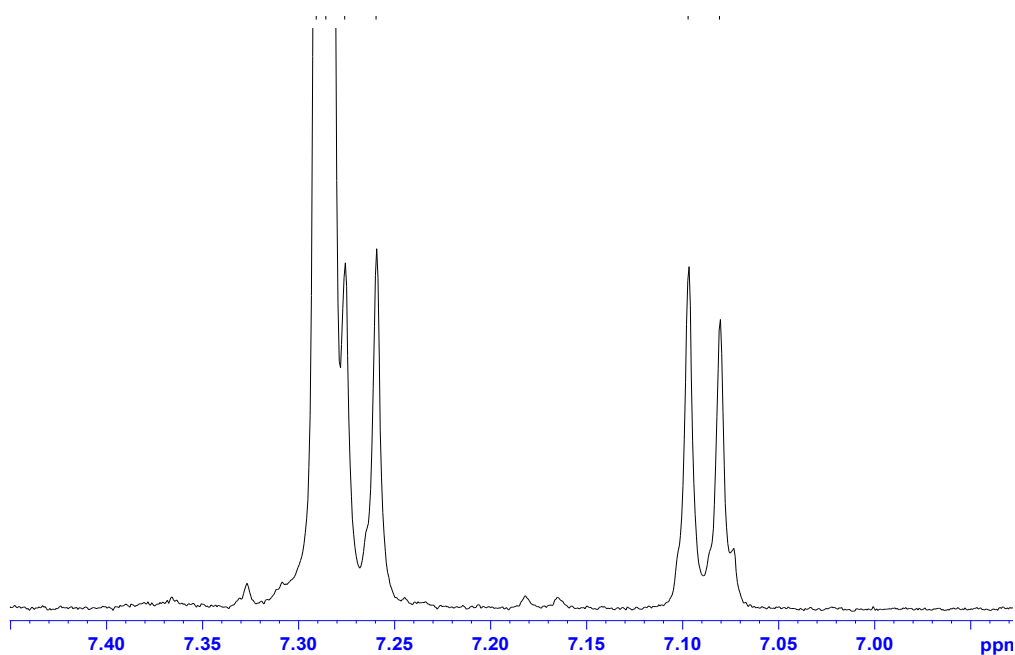


Figure 3.13 – Aromatic region of the ¹H NMR (CDCl₃) spectrum of L₂.

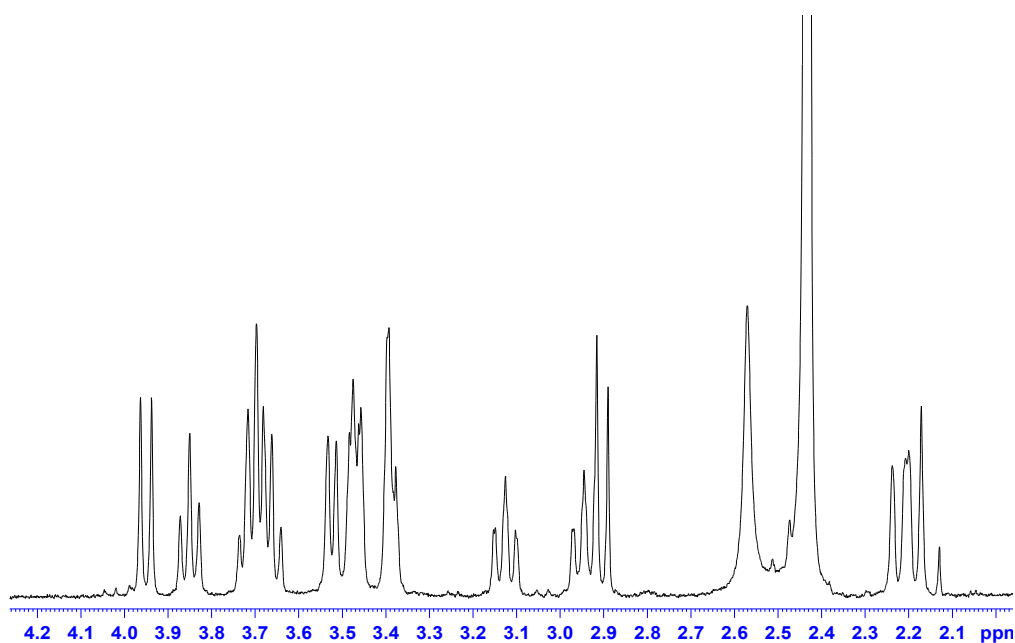


Figure 3.14 – Aliphatic region of the ¹H NMR (CDCl₃) spectrum of L₂.

The ¹H NMR spectra shown in figures 3.13 and 3.14 shows little difference from that of the previous product, however this is expected due to the relatively small change in the environments of the hydrogen atoms within the ligand. Within the large multiplet present at δ 4.0 to 2.1 we can see two doublets, one at 3.95, and one at 3.55, these represent the diastereotopic methylene groups bonded directly to the bipyridine unit.

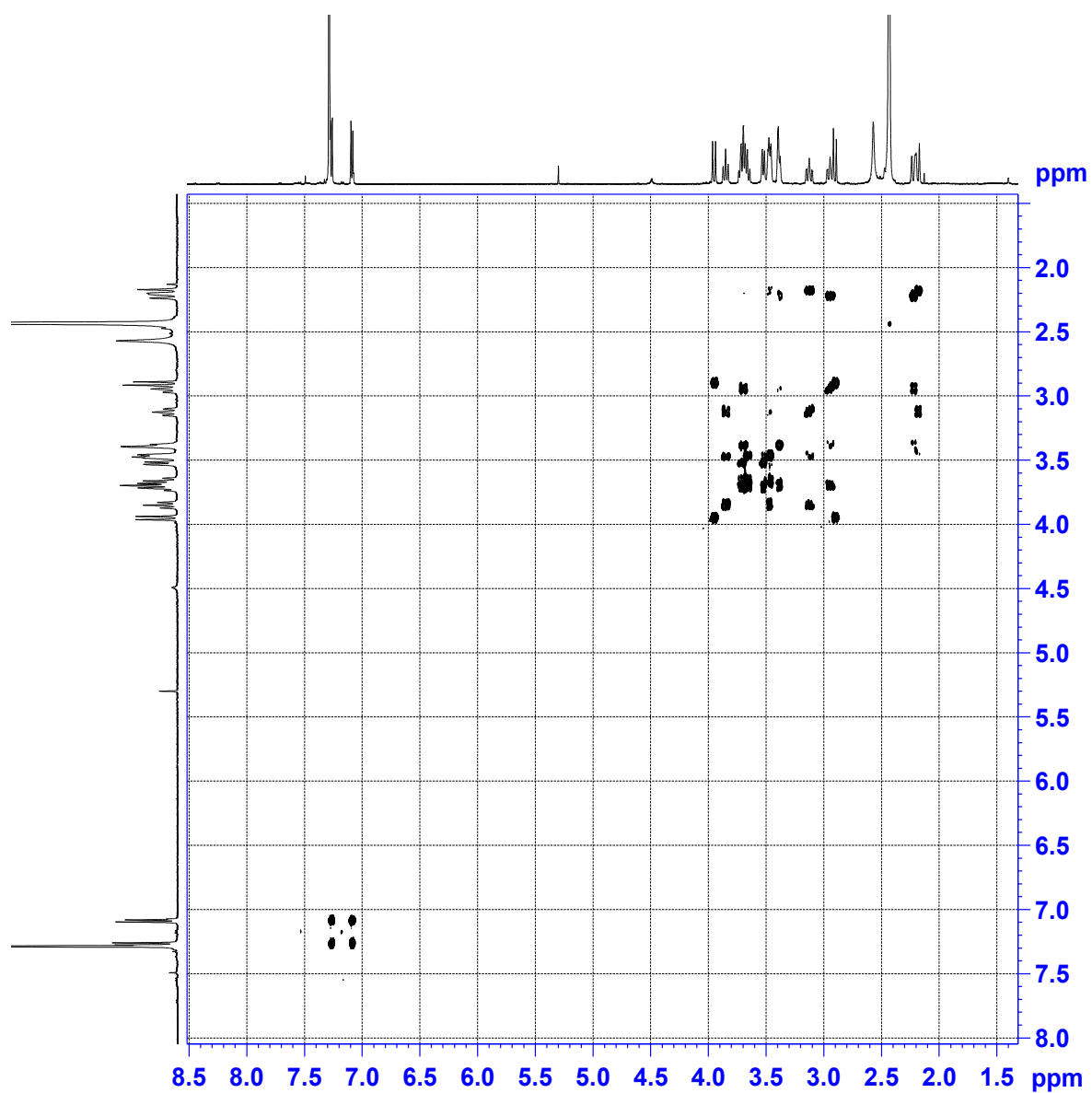


Figure 3.15 – ¹H COSY NMR (CDCl₃) spectra of L₂

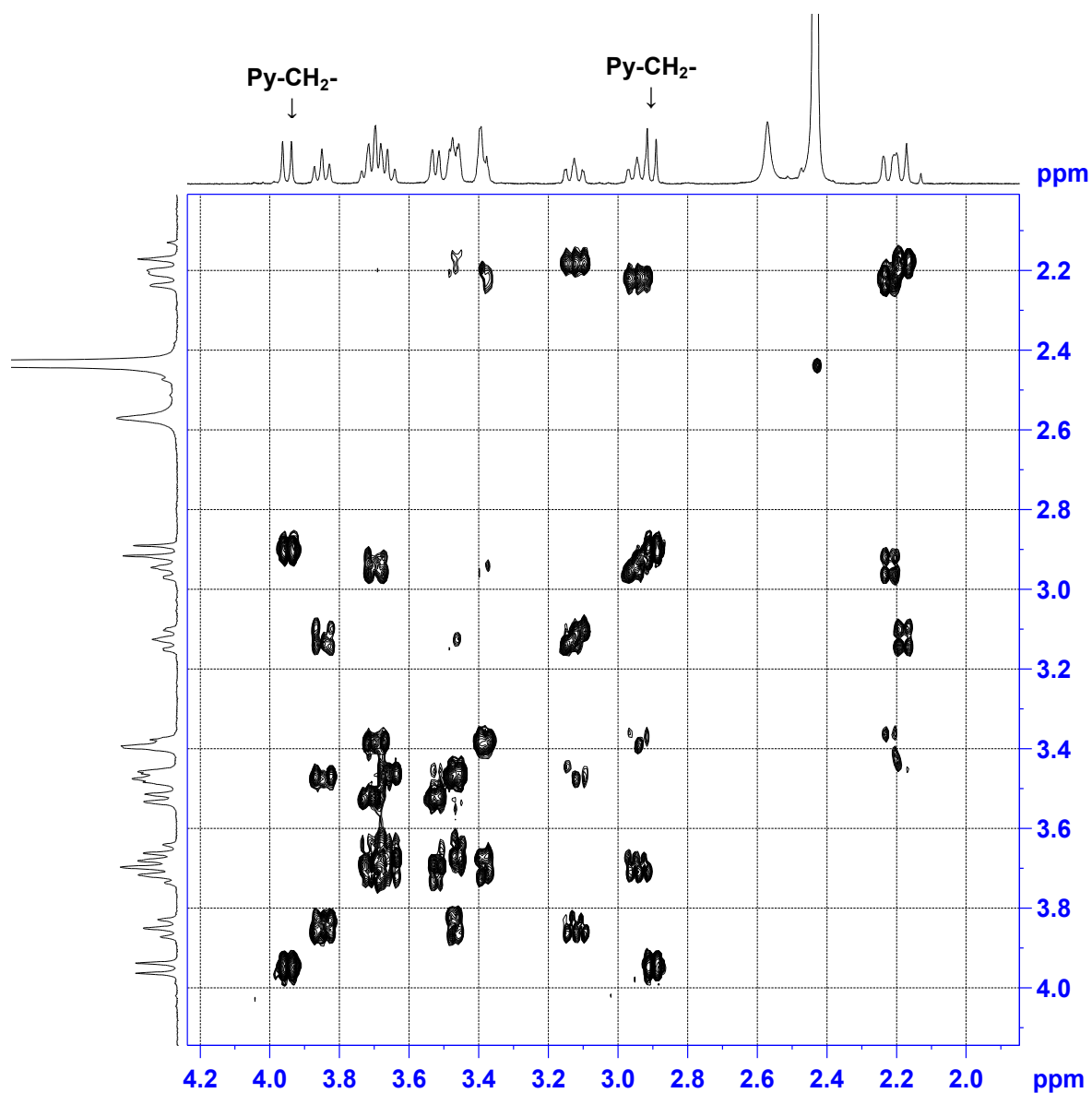


Figure 3.16 – Aliphatic region of the ^1H COSY NMR (CDCl_3) spectra of L_2 .

Further structural elucidation was carried out by ^1H COSY NMR, which can be seen in figures 3.15 and 3.16. The relationships between the peaks clearly demonstrates the correct structure has been assigned. Mass spectrometry was also performed to further clarify the structure, the relative molecular mass of the ligand was concordant with the structure suggested.

3.2 Results and discussion

3.2.1 – Solid State Structure of the Ammonium Iodide salt of L₂

Single crystals of the diamino cryptate species L₂ were obtained by slow evaporation of a solution of CHCl₃ and these were analyzed by single crystal X-Ray diffraction studies. The solid state structure can be seen in figures 3.17, 3.18 and 3.19, and selected bond lengths are shown in figure 3.20. The crystal structure clearly demonstrates the expected 3-dimensional structure has been successfully synthesized. Interestingly, there is an ammonium ion bound within the cryptate, this is present within the cryptate from the neutralization process in the penultimate stage of the synthesis. The hydrogen atoms of the ammonium ion are hydrogen bonded to both of the pyridine nitrogen atoms of the cryptate unit (3.031 and 2.947 Å) and four of the oxygen atoms in the cryptate domain (range 2.947 – 2.837 Å, average length 2.903 Å).

Surprisingly, the salt is that of the iodide (V), even though the anion was used in the penultimate step (HCl was used in the final step). However, the solubility of the iodide salt in DCM must be much greater than that of the chloride and as a result that anion is carried through to the final step. The iodide ion is hydrogen bonded to the molecules of CHCl₃ that are present within the solid state structure, and also with one of the amine groups on the bipyridine unit of the L₂ ligand. These bonds coupled with the solubility of the iodide salt in the DCM have allowed the iodide ion to persist through to the final step. The bipyridine unit of the ligand L₂ shows a large torsional twist (NCCN -57.28°), which can be clearly seen in figure 3.18, this is due to the steric hinderance of the two amine groups which move as far away from each other as possible due to steric repulsion.

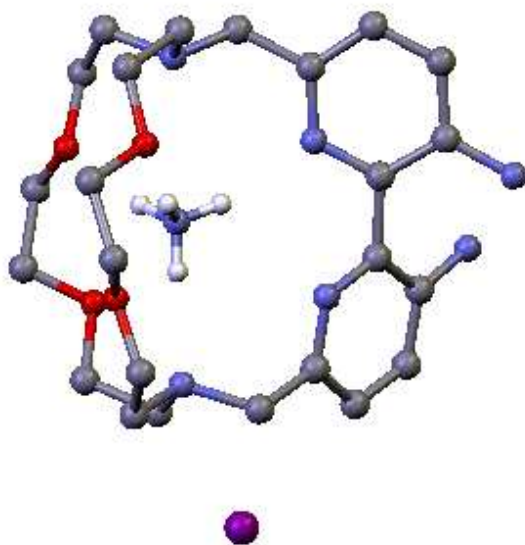


Figure 3.17 – Single Crystal X-ray structure of L_2 ammonium iodide salt.

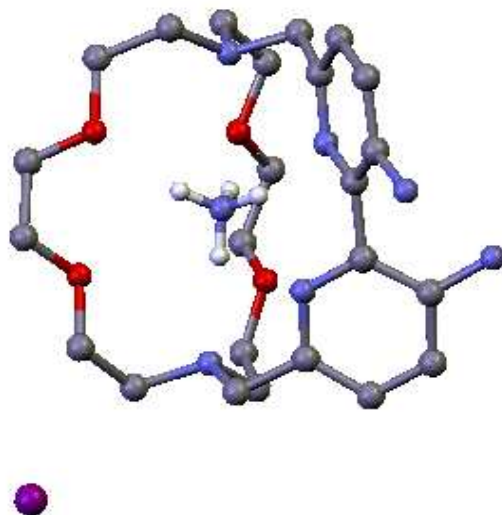


Figure 3.18 – Single Crystal X-ray structure of L_2 ammonium iodide salt, showing large torsional twist in the bipyridine unit.

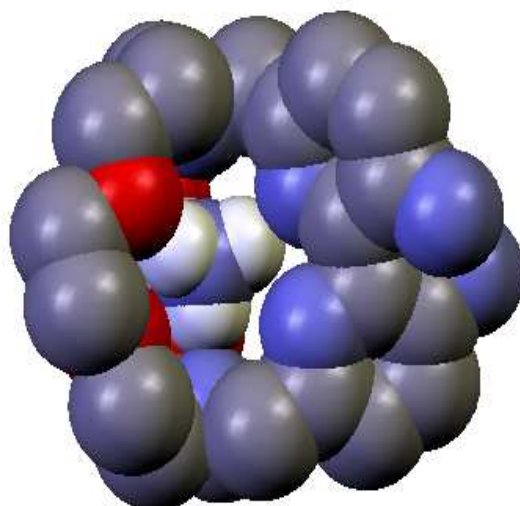


Figure 3.19 – Single Crystal X-ray space-fill structure of L₂ ammonium iodide salt.

Bond distances (Å)

N1G-H1G	0.908(9)	O103-C104	1.435(4)
N1G-H2G	0.905(9)	C104-C105	1.493(5)
N1G-H3G	0.906(9)	C105-O106	1.425(4)
N1G-H4G	0.906(9)	O106-C107	1.422(4)
N11-C16	1.341(4)	C107-C108	1.507(5)
C16-C18	1.519(5)	C108-N109	1.484(4)
C18-N100	1.483(5)	N109-C110	1.480(4)
N21-C26	1.340(4)	C110-C111	1.522(5)
C26-C28	1.506(4)	C111-O112	1.425(5)
C28-N109	1.488(4)	O112-C113	1.430(4)
N100-C101	1.474(5)	C113-C114	1.492(6)
N100-C117	1.480(4)	C114-O115	1.436(5)
C101-C102	1.508(5)	O115-C116	1.429(5)
C102-O103	1.429(4)	C116-C117	1.501(6)

Bond angles (°)

H1G-N1G-H2G	109.7(13)	O106-C105-C104	108.8(3)
H1G-N1G-N3G	109.2(13)	C107-O106-C105	111.8(3)
H2G-N1G-H3G	109.7(13)	O106-C107-C108	109.8(3)
H1G-N1G-H4G	109.3(13)	N109-C108-C107	113.7(3)

H2G-N1G-H4G	109.6(13)	C110-N109-C108	111.0(3)
H3G-N1G-H4G	109.3(13)	C110-N109-C28	109.3(3)
N11-C16-C18	116.8(3)	C108-N109-C28	108.6(3)
N100-C18-C16	114.7(3)	N109-C110-C111	114.9(3)
N21-C26-C28	116.9(3)	O112-C111-C110	110.1(3)
C101-N100-C18	109.5(3)	C111-O112-C113	111.6(3)
C117-N100-C18	108.9(3)	O112-C113-C114	109.7(3)
N100-C101-C102	114.4(3)	O115-C114-C113	109.8(3)
C102-O103-C104	110.8(3)	C116-O115-C114	112.2(3)
O103-C104-C105	109.7(3)	O115-C116-C117	109.9(3)
		N100-C117-C116	114.2(3)

Figure 3.20 – Selected bond lengths for L₂ free ligand

3.2.2 – Reactivity of cryptate with metal ions

Upon successful synthesis of the diamino cryptate the ability of this species to co-ordinate metal ions within the potentially octadentate cryptate domain was investigated by both ¹H NMR and ESI-MS. A ¹H NMR spectrum of the ammonium iodide salt of L₂ was obtained in CD₃CN which showed not only the expected aromatic and aliphatic signals but also present was a triplet at 7.53 ppm corresponding to the NH₄⁺ cation. The difference in the chemical shift between the ammonium present within the cryptate species and that of “free” ammonium (NH₄Cl, 6.1 ppm, CD₃CN) clearly shows that the cation is bound within the cryptate domain both in the solution and solid state.

Metal ions were introduced to the ligand to establish the reactivity of the cryptate domain, the single crystal X-ray structure clearly shows an ammonium ion co-ordinated within the cryptate domain. Several ¹H NMR experiments were performed to investigate whether the ammonium ion could be displaced from within the cryptate and replaced with a metal ion. The spectrum obtained from the ¹H NMR experiments are shown in figure 3.21.

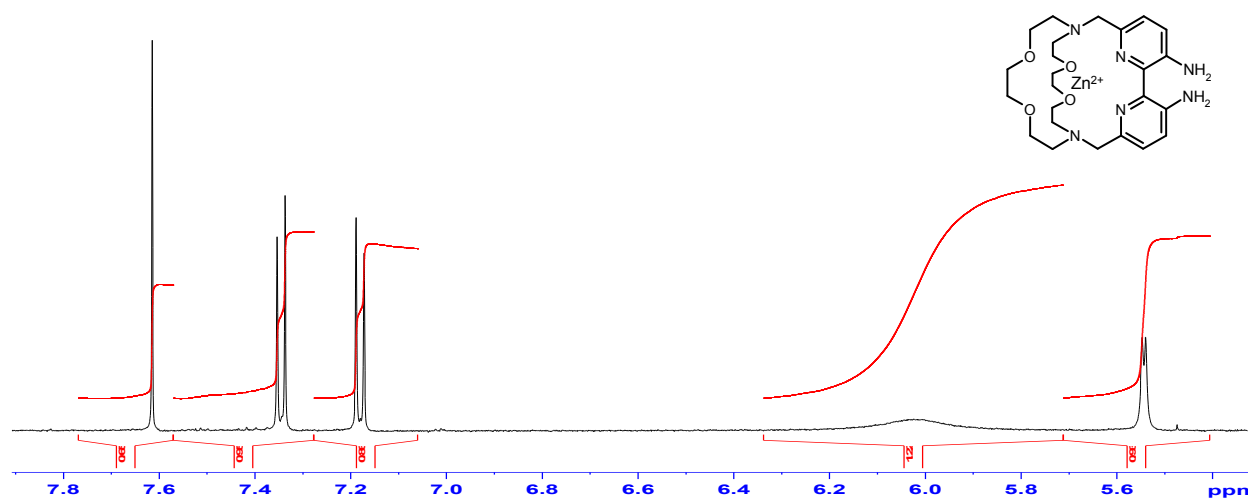
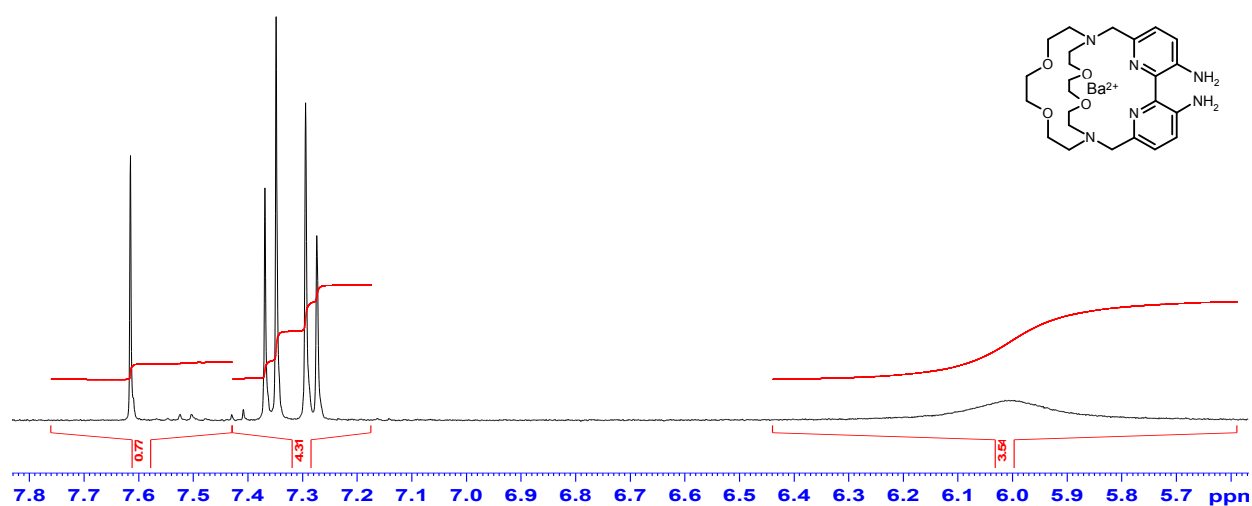
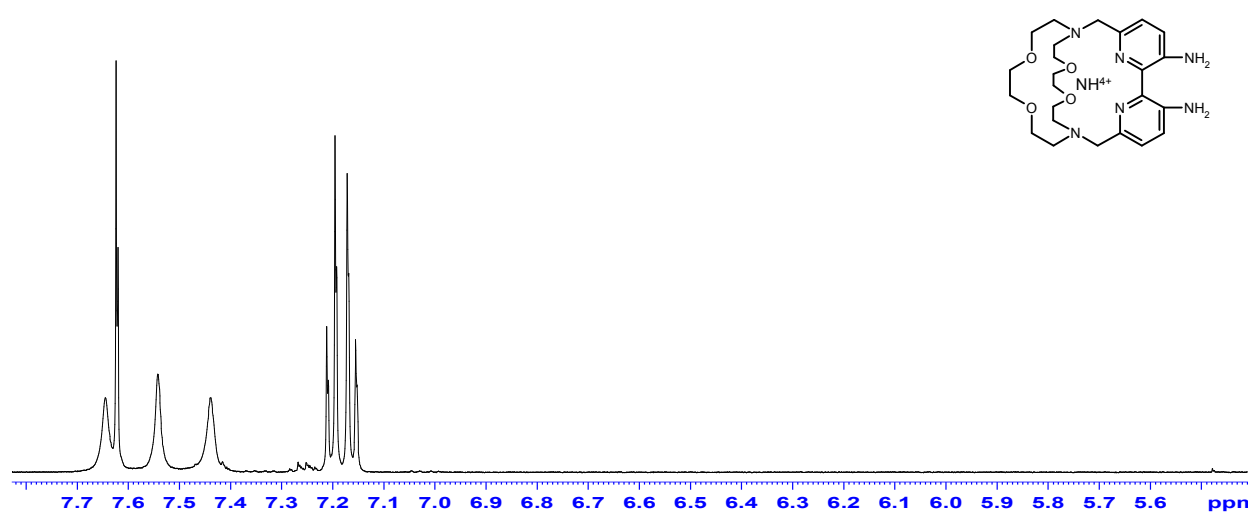


Figure 3.21 – ^1H NMR spectra obtained upon introduction of Ba^{2+} and Zn^{2+} to the ligand L_2 in acetonitrile with a H^+ acid catalyst.

The first spectrum shows the aromatic region of the ligand with an ammonium ion coordinated within the cryptate. The second and third spectra show the response when a metal ion is introduced into the ligand, Ba²⁺ in the second and Zn²⁺ in the third, respectively.

It is clearly demonstrated that upon addition of Ba²⁺ there is a shift in the aromatic signals, indicating that Ba²⁺ is incorporated within the cryptate domain. The Ba²⁺ ion has moved into the cryptate domain and displaced the ammonium situated within, the ammonia is now free in solution and a broad signal characteristic of –NH is observed at δ 6.0. Further evidence for incorporation of this metal cation is obtained by ESI-MS which shows an ion at m/z 736 $\{[L^2Ba]ClO_4\}^+$.

The third spectrum shows the change in signals which occurs upon introduction of zinc to the ligand, again there is a significant shift in the aromatic signals, the initial clue to indicate a change in structure has occurred. A broad signal characteristic of –NH is observed at δ 6.0 indicating the Zn²⁺ has displaced the ammonium ion from within the cryptate. Again an ion is observed with the ESI-MS at m/z 685 which corresponds to the zinc complex $\{[L^2Zn]CF_3SO_3\}^+$

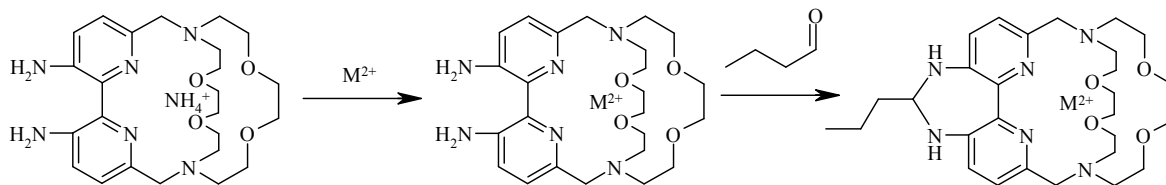
These ¹H NMR experiments demonstrate the ability of the cryptate domain to co-ordinate metal ions, it is believed that the selectivity of the cryptate domain will be based on ionic size as is the case with crown ether domains and this has been demonstrated previously by Rice *et al.*³⁹ The selectivity of the domain for metal ions over cations is demonstrated by the rapid exchange of the ammonium ion for a metal ion. This is due to the number of donor atoms within the cryptate unit and the 3-dimensional shape which allows strong binding of metal ions.

3.2.3 – Cyclisation of Amino Groups

It has been previously observed in similar systems that amino groups react readily with aldehydes and this results in the formation of a seven-membered cyclic cyclic aminal species.⁹⁸ It is thought that this reaction occurs via formation of a Schiff base with one of the amine units. This then undergoes an intramolecular reaction with the other amine resulting in the formation of a 7-membered aza-heterocycle.

To investigate the formation of this cyclic species the ammonium iodide salt of L₂ was reacted with a 10-fold excess of butanal in CDCl₃ and the ¹H NMR spectrum recorded, unfortunately no reaction was observed even with prolonged reaction times or at elevated temperatures. However, upon addition of barium ions to the same reaction a colour change occurred instantaneously and the ¹H NMR showed that the cyclisation had occurred (Scheme 2) as both a shift in the aromatic region was observed, disappearance of the amino

protons and a new signal at 4.15 ppm corresponding to the $-\text{CHCH}_2\text{CH}_2\text{CH}_3$ proton. Further confirmation was given by ESI-MS which gave an ion at m/z 736 corresponding to the barium-containing cyclised species $\{[\text{L}^2\text{Ba}]\text{ClO}_4\}^+$.



Scheme 2 – Cyclization of L_2 upon introduction of M^{2+} and butanal.

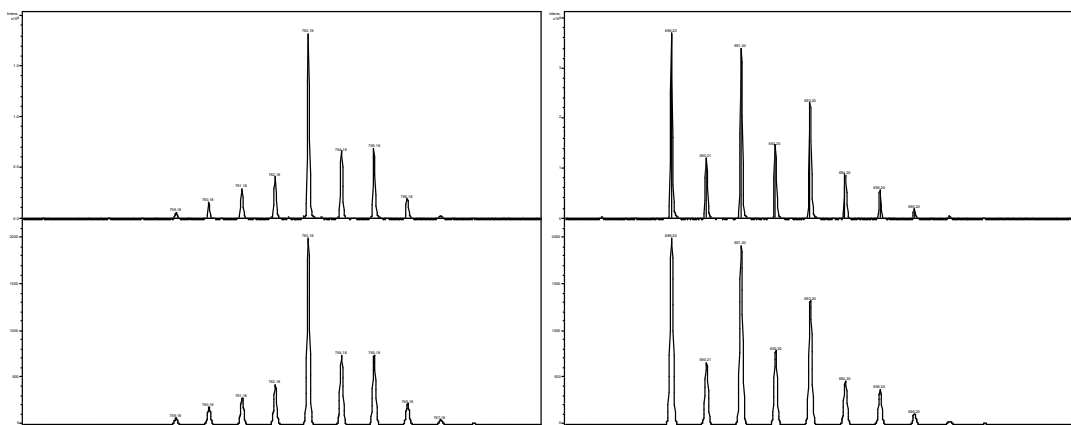


Figure 3.22 – Comparison of the theoretical (above) and obtained (below) isotope distributions from ESI-MS of the Ba^{2+} (left) and Zn^{2+} (right) cyclised complexes.

Single crystals of this cyclised species were grown by reaction of $[\text{L}^2\text{Ba}](\text{ClO}_4)_2$ with butanal in water which slowly deposited dark yellow crystals after 24 hrs. In the crystal structure the formation of the aminal species is confirmed with the barium ion co-ordinated by four oxygen atoms (2.808(5) – 2.887(5) Å) and four nitrogen atoms (2.836(5) – 2.911(5) Å) from the cryptate moiety, along with two oxygen atoms from the perchlorate counter ions (2.887(5) – 3.007(6) Å, omitted for clarity).

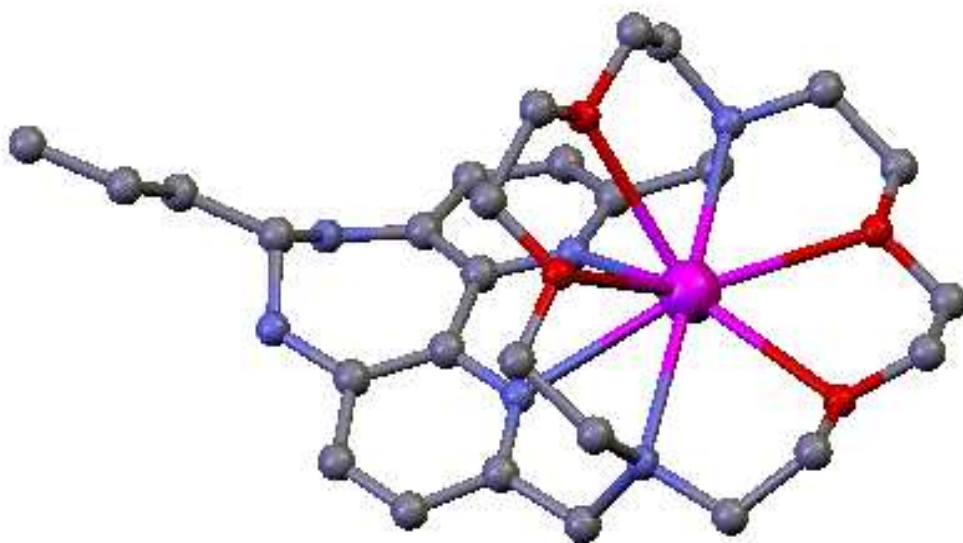


Figure 3.23 – Single Crystal X-ray structure of $L^2\text{-Ba}^{2+}$ cyclised ligand.

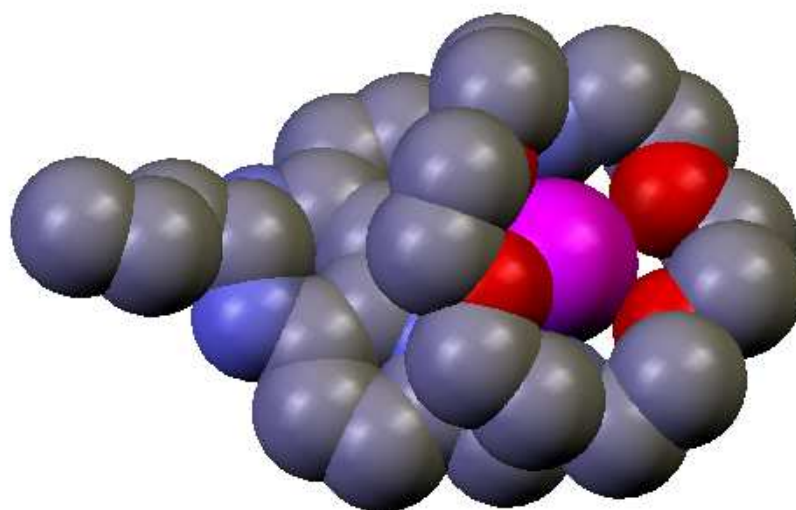


Figure 3.24 – Single Crystal X-ray spacefill structure of $L^2\text{-Ba}^{2+}$ cyclised ligand

Bond distances (Å)

N1-Ba1	2.911(5)
N2-Ba1	2.836(5)
N3-Ba1	2.910(6)
N4-Ba1	2.908(6)
O1-Ba1	2.887(5)
O2-Ba1	2.885(5)
O3-Ba1	2.824(5)
O4-Ba1	2.808(5)
O5-Ba1	2.887(5)
O9-Ba1	3.007(6)

Bond angles (°)

N1-Ba1-N2	61.5 (2)	O5-Ba1-N1	81.6(1)
N1-Ba1-N3	115.7(2)	O5-Ba1-N2	74.8(2)
N1-Ba1-N4	177.8(2)	O5-Ba1-N3	87.9(2)
N2-Ba1-N3	54.6(2)	O5-Ba1-N4	97.9(2)
N2-Ba1-N4	116.4(2)	O9-Ba1-N1	88.5(2)
N3-Ba1-N4	62.1(2)	O9-Ba1-N2	139.1(2)
O1-Ba1-N1	59.1(1)	O9-Ba1-N3	138.3(2)
O1-Ba1-N2	69.9(2)	O9-Ba1-N4	93.5(2)
O1-Ba1-N3	91.7(2)	O1-Ba1-O2	58.9(1)
O1-Ba1-N4	119.9(2)	O1-Ba1-O3	142.3(2)
O2-Ba1-N1	118.4(1)	O1-Ba1-O4	104.5(1)
O2-Ba1-N2	101.7(2)	O1-Ba1-O5	136.6(1)
O2-Ba1-N3	71.5(1)	O1-Ba1-O9	71.0(2)
O2-Ba1-N4	61.6(1)	O2-Ba1-O3	105.1(1)
O3-Ba1-N1	119.5(2)	O2-Ba1-O4	132.8(1)
O3-Ba1-N2	146.6(2)	O2-Ba1-O5	155.8(1)
O3-Ba1-N3	116.7(2)	O2-Ba1-O9	67.0(2)
O3-Ba1-N4	62.2(2)	O3-Ba1-O4	59.2(1)
O4-Ba1-N1	60.4(2)	O3-Ba1-O5	72.5(2)
O4-Ba1-N2	113.6(2)	O3-Ba1-O9	71.3(2)
O4-Ba1-N3	155.4(2)	O4-Ba1-O5	67.7(1)
O4-Ba1-N4	121.4(2)	O4-Ba1-O9	65.7(2)
		O5-Ba1-O9	130.9(2)

Figure 3.25 – Selected bond lengths and bond angles for L²-Ba²⁺ cyclised ligand.

The reaction of the amino groups with aldehydes occurs with any uni- or divalent metal ions but does not occur if these are not present. There are two possible explanations for this behavior; firstly an allosteric effect, as it has been previously shown that proximity of amine groups plays an important role in the cyclisation reaction to form the bis-aminal species. If the two amino groups are too distant then the cyclisation step cannot occur as the nucleophilic nitrogen atom cannot react with the Schiff base. Therefore, upon co-ordination of the cryptate domain with a zinc or barium ion, co-ordination of the nitrogen groups attached directly to the bipyridine unit would force the bipyridine unit planar. This forced planarity moves the two amine groups into closer proximity to each other facilitating the cyclisation with an aldehyde. Therefore, in this case the addition of a barium or zinc ion to ligand L₂ in an excess of butanal would facilitate cyclisation via an allosteric effect. Secondly, the metal ions could act as a simple Lewis acid catalyst simply activating the aldehyde and promoting the formation of the Schiff base.

It is difficult to ascertain which of these effects is predominantly responsible for the catalysis. For example, if sodium was employed as the catalyst then this may slow the reaction but this can be attributed to both an allosteric effect as sodium is smaller than Ba^{2+} or Zn^{2+} and may not result in a planar bipyridine unit (the Na^+ would be coordinated via the 4 oxygen and 2 nitrogen atoms of the cryptate). Retardation of the rate could also be as a result of the monovalent ion which would not be as an effective Lewis acid catalyst compared with the divalent metal ion. However, it is highly probable that the metal ion has a synergistic effect and promotes the reaction via *both* allosteric effects and Lewis acid catalysis.

3.2.4 – Fixing of the Cryptate Domain

The ability of the cyclisation of the two amino functional groups to affect the co-ordination properties was investigated. It was hoped that cyclisation of the amino groups would significantly affect the ability of the cryptate domain to fix a metal cation inside. This “locking” would arise from an allosteric effect as the diamino unit present on the bipyridine prevents it from adopting a planar conformation and as a result the bipyridine cannot easily act as a bidentate unit. Cyclisation of the amino units with an aldehyde would result in reducing the torsion angle allowing bidentate co-ordination. It was envisaged that the metal ions of certain complexes of the uncyclised species could be easily exchanged with other metal ions e.g. addition of excess Ba^{2+} ions to the potassium complex would result in displacement of the K^+ ions with Ba^{2+} . However, cyclisation would lock the metal ion with the cryptate unit.

To investigate this behavior a series of ^1H NMR experiments were performed. In the first experiment the ^1H NMR (CD_3CN) of the potassium-containing complex $[\text{L}^2\text{K}]\text{ClO}_4$ was obtained and to this was added a three-fold excess of $\text{Ba}(\text{ClO}_4)_2$ and the spectrum re-recorded. This clearly showed a difference in the ^1H NMR indicating that the barium had displaced the potassium ion, furthermore the chemical shift was identical to that of the isolated barium complex $[\text{L}^2\text{Ba}](\text{ClO}_4)_2$. A second experiment was then conducted but this time the cyclised species was used, a ^1H NMR spectrum of the cyclised potassium-containing complex $[\text{L}^2\text{K}]\text{ClO}_4$ was obtained in CD_3CN and then a 3-fold excess of barium perchlorate was added and the spectrum re-recorded. Comparison of the ^1H NMR spectra obtained show the potassium ion is easily displaced from the cyclised cryptate in an analogous manner to the uncyclised species.

In retrospect it is somewhat obvious that the cryptate species cannot be “locked” as careful examination of the solid state structure reveals that the distance between the two – $\text{OCH}_2\text{CH}_2\text{O}$ - arms of the cryptate unit is quite large and these “windows” will allow displacement of ions, regardless of whether the bipyridine unit is cyclised or not.

3.2.5 – Luminescence Studies

The unique reactivity of L_2 allows tunable optical and emissive properties. In the free ligand form the probe is shown to absorb with a $\lambda_{max} = 317\text{nm}$ and is weakly emissive at ca. 440nm in aerated aqueous solution. A variety of metal cations ($5 \times 10^{-4} \text{ M}$ as perchlorate salts) were introduced to a $1 \times 10^{-4} \text{ M}$ solution of L_2 and resulted in minor emission wavelength shifts together with general enhancements in emission intensity. The trivalent state of iron is the most common metal ion found within the human body. Comparison of Fe^{3+} and Zn^{2+} was particularly notable as these two species produced the most significant blue ($\text{Fe}^{3+} \lambda_{em} = 428\text{nm}$) and red shifts ($\text{Zn}^{2+} \lambda_{em} = 452\text{nm}$) respectively, therefore allowing differentiation between the ions on the basis of wavelength.

Further evidence for the binding properties of L_2 was observed in the absorption spectra where the lowest energy intraligand band was red shifted in comparison to the $L_2\text{Zn}^{2+}$ complex. In the case of the $L_2\text{-Zn}^{2+}$ complex the absorption is $\lambda_{em} = 365\text{nm}$, however, titration of a micromolar concentrations of Zn^{2+} to a $1 \times 10^{-4} \text{ M}$ solution of L_2 induced approximately a 10-fold increase in the emission intensity. The emission intensity with increasing concentrations of Zn^{2+} is shown in figure 3.26, the dramatic increase in intensity can be seen following the increase in concentration of Zn^{2+} present.

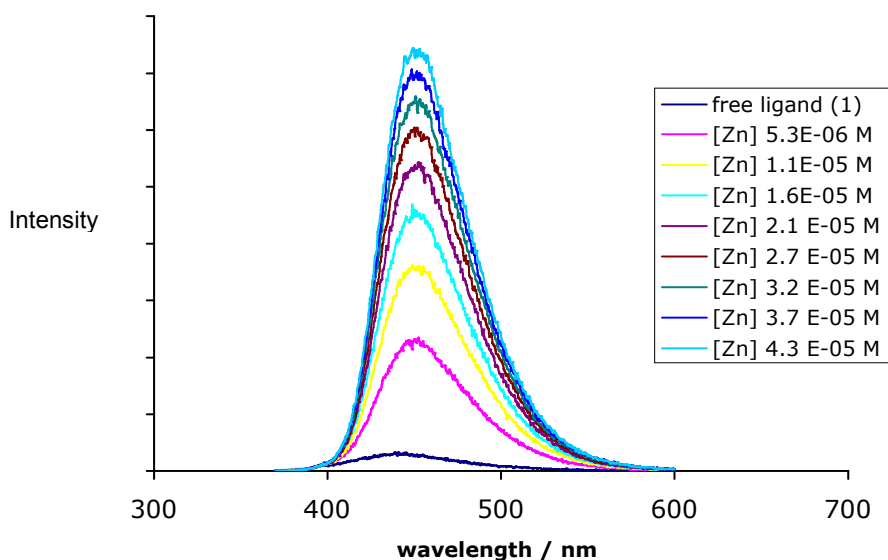


Figure 3.26 – Luminescence titration of $\text{Zn}(\text{ClO}_4)_2$ with L_2 ($1 \times 10^{-4} \text{ M}$ in water)

The addition of excess butanal to the solution of L_2 resulted in the formation of the cyclised bis-aminal species, this further optimized the optical properties of the ligand. The derivatisation resulted in formation of a yellow solution as a consequence of the red shift in the lowest energy absorption band.

A further example of this was shown in the electronic spectrum of cyclised zinc complex (cyclised L_2Zn^{2+}) with $\lambda_{max} = 439$ and 282 nm, demonstrating a dramatic low energy shift upon cyclisation, and thereby facilitating visible sensitisation, this is shown in figure 3.27. It should be noted that in contrast to the cyclised species neither the uncyclised free L_2 ligand or the L_2Zn^{2+} uncyclised species are strongly absorbing above 420 nm. This indicates that excitation wavelengths at or above 420 nm are selective for the cyclised L_2Zn^{2+} ligand.

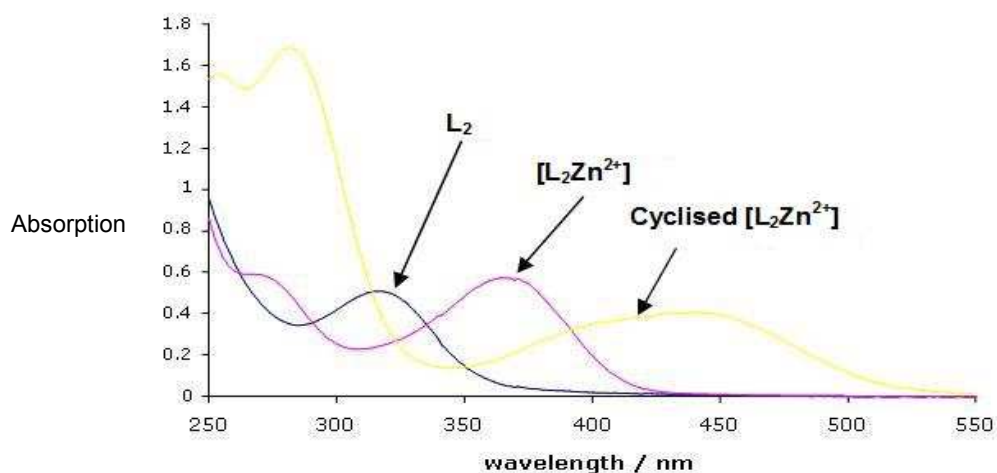


Figure 3.27 – Electronic absorption spectra obtained in aqueous solutions at a concentration of 7×10^{-5} M

The photophysical properties of the cyclised L_2 ligand were even more varied in response to various complexes than the uncyclised L_2 ligand. The data associated with the wavelength and fluorescent lifetime responses of the ligand with various metal ions are shown in table 3.1 and in graphical form in figures 3.28 and 3.29. Table 3.1 and figure 3.29 also display the relative intensity compared to the zinc complex. The cyclised ligand produced the most intense emission when co-ordinated with zinc by a significant margin.

Table 3.1 Luminescent properties of L^{2a} (uncyclised L₂ ligand) and L^{2b} (cyclised L₂ ligand) + metal ions (Mⁿ⁺).

M ⁿ⁺	[L ^{2a} + M]/nm ^a	[L ^{2b} + M]/nm ^b	Relative intensity (I/I ₀) ^c	[2-M]□/ns ^d
Li ⁺	442	559	0.03	1.3
Na ⁺	442	563	0.03	1.3
K ⁺	441	560	0.03	1.2
Mg ²⁺	440	560	0.03	1.3
Ca ²⁺	444	562	0.03	1.3
Ba ²⁺	437	543	0.23	9.0
Fe ³⁺	428	568	0.16	1.0
Co ²⁺	440	556	0.07	1.5
Ni ²⁺	440	566	0.05	1.4
Cu ²⁺	Weak	Weak	-	-
Zn ²⁺	452	533	1	5.9
Cd ²⁺	442	528	0.29	5.3
Hg ²⁺	441	520 Weak	0.01	-

^a λ_{ex} = 350 nm; ^b λ_{ex} = 425 nm; ^c where I = L^{2a} + Mⁿ⁺, I₀ = L^{2b} + Zn²⁺; ^d λ_{ex} = 372 or 459nm. Measurements obtained using 1 × 10⁻⁴ M of 1 and 5 × 10⁻⁴ M Mn+. All solutions were allowed to equilibrate for 10 min and the pH remained between 6.5 and 7.5 in all cases. For [2-M]^{+/2+}, samples were re-recorded after 24 h demonstrating no further changes. Measurement were taken at a fixed excitation wavelength, therefore changes in emission intensity may not necessarily reflect changes in quantum yield.

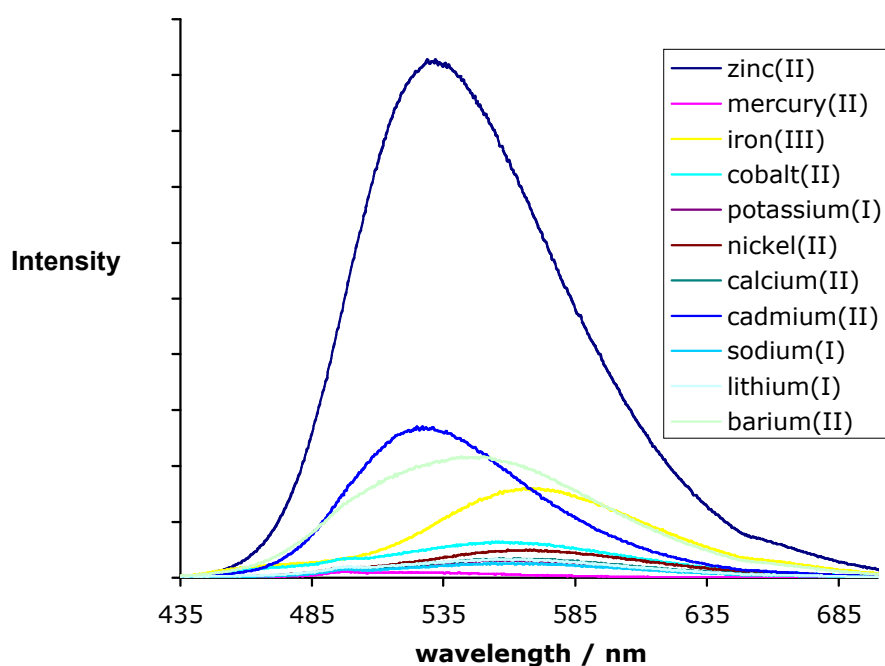


Figure 3.28 - Comparison of emission spectra of L_2M^+ in water following exposure to an excess of butanal.

It can be clearly seen that the zinc and cadmium complex of cyclised L_2 ligands emit at a slightly shorter wavelength than the other metal ions, they both emit at below 535nm, the other ions emit in the 550 to 585 nm range, with the majority emitting at approximately 575nm. This may allow a degree of wavelength selectivity based on metal ions co-ordinated and their emission wavelengths.

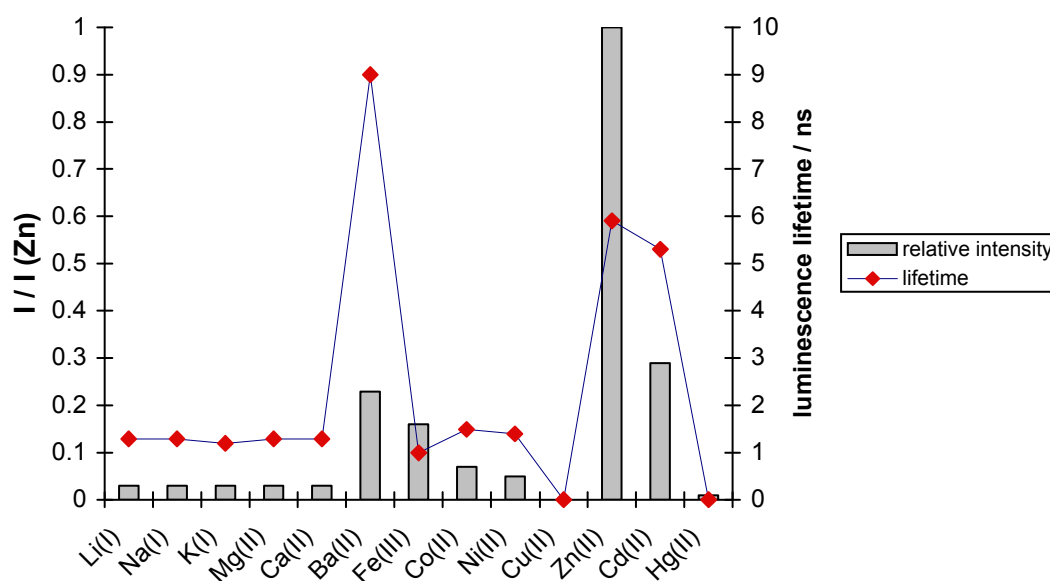


Figure 3.29 – Graphical summary of the luminescence responses of the cyclised L_2M^+ species in water.

Generally it was found that the emission maxima from the cyclised bisaminal species lay between 515 and 570 nm for the various metal complexes, following excitation at 425 nm, this indicated a significant Stokes shift which is commonly associated with emissive transition metal complexes, the Stokes shift for the cyclised L_2Zn^{2+} ligand is shown in figure 3.30. A large Stokes shift is preferable for luminescent sensors as there is a large difference between the wavelength in which excitation occurs and the wavelength at which emission occurs, this means there is no confusion between the two signals.

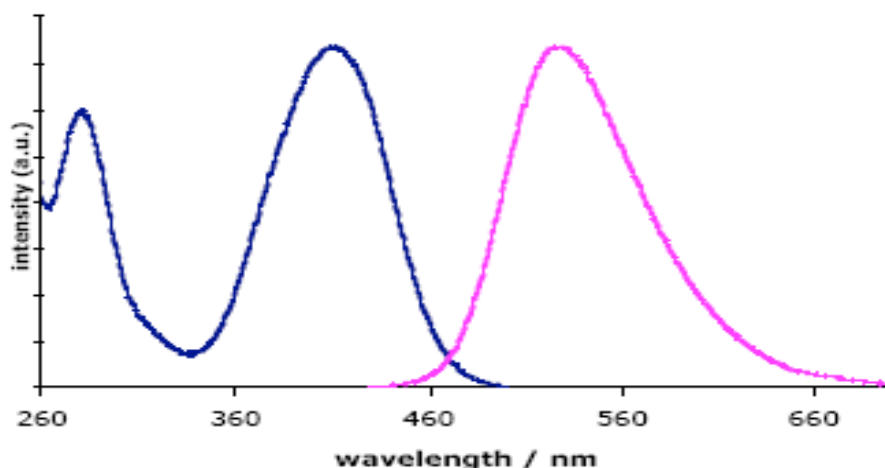


Figure 3.30 – Example of excitation (left) and emission spectra of the cyclised L_2Zn^{2+} ligand obtained in aerated water.

The ligand L_2 showed a dramatic increase in luminescence intensity when co-ordinated to zinc ions when compared to other metal cations, the reasons for this can be ascribed to a number of factors. Zn^{2+} has a higher affinity for the bipyridine unit than the group 1 and 2 cations, and is therefore more likely to co-ordinate the nitrogen atoms present in the bipyridine unit forcing the bipyridine unit planar. Increased planarity and rigidification allow greater luminescence intensity due to the reduced vibrational activity of the ligand. Zn^{2+} also possesses a closed shell d^{10} configuration, whereas paramagnetic metal ions (such as Ni^{2+} , Co^{2+} and Cu^{2+}) are known to be efficient luminescence quenchers. Comparison of the L_2Zn^{2+} complex with other metal complexes from Group 10 reveal a gradual decrease in luminescent intensity as we move down the group, this is due to quenching via the heavy atom effect.

The fluorescence lifetimes of the L_2Zn^{2+} complex were found to be far longer than those species which emitted at approximately 560nm, (such as Ca^{2+} , Ni^{2+} , Mg^{2+} , K^+ , Na^+ , Li^+ , Co^{2+} and Fe^{3+}), these are all analytes of biological interest, and this lifetime dependence allows screening for zinc in an ionically competitive buffered HEPES aqueous medium at pH 7.4. The HEPES buffered aqueous solution consists of 4mM $ZnCl_2$ in 140mM NaCl, 4mM KCl, 1.2 mM $MgCl_2$ and 2.3mM $CaCl_2$.

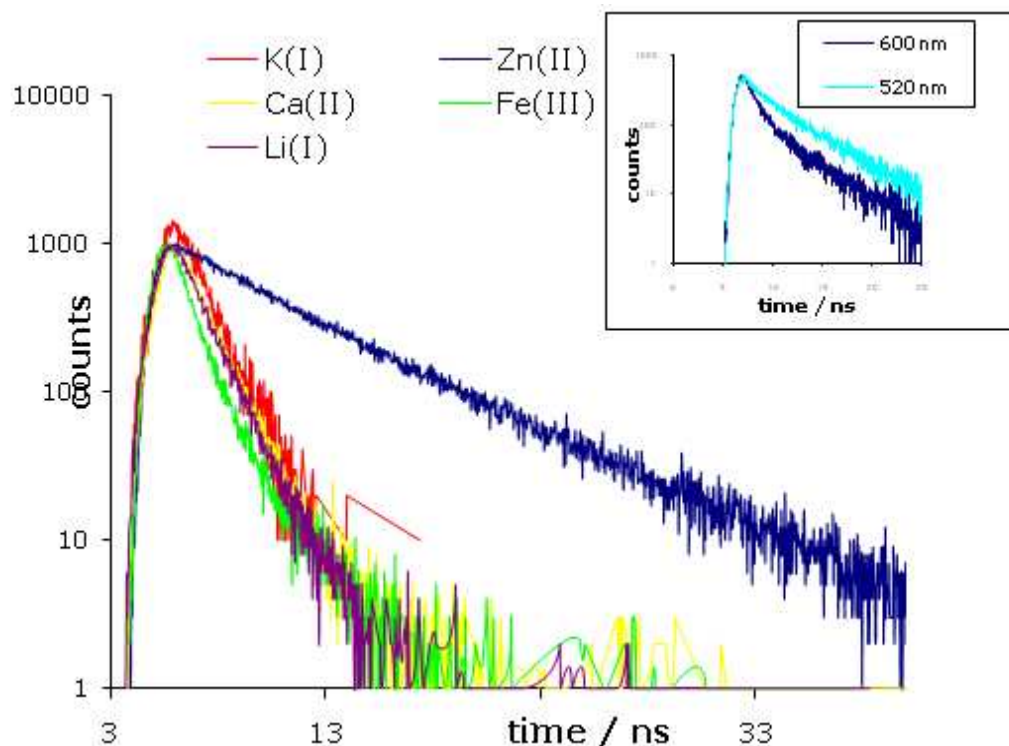


Figure 3.31 – Comparison luminescent lifetime decay profiles of cyclised L_2M^{n+} where $M = K^{(I)}$, $Zn^{(II)}$, $Fe^{(III)}$, $Ca^{(II)}$ and $Li^{(I)}$. Inset- wavelength dependent lifetime decays of cyclised L_2Zn^{2+} in an ionic mixture.

The response is shown in figure 3.31, and it can be seen that the profiles for $K^{(I)}$, $Fe^{(III)}$, $Ca^{(II)}$ and $Li^{(I)}$ begin to decay after approximately 6 nano seconds. However Zn^{2+} has a much longer lifetime and less dramatic decay profile. The inset shows the lifetime decay profile for an ionic mixture at different wavelengths. At longer wavelengths (550nm) the shorter lifetime contributions of Na^+ , K^+ , Mg^{2+} and Ca^{2+} are notable, however the long lifetime of the Zn^{2+} is also clearly demonstrated. At lower wavelengths, (550nm), the long lived emission of Zn^{2+} is dominant, this supports the emission wavelength data shown in figure 3.28, where the zinc emits at a shorter wavelength than the majority of the other ions tested. Thus, for the cyclised L_2Zn^{2+} species the luminescence lifetime measurement can be used as a discriminatory technique for the detection of zinc, even in a competitive ionic medium.

4: Luminescent Transition Metal Helicates

The chapter describes the synthesis of a potentially hexadentate ligand L_3 , which contains two coumarin fluorophores. The ligand is potentially capable of forming a dinuclear double helicate when in the presence of dicationic metal ions.

The ability of polydentate ligands to form helicate assemblies with transition metals has and continues to receive a large amount of interest within chemical research. Luminescent helicates are a specific area of interest and most commonly involve the incorporation of luminescent lanthanide ions. The lanthanide ions are capable of participating in f-f transitions and can produce interesting and useful properties. However, the frequency of helicates containing organic lumophores is considerably less common, and although some examples have been reported, these generally form mononuclear complexes with divalent metal ions, or helicates with monovalent metal ions.¹⁰¹

4.1 Ligand synthesis

4.1.1 Synthesis of ligand L_3

The aim of the chapter was to synthesise a hexadentate ligand which possessed two coumarin fluorophores. It is envisaged that co-ordination of the ligand with certain metal ions will result in a dinuclear double helicate. The coumarin fluorophores may enable a modulation of luminescence emission upon co-ordination of the ligand with metal ions.

The ligand L_3 incorporates a well known fluorophore in the form of coumarin, which is attached to the thiazole moiety in the final step of the synthesis. The ligand was prepared from the starting pre-cursor 3,3'-dimethoxy-2,2'-bipyridine via a 4 step linear reaction. The luminescence and co-ordination properties of the ligand were subsequently investigated.

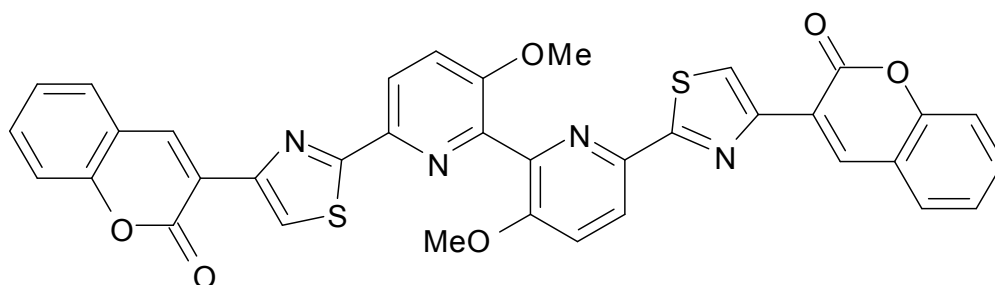
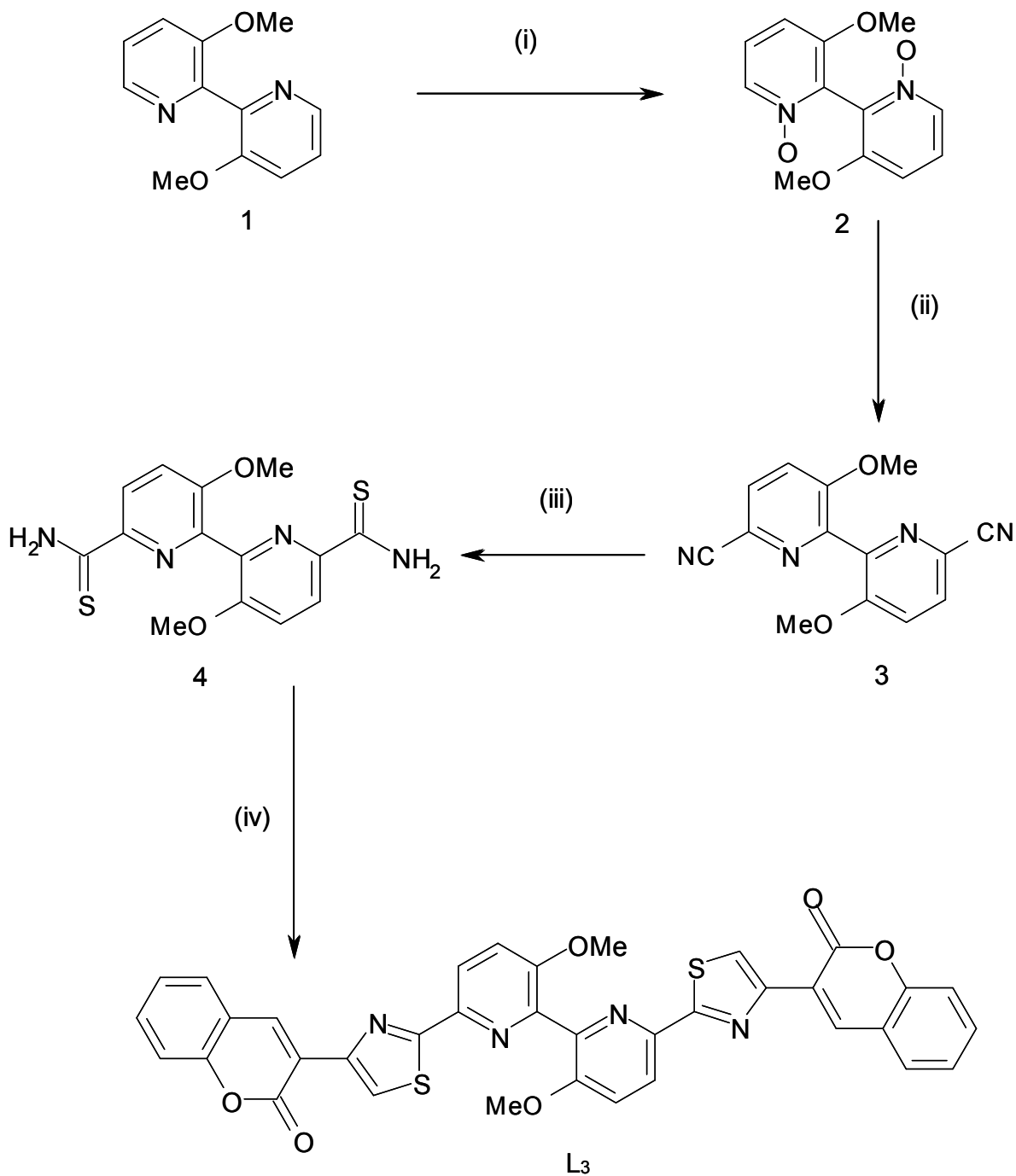


Figure 4.1 – Structure of helicate ligand L_3 .



Scheme 3 – Synthesis of L₃ from 3,3'-dimethoxy-2,2'-bipyridine (1). Reagents and conditions; (i) mCPBA, RT, (ii) trimethylsilyl cyanide, Et₃N, CH₂Cl₂, reflux, (iii) H₂S, (iv) 3-bromoacetyl coumarin, EtOH, reflux, aqueous NH₃.

The ligand L₃ was prepared from the initial starting material 3,3'-dimethoxy-2,2'-bipyridine via bis-N-oxidation and cyanation, reaction with hydrogen sulphide yielded the 6,6'-dithioamide. The final ligand L₃ was prepared by reaction of the 6,6'-dithioamide (4) with 3-bromoacetyl coumarin in ethanol at reflux. The ligand L₃ formed an insoluble precipitate which was isolated and washed. Once thoroughly dried any impurities were removed by suspension in ammonia solution, and once filtered and dried, analytically pure L₃ was obtained.

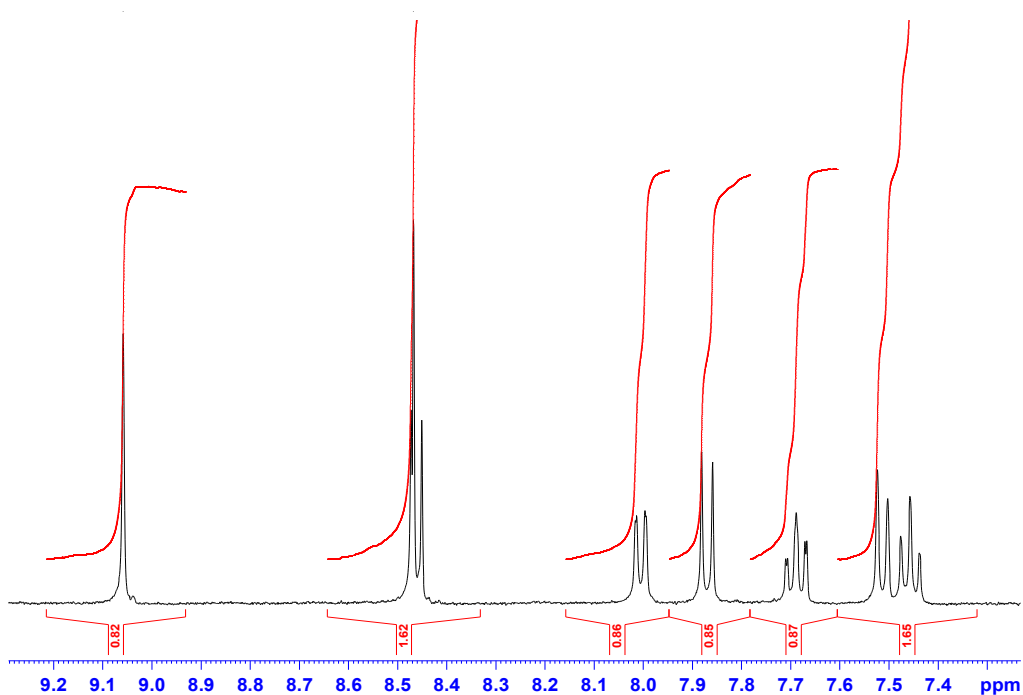


Figure 4.2 – Aromatic region of the ¹H NMR (DMSO) spectrum of L₃.

Due to the poor solubility of the L₃ ligand, it was difficult to obtain a ¹H NMR spectrum in most solvents; eventually a ¹H NMR spectrum was obtained in DMSO at 50°C, and is shown above in figure 4.2. The symmetrical nature of the ligand means that 8 aromatic signals are observed in the aromatic region, as is expected from the proposed structure, and a methyl group is clearly observed at δ 3.4, representing the methoxy group present.

4.2 Discussion and results

4.2.1 Solid State analysis

Reaction of the ligand with one equivalent of $\text{Cu}(\text{ClO}_4)_2 \cdot 6\text{H}_2\text{O}$ in MeCN yielded a dark red solution, from which a red crystalline material was produced by slow diffusion of which with diethyl ether. ESI-MS indicated a dinuclear double stranded helicate had been formed with peaks at m/z 1767 $\{[\text{Cu}_2(\text{L}^3)_2](\text{ClO}_4)_3\}^+$ and m/z 832 $\{[\text{Cu}_2(\text{L}^3)_2](\text{ClO}_4)_2\}^{2+}$.

The single crystal X-ray crystal structure confirmed the presence of the helicate species. The ligand can be seen to partition into two tridentate domains comprising of two N-donor atoms from the pyridyl and thiazole units and one O-donor atom from the carbonyl oxygen atom of the coumarin moiety. The copper ion is co-ordinated by two of these tridentate units, one from each of the two ligands forming the helicate structure.

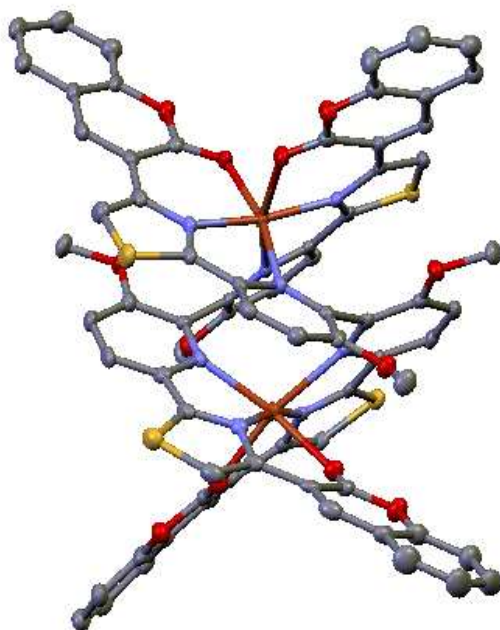


Figure 4.3 – Single crystal X-ray structure of $[\text{Cu}_2(\text{L}^3)_2]^{4+}$

Bond distances (Å)

Cu1 N81	1.955(3)
Cu1 N21	1.983(3)
Cu1 O71	2.091(3)
Cu1 N91	2.133(3)
Cu1 O11	2.203(3)
Cu1 N31	2.272(3)
Cu2 N51	1.947(3)
Cu2 N111	1.980(3)
Cu2 O61	2.083(3)
Cu2 N41	2.146(3)
Cu2 O121	2.239(3)
Cu2 N101	2.311(3)

Bond Angles (°)

N81-Cu1-N21	167.3(1)	N51-Cu2-N111	169.1(1)
N81-Cu1-O71	86.7(1)	N51-Cu2-O61	85.9(1)
N21-Cu1-O71	88.7(1)	N111-Cu2-O61	91.5(1)
N81-Cu1-N91	80.6(1)	N51-Cu2-N41	80.9(1)
N21-Cu1-N91	103.1(1)	N111-Cu2-N41	102.1(1)
O71-Cu1-N91	166.9(1)	O61-Cu2-N41	166.4(1)
N81-Cu1-O11	83.8(1)	N51-Cu2-O121	85.3(1)
N21-Cu1-O11	84.4(1)	N111-Cu2-O121	84.5(1)
O71-Cu1-O11	90.7(1)	O61-Cu2-O121	96.4(1)
N91-Cu1-O11	85.2(1)	N41-Cu2-O121	85.8(1)
N81-Cu1-N31	112.4(1)	N51-Cu2-N101	112.5(1)
N21-Cu1-N31	78.5(1)	N111-Cu2-N101	77.2(1)
O71-Cu1-N31	81.0(1)	O61-Cu2-N101	79.0(1)
N91-Cu1-N31	106.4(1)	N41-Cu2-N101	103.1(1)
O11-Cu1-N31	161.0(1)	O121-Cu2-N101	161.0(1)

Figure 4.4 – Selected bond lengths for L₃ free ligand

The solid state structure demonstrates that each of the Cu²⁺ centres has a distorted pseudo-octahedral co-ordination geometry with Cu-N and Cu-O distances ranging from 1.980(3)-2.311(3)Å and 1.980(3)-2.311(3)Å respectively. Surprisingly the Cu²⁺ centres appear to interact directly with the carbonyl O-donors of the coumarin fluorophores, which was unexpected as ester groups are generally considered to be poor donor units. The most probable explanation for this is unfavourable steric interaction between the two methoxy groups present in the 3,3'-position of the central bipyridine unit which prevent the ligand from adopting the coplanar geometry, required for all four of the N-donors to co-ordinate a common Cu²⁺ centre. Removal of these methoxy groups would almost certainly result in the

preferential formation of a single stranded mononuclear complex, observation of which has previously occurred in the study of Cu^{2+} complexes of related ligands based on a similar N-donor array.^{102, 103} In the ligand L_3 however, the partitioning of the ligand by the 3,3'-substituents allows the carbonyl oxygen groups to stabilize the Cu^{2+} centres within the dinuclear double-stranded complex.

ESI-MS studies have demonstrated that the latter 1st row d-block metal ions ($\text{M} = \text{Ni}^{2+}$, Zn^{2+} , Cu^{2+} and Co^{2+}) form the dinuclear double helicate species $[(\text{L}^3)_2\text{M}_2]^{4+}$, as do the 2nd and 3rd row d¹⁰ metal ions, giving $[\text{Cd}_2(\text{L}^3)_2]^{4+}$ and $[\text{Hg}_2(\text{L}^3)_2]^{4+}$ respectively. For the zinc complex a ^1H NMR spectrum (CD_3CN) was obtained and reveals eight signals in the aromatic region, which is consistent with the formation of the expected symmetrical helicate.

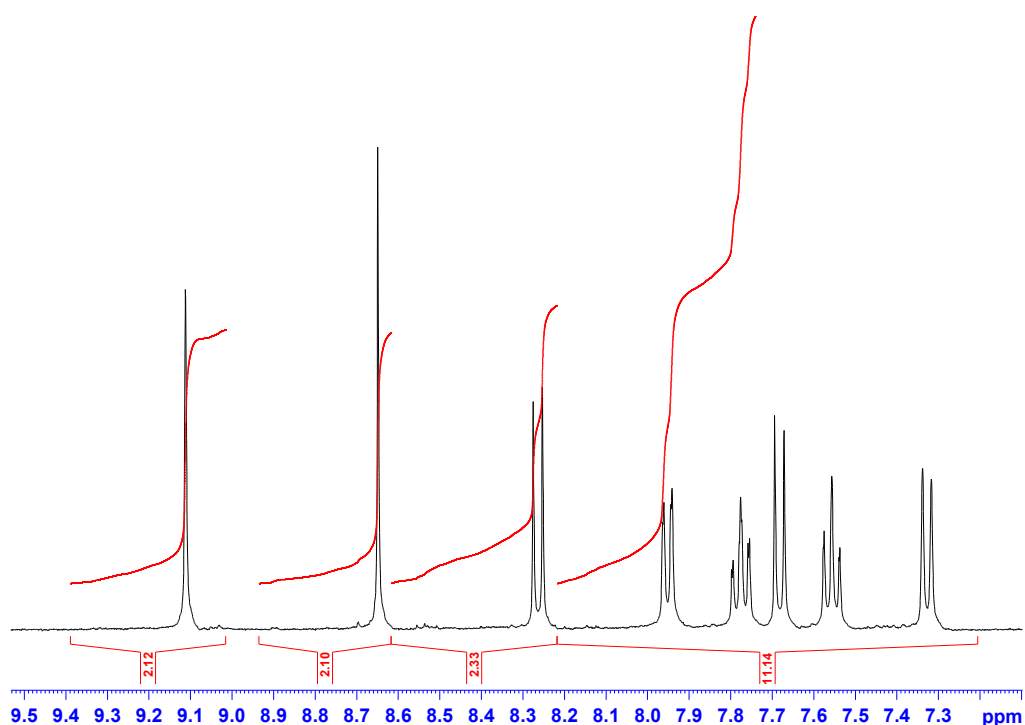


Figure 4.5 - Aromatic region of the ^1H NMR (CD_3CN) spectra of $[(\text{L}^3)_2\text{Zn}_2]^{4+}$.

A single crystal X-ray crystal structure has been obtained for the zinc complex $[\text{Zn}_2(\text{L}^3)_2]^{4+}$, however the data achieved for this structure is poor and show extensive disorder. The structure clearly demonstrates the structure is very similar to that obtained for the $\text{Cu}(\text{II})$ complex, however there is little further information available apart from the structure and the data do not merit detailed discussion.

^1H NMR studies of the larger Group 12 metal ions are more complex and two sets of 8 signals are observed, thus indicating the formation of two different species. Titration of an

excess metal ion results in the disappearance of one set of signals leaving a single species present.

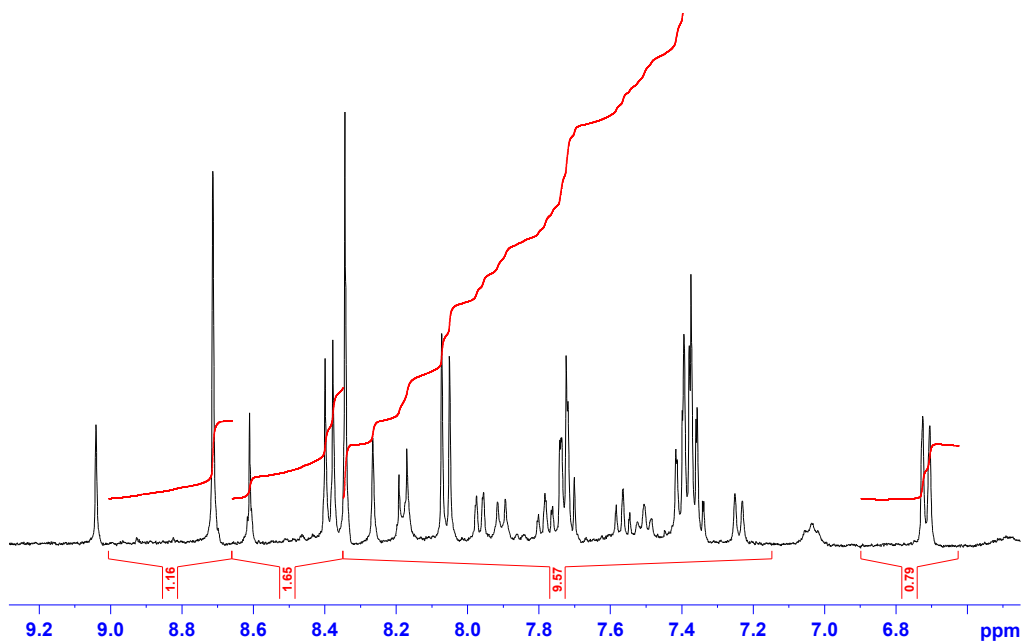


Figure 4.6 - Aromatic region of the ^1H NMR (CD_3CN) spectra of ligand L_3 and one equivalent of Cd^{2+} .

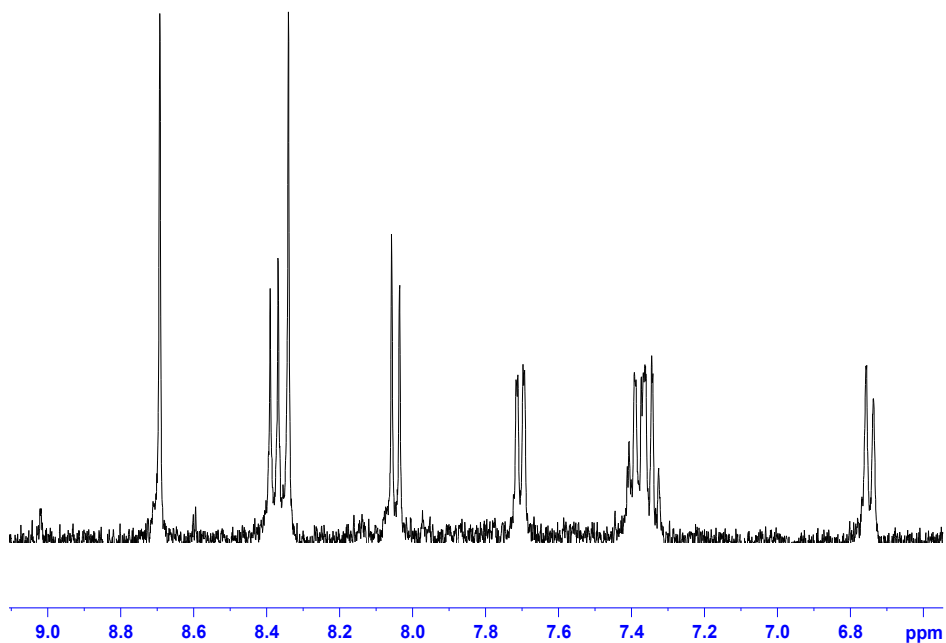


Figure 4.7 - Aromatic region of the ^1H NMR (CD_3CN) spectra of ligand L_3 and excess Cd^{2+} .

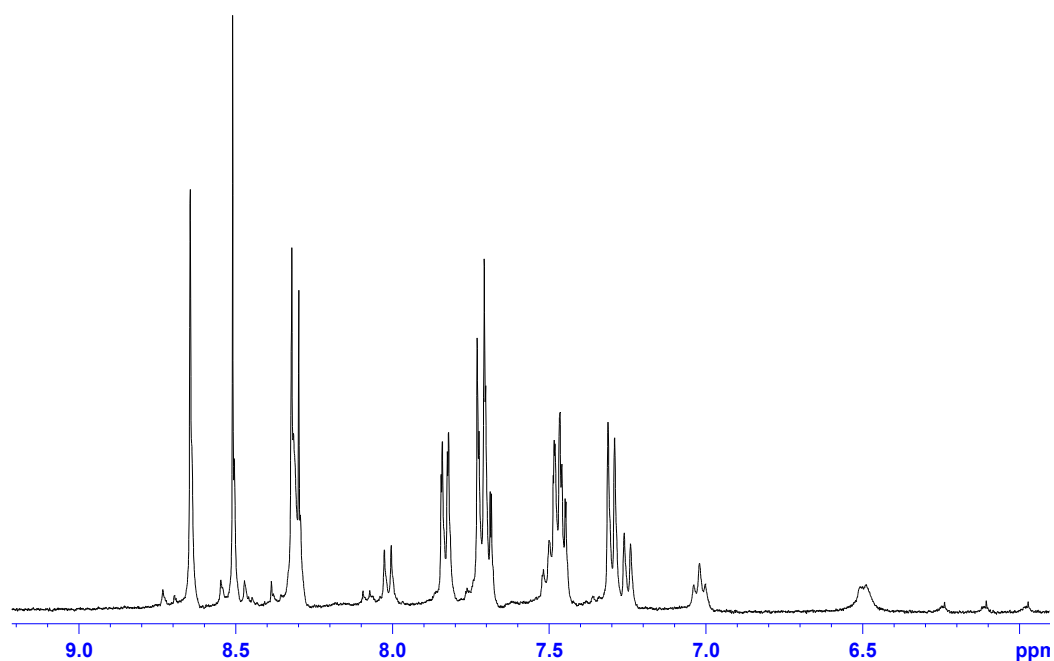


Figure 4.8 - Aromatic region of the ^1H NMR (CD_3CN) spectra of ligand L_3 and one equivalent of Hg^{2+} .

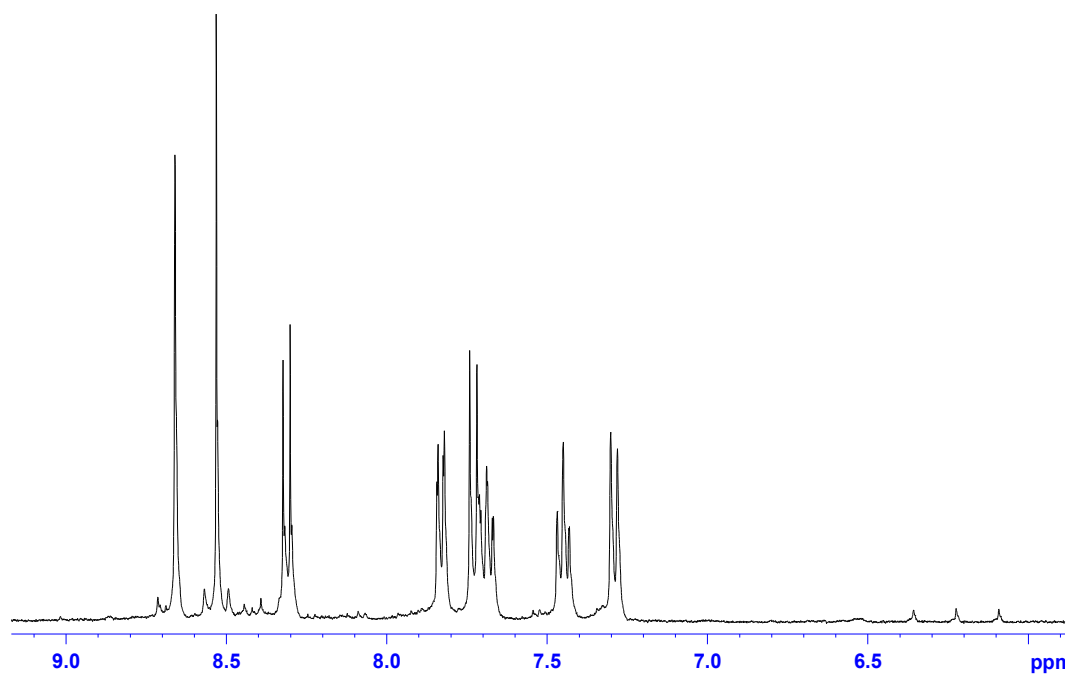


Figure 4.9 - Aromatic region of the ^1H NMR (CD_3CN) spectra of ligand L_3 and excess Hg^{2+} .

It is possible that with Cd^{2+} and Hg^{2+} that complexes of the complex $[\text{M}(\text{L}^3)_2]^{2+}$ are present and the metal is co-ordinated by 8 N-donor atoms, four from each ligand, giving rise to an 8-

co-ordinate metal centre. However, Cd^{2+} and Hg^{2+} are both capable of displaying coordination numbers of greater than six and are less oxophilic than Zn^{2+} , which would facilitate the formation of the diligand containing species $[\text{M}(\text{L}^3)_2]^{2+}$. Formation of the mononuclear species would be unfavourable upon addition of the excess metal ion as this would give preference to the formation of $[\text{M}_2(\text{L}^3)_2]^{4+}$. This theory is supported by the ESI-MS as ions which correspond to $[\text{M}(\text{L}^3)_2]^{2+}$ are observed at m/z 1553 for Cd^{2+} and m/z 1641 for Hg^{2+} . In contrast to this addition of excess metal salt to the zinc complex $[\text{Zn}_2(\text{L}^3)_2]^{4+}$ yields no changes.

4.2.2 Luminescence Studies

The emissive properties of the complexes of $[\text{M}_2(\text{L}^3)_2]^{4+}$ were examined in MeCN solution ($[\text{complex}]_{\text{tot}} \sim 10^{-3}$ M) of samples prepared in situ by combining stoichiometric amounts of the ligand and metal ion in question. The studies revealed the zinc complex to be the most emissive by a considerable margin, whilst the addition of all the other metal ions caused quenching of the coumarin based fluorescence by varying degrees. Paramagnetic metal ions (such as Co^{2+} and Cu^{2+}) are commonly known to demonstrate efficient quenching of ligand centred excited states, as are the heavier 2nd and 3rd row d^{10} metal ions, the results corresponded with this showing emission intensities decreasing dramatically in the order $\text{Zn}^{2+} \gg \text{Cd}^{2+} > \text{Hg}^{2+}$.

M^{n+}	λ_{em} (nm) ^a	$I/I_{(\text{lig})} \times 100$ (%)
-	437	100
Co^{2+}	435	8
Cu^{2+}	435	0.3
Zn^{2+}	453	120
Cd^{2+}	448	31
Hg^{2+}	442	0.5

^a $\lambda_{\text{ex}} = 390$ nm.

Table 4.1 – Solution state luminescence properties of the ligand L_3 and corresponding dimetallic helicates.

The 2nd and 3rd row d^{10} metal ions induce heavy atom mediated intersystem crossing to ligand centred triplet states, with Hg^{2+} being extremely sensitive to quenching via triplet oxygen. However, the greatest quenching effect was observed in the presence of Cu^{2+} , which resulted in extremely weak ligand fluorescence

Recently theoretical studies on a related picolyl-functionalised coumarin species have revealed that nonradiative quenching by Cu^{2+} may be caused by a combination of energy transfer and charge transfer ($\text{L}_{\text{coum}}\text{M}_{\text{Cu}}\text{CT}$).¹⁰⁴ Measurements at 77 K on an ethanolic glass of L and excess Cu^{2+} resulted in the restoration of the fluorescence signal. Energy transfer via Dexter electron exchange should be independent of solvent reorganisation, therefore it is probable that fluorescence quenching by Cu^{2+} at room temperature is due to solvent-mediated photoinduced electron transfer, though an additional Förster contribution cannot be ruled out on the basis of spectral overlap, ($\{[\text{Cu}_2(\text{L}^3)_2](\text{ClO}_4)_4\}$ is red).

The ligand L_3 was fairly insoluble in MeCN at mM concentration, and deposition of precipitate often resulted in turbid solutions. This causes difficulties in ascertaining any changes in the free ligand emission intensity upon co-ordination of the coumarin unit; the relative emission intensities of the resultant complexes however, could be examined. Therefore in order to monitor any modulation in the luminescence of the free ligand the emission spectrum of a saturated solution of L_3 in MeCN (filtered to remove any undissolved L_3) was obtained and an excess of metal ion added to it, results are shown in figure 4.10.

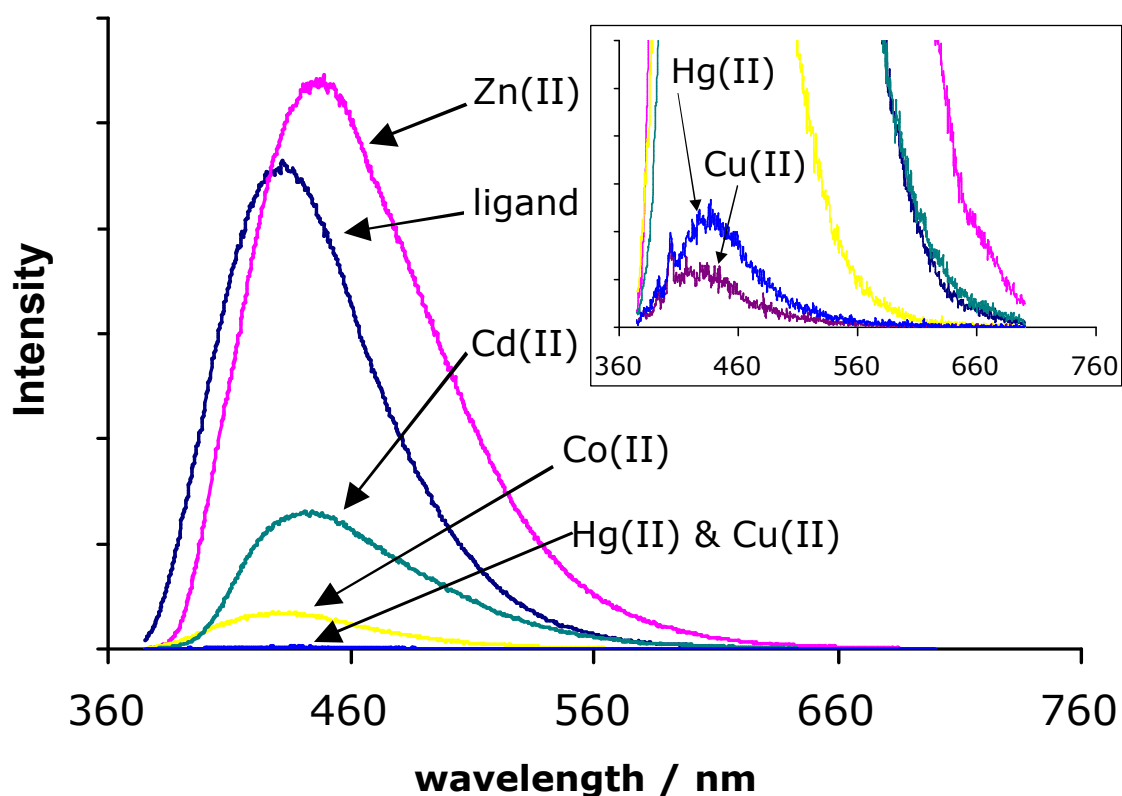


Figure 4.10 - Emission spectra for $[(\text{L}^3)_2\text{M}_2]^{4+}$ complex with a variety of metal ions.

Studies utilising both ^1H NMR and ESI-MS demonstrated that when in the presence of excess metal ion the sole species present was the dinuclear helicate. The resulting emission data are therefore representative of the latter complexes and not other higher nuclearity species. The spectral changes observed follow the same general trend as was previously observed for the stoichiometric addition of metal ions to L_3 , but highlight the enhancement of the ligand emission intensity following the addition of zinc ions.

The Zn^{2+} helicate has been shown to be more emissive (i.e. increased integrated intensity) than the unco-ordinated L_3 ligand, whereas all other transition metal complexes show varying degrees of luminescent quenching of the coumarin based emission. There is very little difference displayed in emission wavelength upon the co-ordination of the transition metal ions (Cu^{2+} , Co^{2+}), the group 12 metal ions however, do induce subtle shifts relative to the free ligand.

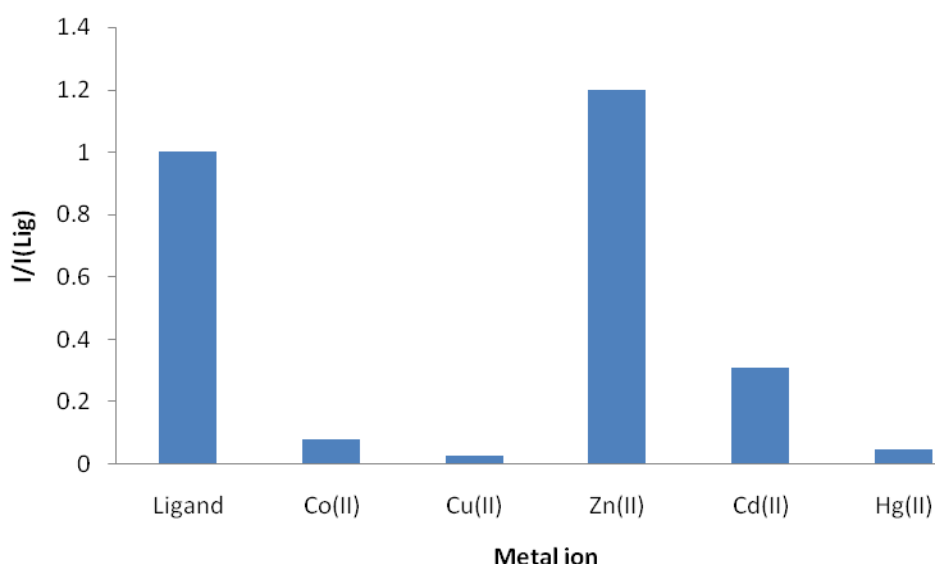


Figure 4.11 - Relative intensity of emission compared to unco-ordinated ligand L_3 .

The ligand L_3 which contains luminescent coumarin units has been shown to form helicates with divalent metal ions. The carbonyl oxygen atoms participate in co-ordination with metal ions due to steric constraints and due to this interaction results in a large change in the luminescent properties of the coumarin-based fluorophores present in the complexes. Solution state speciation studies utilising ^1H NMR and ESI-MS confirm that the dinuclear helicates form exclusively in solution, with addition of zinc ions causing an increase in

emission intensity, addition of paramagnetic (Co^{2+} and Cu^{2+}) and heavier ions however, induce varying amounts of fluorescent quenching.

5: Conclusions

In conclusion three novel and specific ligands were successfully synthesized, an aza crown macrocycle, a ligand containing a cryptate domain and a helicate ligand. The ligands were characterised using ^1H NMR spectroscopy, mass spectrometry and in some cases COSY NMR and single crystal X-ray diffraction.

The aza crown macrocycle described in chapter 1 contained both a bipyridine domain and an aza crown domain. The ligand was able to co-ordinate a Cu^{2+} ion within either domain, and formed a variety of different complexes depending on the ratio of Cu^{2+} ions to ligand present. The aza crown domain was able to co-ordinate a Cu^{2+} ion within the crown by all four of the available nitrogen groups, acting as a tetradentate donor. However, upon co-ordination of a second Cu^{2+} ion by the bipyridine unit, torsional changes meant the aza crown domain was no longer able to behave as a tetradentate donor. The aza crown co-ordinated the Cu^{2+} ion by just three of the available nitrogen ions when a second Cu^{2+} was co-ordinated by the bipyridine unit. The ligand was reprogrammed by the second Cu^{2+} ion, meaning the aza crown was changed from a tetradentate unit to a tridentate unit when both the aza crown and bipyridine domains were co-ordinated to a Cu^{2+} ion. This type of behavior is termed a negative allosteric effect, as the denticity of the aza crown is adversely affected by the co-ordination of a second Cu^{2+} ion at the bipyridine unit.

Further research could be performed by modulation of the size of the aza crown unit, aza crown domains are similar to crown ether units as they demonstrate selectivity based on ionic radius. Therefore, further ligands could be synthesized with differently sized aza crown domains in order to investigate whether larger or smaller crown unit can be reprogrammed in a similar way.

The second chapter described the synthesis and characterisation of a ditopic cryptate ligand, which possessed a cryptate domain and a pair of amine groups. The ligand reacted irreversibly with butanal when in the presence of various metal ions. The metal ion is able to co-ordinate within the cryptate domain, which enforces a smaller torsional angle within the bipyridine unit. The decreased torsional angle enabled the amine groups attached to the bipyridine unit to move into closer proximity to each other, which allowed cyclisation with butanal to occur. The cyclisation resulted in a seven membered bis-aminal species, which was found to display luminescent properties.

A variety of metal ions were introduced to the cryptate domain and cyclisation of the amine groups was performed, general enhancements of luminescence resulted. However the most intense increase in luminescence resulted when the ligand was complexed with Zn^{2+} ions.

The complex of the cyclised ligand with Zn^{2+} ions was observed to emit at a shorter wavelength when compared to the other metal ion complexes, allowing a degree of wavelength selectivity. The luminescent lifetime of the Zn^{2+} was found to be far longer than those associated with other metal ion complexes of the ligand, allowing discrimination from other ions within a competitive media.

The ligand was demonstrated to be selective for the detection of zinc ions in a competitive biological media by both wavelength selectivity and luminescent lifetime. The detection of Zn^{2+} ions is particularly interesting as Zn^{2+} ions have been implicated in a variety of diseases and in particular age related disorders. The role of Zn^{2+} ions within the body is not fully understood, consequently accurate measurement of concentration and distribution of Zn^{2+} ions within the body would be a useful diagnostic tool.

The third chapter described a ligand which was hexadentate in nature, and was able to coordinate dicationic metal ions to form a dinuclear double stranded helicate species. The symmetrical ligand consisted of a central thiazole-pyridyl-pyridyl-thiazole unit, with a coumarin unit on each terminus. Upon co-ordination of a Cu^{2+} ion the ligand partitions into two separate binding domains. These domains consist of a pyridyl-thiazole unit and an O-donor from a carbonyl oxygen group on the coumarin unit. It was found that the two methoxy groups prevented the ligand from adopting a coplanar unit due to unfavourable steric interactions. Therefore the O-donor from the carbonyl group is required to stabilize the Cu^{2+} centre forming a distorted octahedral geometry.

Coumarin is a well known fluorophore, luminescence studies revealed complexes of the ligand with various metal ions gave varying degrees of luminescent emission. The zinc complex of the ligand was found to be the most emissive by a considerable margin, while paramagnetic metal ions and heavier 2nd and 3rd row d^{10} metal ions demonstrated efficient quenching of the emission intensities.

Research concerning helicates containing organic lumophores has been relatively uncommon, therefore further ligands could be investigated based on a similar design. The addition of further binding units within the helicate ligand may allow modification of the metal centres, and therefore the emission intensity. The pyridyl-thiazole ligands are a versatile type of helicate structure, and have been utilized in reprogramming helicate ligands previously.⁹⁵⁻⁹⁸ The addition of organic lumophores to the terminal ends of these ligands may allow modification of the luminescence upon reprogramming of the ligand.

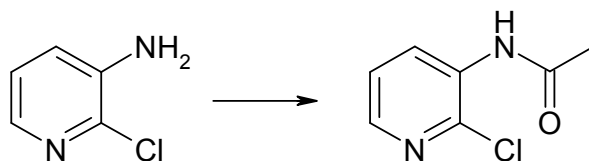
6: Experimental

General details

All starting materials and solvents were purchased from Lancaster or Aldrich and used as received (unless otherwise stated). Anhydrous solvents (DMF, THF) were purchased from Aldrich and used as supplied. The following instruments were used for routine spectroscopic analyses: Bruker DPX400 (^1H NMR) and VG Quattro II mass spectrometer with Z-spray source (ESI).

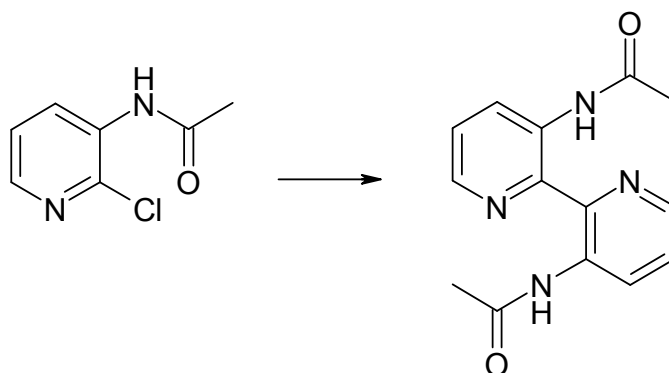
6.1 - Preparation of Aza Crown L₁

6.1.1. Synthesis of Acetylated-amino-chloropyridine



3-amino-2-chloropyridine (5 g, 0.039 mol) was dissolved in acetic anhydride under stirring, this was allowed to stir for 12 hours. The solvent was reduced by rotary evaporation, toluene added and the solvent removed again. The product was recrystallised from toluene giving a fine white crystalline powder (6.46 g, yield = 97 %). A ¹H NMR was obtained and was identical to literature values.¹⁰⁵

6.1.2. Synthesis of 3,3'-Diacetylamino-2,2'-bipyridine

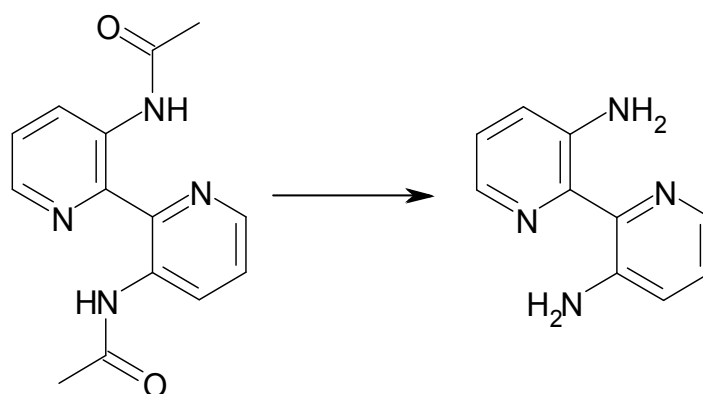


Activation of copper bronze. Copper powder (15 g, 0.24 mol) and iodine bead (3 g, 0.012 mol) were combined in acetone (150 ml) and stirred and sonicated until a grey/pink colour appeared, indicating the formation of CuI. This was filtered through a sintered glass funnel, washed with a 1:1 solution of acetone and concentrated hydrochloric acid (150ml), then washed with acetone (400 ml) and allowed to dry. The activated metal was then used immediately.

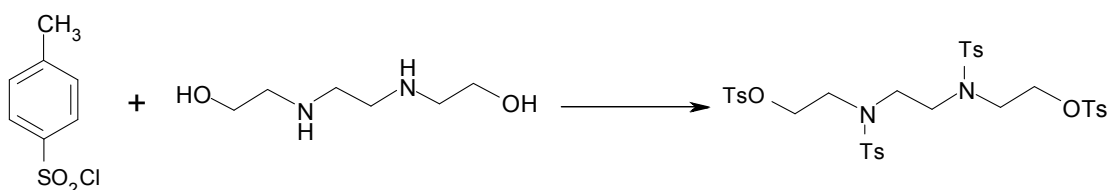
The acetylated amide (6.46 g, 0.038 mol) and copper bronze (7.0 g, 0.11 mol) were added to the two necked flask and anhydrous DMF (60 ml) was added. The solution was heated at 100 °C for 4 hours and after this time poured over water (400 ml) to give a very fine yellow brown precipitate. The precipitate was filtered off through a celite filter medium and then washed with concentrated ammonia solution (2 x 200 ml). The precipitate was allowed to dry on the celite medium for several days in a fume cupboard. One completely dry the celite

was broken up and the product extracted into DCM (5 x 100 ml), the solvent was then filtered and the solution treated with magnesium sulphate powder. Evaporation gave 3,3'-diacetylamino-2,2'-bipyridine as a pale yellow powder (4.10 g, yield = 78 %). $^1\text{H NMR}$ [500 MHz, CDCl_3], (δ); 13.1 (s, 2H, -NH), 9.1 (dd, $J = 1.4, 8.5$ Hz, 2H, -py), 8.3 (dd, $J = 1.6, 4.5$ Hz, 2H, -py), 7.4 (dd, $J = 4.5, 8.5$ Hz, 2H, -py), 2.2 (s, 6H, - CH_3).

6.1.3. Synthesis of 3,3'-Diamino-2,2'-bipyridine

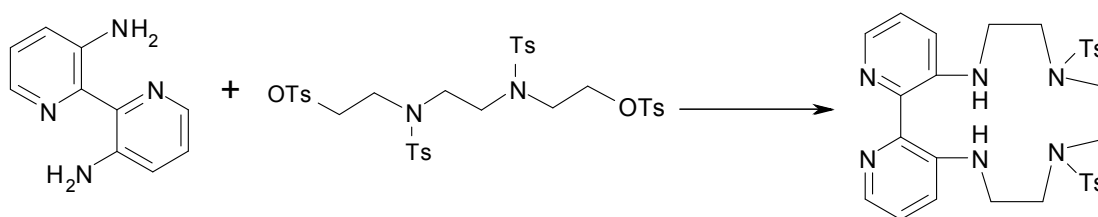


3,3'-Diacetylamino-2,2'-bipyridine (5.36 g, 0.0198 mmol) was suspended in concentrated hydrochloric acid (20 ml) and refluxed for 1 hour. Once the solution had cooled it was neutralised with concentrated ammonia solution, and the product extracted into DCM (4 x 100 ml). The solvent was removed at reduced pressure giving an iridescent yellow powder (1.85 g, yield = 50 %). $^1\text{H NMR}$ [500 MHz, CDCl_3], (δ); 8.0 (dd, $J = 1.9, 3.9$ Hz, 2H, -py), 7.0 (m, 4H, overlapping -py) 6.2 (s, 4H, - NH_2).

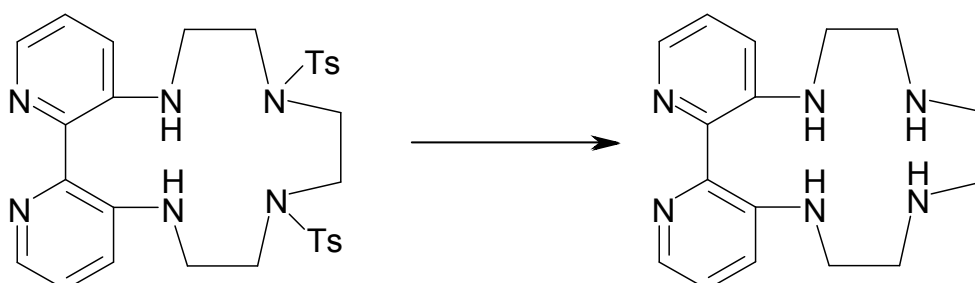


A solution of p-toluenesulfonylchloride (7.7 g, 0.04 mol) suspended in pyridine (20 ml) was added drop wise, over 2 hours to a vigorously stirred solution of N,N'-bis(2-hydroxy-ethyl) ethylene diamine (1.48 g, 0.01 mol) in pyridine (20 ml) at 0 °C. The solution was then stirred

for 4 hours while the solution returned to room temperature. This was poured over ice (50 ml) and concentrated hydrochloric acid (50 ml) and chilled for 12 hours. The solution was decanted off leaving an oily yellow brown residue. The product was recrystallised from methanol giving the product as a yellow powder which was isolated by filtration (5.67 g, yield = 74 %). $^1\text{H NMR}$ [400 MHz, CDCl_3], (δ); 7.8 (d, $J = 8.3$ Hz, 4H, -ph), 7.7 (d, $J = 8.3$ Hz, 8H, -ph), 7.4 (d, $J = 8.16$ Hz, 8H, -ph), 4.2 (t, $J = 5.3$ Hz, 4H, $-\text{NCH}_2\text{CH}_2-$), 3.4 (t, $J = 4.6$ Hz, 4H, $-\text{NCH}_2\text{CH}_2\text{O}-$), 3.3(s, 4H, $-\text{NCH}_2\text{CH}_2\text{N}-$), 2.5 (s, 12H, CH_3).



To a solution of 3,3'-diamino-2,2'-diamine (0.5 g, 2.69 mmol) in dry THF (30 ml), at -78°C , *n*-butyl lithium (7.4 ml, 1.0 M solution in hexanes) was added slowly. Upon addition, a yellow precipitate formed which was replaced by a red precipitate after more than half of the base was added. The reaction was allowed to warm to room temperature, after which the tetra-tosylate (2.06 g, 2.69 mmol) in THF (10 ml) was added and the resulting solution refluxed for 3 hours. The reaction was evaporated to dryness and purified by column chromatography (SiO_2 , 5% MeOH in DCM) giving the tosylated aza-crown as a yellow solid (0.14 g, yield = 8 %). $^1\text{H NMR}$ [400 MHz, CDCl_3], (δ); 8.21 (2H, d, $J = 4.5$; pyridyl H), 7.62 (4H, d, $J = 8.3$; tsH), 7.33 (4H, d, $J = 8.1$; tsH), 7.25 (2H, dd, $J = 7.3, 4.4$; pyridyl H), 7.10 (2H, d, $J = 7.4$; pyridyl H), 4.76 (2H, t, $J = 4.7$; pyridyl-NH), 3.8 – 2.8 (12H, m (overlapping); $-\text{CH}_2-$), 2.47 (6H, s; $-\text{CH}_3$). ESI-MS m/z 607 $\text{M} + \text{H}^+$.

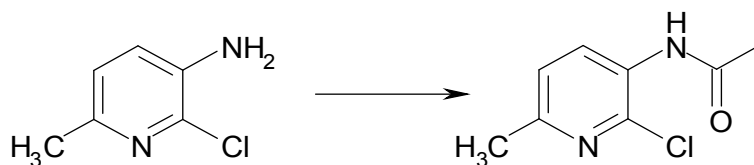


The ditosylated aza crown (0.14 g, 0.23 mmol) was suspended in concentrated H_2SO_4 and heated at 100°C for 48 hours, in a sealed vessel under an atmosphere of dinitrogen. The acidic solution was poured over ice and adjusted to pH 14 with NaOH. Extraction into DCM

(4 x 100ml), followed by evaporation gave the bipyridine aza-crown as a pale yellow solid (0.031 g, yield = 45 %). ¹H NMR [400 MHz, CDCl₃], (δ); 8.00 (2H, t, *J* = 3; pyridyl H), 7.09 (4H, d, *J* = 3; pyridyl H), 4.78 (2H, t, *J* = 4.3; pyridyl-NH), 3.40 (2H, m; -CH₂-), 3.10 (2H, m; -CH₂-), 2.70 (2H, m; -CH₂-), 2.60 (2H, d, *J* = 9.4; -CH₂-), 2.5 (m, 2H; -CH₂-), 2.3 (2H, d, *J* = 9.4 Hz; -CH₂-), terminal NH too broad to be observed. ESI-MS *m/z* 299 M + H⁺.

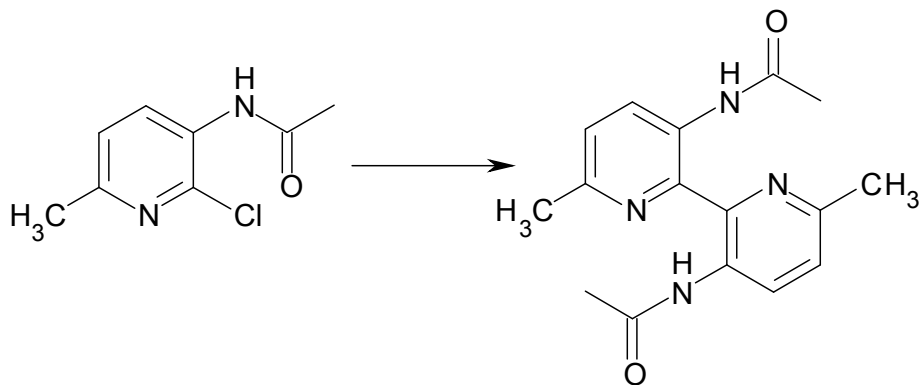
6.2 – Preparation of Diamino-Cryptate, L₂

6.2.1. Synthesis of 5-Acetylamino-6-chloro-2-picoline



5-amino-6-chloro-2-picoline (1.0 g, 7.02 mmol) and acetic anhydride (20 ml) were placed in a 50ml round bottom flask and allowed to stand for 12 hours. The solvent was removed at reduced pressure, toluene added and the solvent removed again. The product was recrystallised from toluene to give a fine brown crystalline powder (0.90 g, yield = 69 %). Structural elucidation was not performed on this product. A ¹H NMR was obtained and was identical to literature values.¹⁰⁴

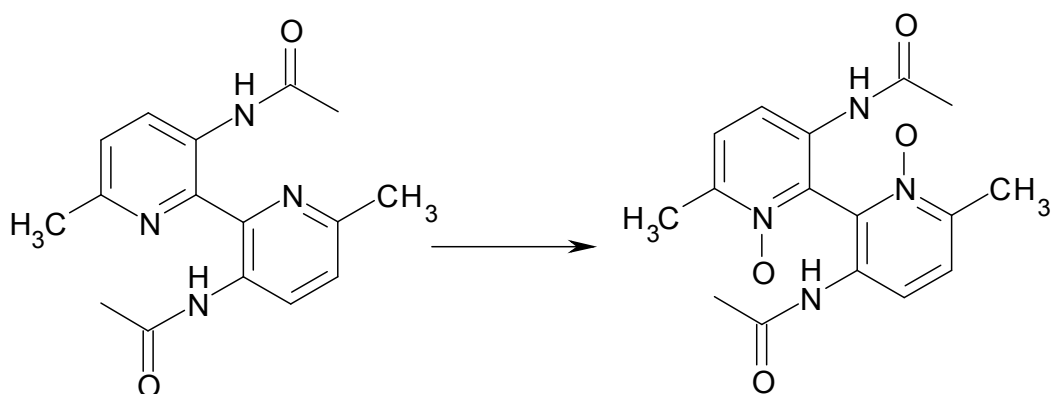
6.2.2. Synthesis of 3,3'-Diacetylamino-6,6'-dimethyl-2,2'-bipyridine



A two necked round bottom flask was charged with one equivalent of tetraethylammonium iodide (1.3 g, 3.5 mmol), 1 equivalent of [(Ph₃P)₂NiCl₂] (3.5 g, 5.3 mmol) and 2 equivalents of zinc dust (0.5 g, 7.6 mmol) and was purged with nitrogen while being heated at 80 °C for 15 minutes. Absolute DMF (20 ml) was added to the flask and the solution stirred for 30 minutes until the blue colour turned to dark red. In a separate round bottom flask 2-chloro-3-acetylamino-6-methylpyridine (0.90 g, 5.3 mmol) was purged with dinitrogen for 15 minutes and absolute DMF (10 ml) added. The solution of the amide was then transferred to the two neck flask and the resulting solution was heated at 100 °C for 24 hours. Upon cooling the solvent was removed and concentrated ammonia solution was added to the residue and the

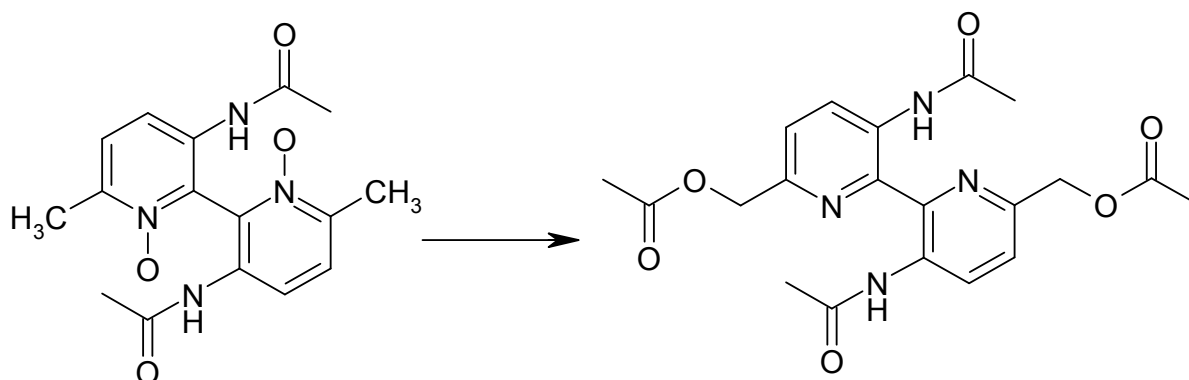
resulting suspension stirred for 1 hour. The product was extracted into DCM (3 x 150 ml), dried with magnesium sulphate powder, filtered and the solvent removed by rotary evaporation. The product was recrystallised from toluene to give beige colour crystals (0.293 g, yield = 37 %). $^1\text{H NMR}$ [400 MHz, CDCl_3] (δ); 9.0 (d, $J = 8.6$, 2H, py), 7.2 (d, $J = 8.6$ Hz, 2H, py), 2.6 (s, 6H, $-\text{CH}_3$), 2.3 (s, 6H, $-\text{CH}_3$).

6.2.3. Synthesis of 3,3'-Diacetylamino-6,6'-dimethyl-2,2'-bipyridine-N,N'-dioxide



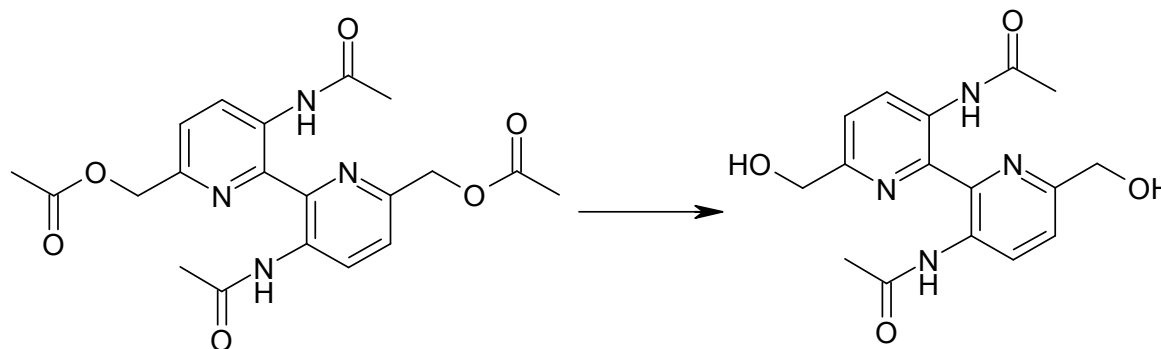
The acetylated diamine (0.293 g, 0.98 mmol) and 3 equivalents mCPBA (70%, 0.725 g, 2.94 mmol) were suspended in DCM (20 ml) and allowed to stand for 8 days. The resulting solution was passed through a pad of alumina and washed with 10% MeOH : DCM. The eluent was filtered and the solvent removed at reduced pressure. The residue was washed with hexane to give 3,3'-diacetylamino-6,6'-dimethyl-2,2'-bipyridine-N,N'-dioxide as a white solid (0.26 g, yield = 79 %). $^1\text{H NMR}$ [400 MHz, CDCl_3] (δ); 9.6 (s, -NH), 8.3 (d, $J = 8.9$, 2H, -py), 7.6 (d, $J = 8.6$ Hz, 2H, -py), 2.5 (s, 6H, $-\text{CH}_3$), 2.1 (s, 6H, $-\text{CH}_3$)

6.2.4 Synthesis of 3,3'-Diacetylamino-2,2'-bipyridine-6,6'-diacetate



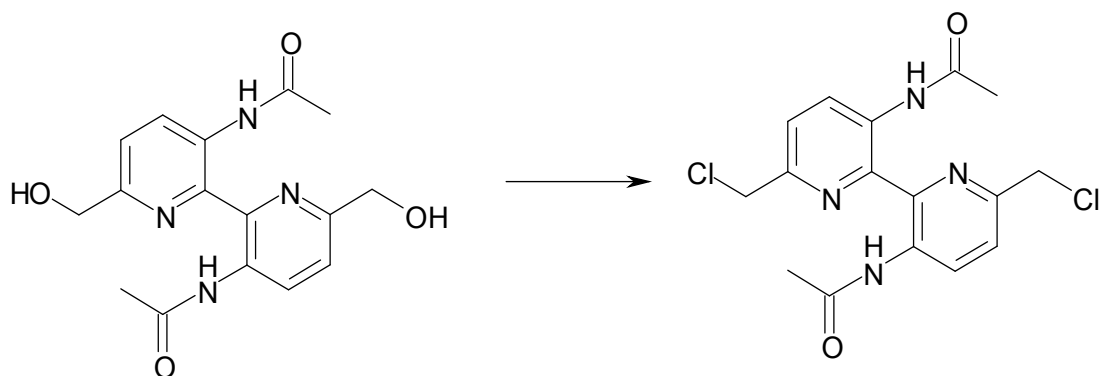
Acetic anhydride (20 ml) was added to the bis-N-oxide (0.260 g, 0.78 mmol) and the solution heated for 12 hours at 80 °C. Once the solution has cooled the solvent was removed and the product purified by column chromatography (Al₂O₃, 2% MeOH:DCM). The product was collected and the solvent removed by rotary evaporation (0.133 g, yield = 41 %). ¹H NMR [400 MHz, CDCl₃] (δ); 13.0 (s, -NH), 9.1 (d, *J* = 8.6, 2H, -py), 7.5 (d, *J* = 9.0 Hz, 2H, -py), 5.3 (s, 4H, -CH₂), 2.3 (s, 6H, -CH₃), 2.2 (s, 6H, -CH₃)

6.2.5 Synthesis of 3,3'-Diacetylamino-2,2'-bipyridine-6,6'-dimethanol



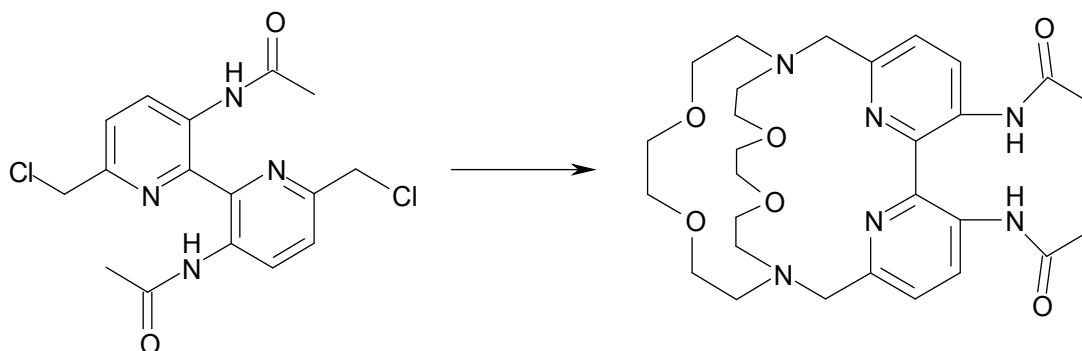
The diacetate (0.041 g, 0.1 mmol) was dissolved in MeOH (10 ml) with 3 equivalents of NaOH (0.012 g, 0.3 mmol) and stirred at room temperature for 10 hours. The resulting creamy white precipitate was filtered off at the pump (0.024 g, yield = 73 %). ¹H NMR [500 MHz, DMSO] (δ); 13.0 (s, -NH), 8.9 (d, *J* = 8.6, 2H, -py), 7.5 (d, *J* = 8.6, 2H, -py), 5.6 (t, br, -OH), 4.6 (d, *J* = 5.0 Hz, 4H, -CH₂), 2.2 (s, 6H, -2.6, -CH₃).

6.2.6 Synthesis of 3,3'-Diacetylamino-2,2'-bipyridine-6,6'-dimethylenechloride



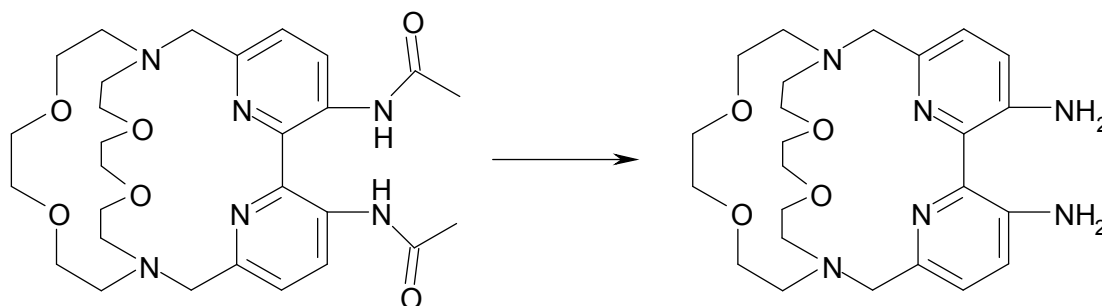
The dimethanol (0.024 g, 0.0726 mmol) was suspended in DCM with K_2CO_3 (0.10 g, 0.7 mmol) and thionyl chloride (1 ml) and the solution was refluxed until the precipitate dissolved. After cooling the solution was poured over water and extracted into DCM (3 x 150ml), the extracts were treated with magnesium sulphate, filtered and the solvent removed. The product was purified by column chromatography (Al_2O_3 , 1% MeOH:DCM) to give dimethylene chloride as a pale yellow powder (0.019 g, yield = 72 %). 1H NMR [500 MHz, $CDCl_3$] (δ); 12.4 (s, -NH), 9.1 (d, $J = 8.6$, 2H, -py), 7.4 (d, $J = 8.6$, 2H, -py), 4.6 (s, $J = 3.9$ Hz, 4H, $-CH_2$), 2.2 (s, 6H, $-CH_3$)

6.2.7 Synthesis of Diacetyl-functionalised cryptate



The dichloro derivative (0.055 g, 0.15 mmol), 1 equivalent of diaza-18-crown-6 (0.311 g, 0.118 mmol), a catalytic amount of NaI and Na_2CO_3 were dissolved in acetonitrile (20 ml) and refluxed for 3 days. Once cooled the solvent was removed and the product was purified using column chromatography (Al_2O_3 , 5% MeOH:DCM), giving the product was a orange oily solid (0.022 g, yield = 26 %). 1H NMR [500 MHz, CD_3CN] (δ); 10.0 (s, -NH), 8.1 (d, $J = 8.2$, 2H, -py), 7.3 (d, $J = 8.3$ Hz, 2H, -py), 4.0-2.1 (m, 24H, $-CH_2$)

6.2.8 Synthesis of Diamino-functionalised cryptate



The acetylated cryptate (0.02 g, 0.05 mmol) was suspended in HCl (3M, 10 ml) and allowed to stand for 3 days. After this time the solution was neutralised with concentrated ammonia solution and extracted immediately with DCM (3 x 100ml) and the solution dried and the solvent removed by rotary evaporation. Recrystallisation from CHCl_3 gave the cryptate (as the ammonium iodide salt) as a pale orange crystalline solid (0.016 g, yield = 62 %). $^1\text{H NMR}$ [500 MHz, CD_3CN] (δ); 7.50, (t, $J = 51.5$, 4H, NH_4^+), 7.16, (d, $J = 8.2$, 2H, py), 7.12, (d, $J = 8.2$, 2H, py), 4.46, (s, 4H, $-\text{NH}_2$), 3.96, (d, 2H, $J = 12.6$ Hz), 3.82, (t, 2H), 3.70, (m, 2H); 3.58 – 3.37, (d, m, m overlapping, 12H), 3.16, (t, 2H), 2.86, (m, 4H), 2.16, (m, 4H). ESI-MS 473 M + H^+ .

6.2.9 Formation of Barium complex $[\text{LBa}](\text{ClO}_4)_2$

In a typical experiment the ammonium cryptate $[\text{L}_2\text{NH}_4]\text{I}$ (5 mg, 8.1×10^{-3} mmol) in MeCN (1 ml) was added to an excess of $\text{Ba}(\text{ClO}_4)_2 \cdot 6\text{H}_2\text{O}$ (15 mg, 4.0×10^{-2} mmol), diethyl ether was then slowly diffused over 24 hrs. After which time, yellow crystals were deposited, which were collected by filtration (1.2 mg, 48%). $^1\text{H NMR}$ [500 MHz, CD_3CN] (δ); 7.39, (d, $J = 8.3$, 2H, py), 7.32, (d, $J = 8.3$ Hz, 2H, py), 4.69, (s, 4H, $-\text{NH}_2$); 3.92 – 3.53, m overlapping, 18H) 3.42, (m, 2H) 3.10, (m, 2H) 2.90, (m, 2H), 2.82, (m, 2H) 2.60, (m, 2H). ESI-MS 305 $[\text{L}_2\text{Ba}]^{2+}$

6.2.10 Formation of Barium cyclised complex $[\text{L}_2\text{Ba}](\text{ClO}_4)_2$

In a typical experiment the ammonium cryptate $[\text{L}_2\text{NH}_4]\text{I}$ (5 mg, 8.1×10^{-3} mmol) in MeCN (1 ml) was added to an excess of $\text{Ba}(\text{ClO}_4)_2 \cdot 6\text{H}_2\text{O}$ (15 mg, 4.0×10^{-2} mmol) and one drop of butyaldehyde, diethyl ether was then slowly diffused over 24 hrs. After which time, yellow crystals were deposited, which were collected by filtration (3.2 mg, 53%). $^1\text{H NMR}$ [500 MHz, CD_3CN] (δ); 7.30 (d, $J = 8.2$, 2H, py), 7.14 (d, $J = 8.2$, 2H, py), 5.50 (d, $J = 3.6$, 2H, $-\text{NH}$) 4.33 (m, 1H, $\text{CH}_3\text{CH}_2\text{CH}_2\text{CH}-$) 4.16 (d, $J = 13.6$, 2H), 3.78 – 3.57 (m, overlapping, 14H), 3.28 (m, 2H, 3.10 (m, 2H), 2.94 (m, 2H), 2.78 (m, 2H), 2.65 (m, 2H), 2.53 (m, 2H), 1.77 (m, 2H, $\text{CH}_3\text{CH}_2\text{CH}_2\text{CH}-$), 1.52 (m, 2H, $\text{CH}_3\text{CH}_2\text{CH}_2\text{CH}-$), 0.95 (t, $J = 7.3$ Hz, 3H, $\text{CH}_3\text{CH}_2\text{CH}_2\text{CH}-$).

ESI-MS 736 $\{[2\text{Ba}]\text{ClO}_4\}^+$ HR ESI-MS found 736.178126 $\text{C}_{28}\text{H}_{42}\text{BaClN}_6\text{O}_8$ requires 763.179957 (error 2.4 ppm).

6.2.11 Formation of Zinc complex $[\text{L}_2\text{Zn}](\text{CF}_3\text{SO}_3)_2$

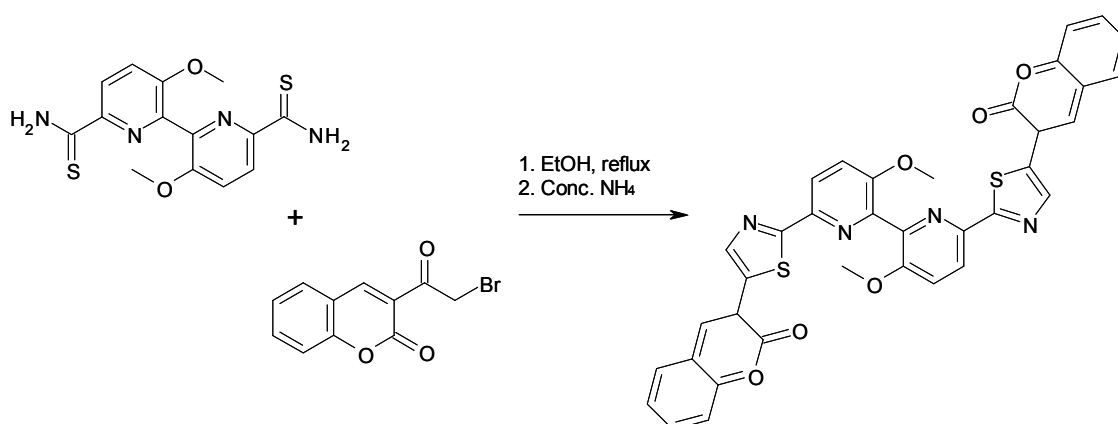
In a typical experiment the ammonium cryptate $[\text{L}_2\text{NH}_4]\text{I}$ (5 mg, 8.1×10^{-3} mmol) in MeCN (1 ml) was added to an excess of $\text{Zn}(\text{ClO}_4)_2 \cdot 6\text{H}_2\text{O}$ (15 mg, 4.0×10^{-2} mmol), diethyl ether was then slowly diffused in over 24 hrs. After which time orange crystals were deposited, which were collected by filtration (2.8 mg, 50%). ^1H NMR [500 MHz, CD_3CN] (δ); 7.55 (d, $J = 8.4$ Hz, 2H, py), 7.39 (d, $J = 8.4$, 2H, py), 5.17 (s, 4H, $-\text{NH}_2$), 4.00 (s, 4H), 3.69 (m, 4H), 3.60 – 3.50 (m overlapping, 8H), 3.36 – 3.26 (m overlapping, 8H), 2.86 (m, 4H). ESI-MS 685 $\{[1\text{Zn}]\text{CF}_3\text{SO}_3\}^+$ HR ESI-MS found 685.160315 $\text{C}_{25}\text{H}_{36}\text{F}_3\text{N}_6\text{O}_7\text{SZn}$ requires 685.160426 (error 0.16 ppm)

6.2.12 Formation of Zinc cyclised complex $[\text{L}_2\text{Zn}](\text{ClO}_4)_2$

In a typical experiment the ammonium cryptate $[\text{L}_2\text{NH}_4]\text{I}$ (5 mg, 8.1×10^{-3} mmol) in MeCN (1 ml) was added an excess of $\text{Zn}(\text{ClO}_4)_2 \cdot 6\text{H}_2\text{O}$ (15 mg, 4.0×10^{-2} mmol) and one drop of butyaldehyde, diethyl ether was then slowly diffused in over 24 hrs. After which time orange crystals were deposited, which were collected by filtration (3 mg, 47 %). ^1H NMR [500 MHz, CD_3CN] (δ); 7.48 (d, $J = 8.4$, 2H), 7.22 (d, $J = 8.4$, 2H), 5.91 (s, 2H), 4.15 (m, 1H, $\text{CH}_3\text{CH}_2\text{CH}_2\text{CH}-$), 4.01 (m, 4H), 3.74 – 3.32 (m overlapping, 18H), 3.15 (m, 2H) 2.87 (m, 4H), 1.86 (m, 2H, $\text{CH}_3\text{CH}_2\text{CH}_2\text{CH}-$), 1.56 (m, 2H, $\text{CH}_3\text{CH}_2\text{CH}_2\text{CH}-$), 0.97 (t, $J = 7.3$ Hz, 3H, $\text{CH}_3\text{CH}_2\text{CH}_2\text{CH}-$). ESI-MS 689 $\{[2\text{Zn}]\text{ClO}_4\}^+$ HR ESI-MS found 689.201874 $\text{C}_{28}\text{H}_{42}\text{ClN}_6\text{O}_8\text{Zn}$ requires 689.203863 (error 2.89 ppm).

6.3 – Preparation of Luminescent Transition Metal Helicate, L₃

6.3.1 Synthesis of Coumarin-containing helicate, L₃



A suspension of 3,3'-dimethoxy-2,2'-bipyridine-6,6'-dithioamide ¹⁰⁶ (0.57 g, 2.13 mmol) and 3-bromoacetylcoumarin (1.57 g, 4.69 mmol) in ethanol (50 ml) was refluxed for 8 hours and subsequently stirred for 12 hours. The resulting solid was isolated by filtration and washed with ethanol (4 ml) and then ether (4 ml). The free ligand was isolated from the HBr complex by suspension in aqueous ammonia solution overnight. The solid precipitate was filtered and washed with water (4 ml), ethanol (4 ml) and ether (4 ml), and then dried (0.8 g, 56%). ¹H NMR [400MHz, DMSO], (δ); 9.05 (s, 2H, tz), 8.47 (s, 2H, Ar), 8.46 (d, J = 7.2 Hz, 2H, py), 8.00 (d, J = 7.2 Hz, 2H, py), 7.87 (d, J = 8.7 Hz, 2H, Ar), 7.69 (t, J = 7.4 Hz, 2H, Ar), 7.51 (d, J = 8.5 Hz, 2H, Ar), 7.46 (t, J = 7.5 Hz, 2H, Ar), 3.91 (s, 6H, -OMe). ESI-MS 671 [M + H⁺].

6.3.2 Formation of the helicate complexes [M₂(L₃)₂](ClO₄)₄ (M = Zn²⁺, Cd²⁺, Hg²⁺ and Cu²⁺)

In a typical procedure: Zn(ClO₄)₂·6H₂O (0.003 g, 7.45 μmol) was added to a suspension of L₃ (0.005 g, 7.45 μmol) in MeCN (2 ml) and the solution stirred until dissolved. The solution was filtered and slow vapour diffusion with ethyl acetate yielded colourless crystals (8.2 mg, 59 %); Cu²⁺ (7.1 mg, 51 %); Cd²⁺ (6.3 mg, 43 %); Hg²⁺ (8.4 mg, 53 %). For ¹H NMR see text.

References

1. P. D. Beer, P. A. Gale and D. K. Smith, *Supramolecular Chemistry*, Oxford University Press, Oxford, 1999.
2. J. W. Steed and J. L. Atwood, *Supramolecular Chemistry*, John Wiley and Sons, Chichester, 2000.
3. J. M. Lehn, *Angewandte Chemie-International Edition in English*, 1988, **27**, 89-112.
4. N. F. Curtis, *Journal of the chemical society* 1964, 2644-2650.
5. C. J. Pedersen, *Journal of the American Chemical Society*, 1967, **89**, 7017 - 7036.
6. E. G. Jager, *Zeitschrift für Chemie*, 1964, **4**, 437.
7. J. D. Curry and D. H. Busch, *Journal of the American Chemical Society*, 1964, **86**, 592 -594.
8. B. Dietrich, J. M. Lehn and J. P. Sauvage, *Tetrahedron Letters*, 1969, **34**, 2889 - 2892.
9. N. F. Curtis and D. A. House, *Journal of the American Chemical Society*, 1962, **84**, 3248-3250.
10. C. J. Pedersen, *Angewandte Chemie-International Edition*, 1988, **27**, 1021 - 1027.
11. E. Fischer, *Berichte der Deutschen Chemischen Gesellschaft* 1894, **27**, 2985 - 2993.
12. J. M. Lehn, *Pharmaceutica Acta Helvetiae*, 1995, **69**, 205-211.
13. C. J. Pedersen, *Journal of the American Chemical Society*, 1970, **89**, 391-394.
14. G. W. Gokel, *Chemical Society Reviews*, 1992, **21**, 39-47.
15. H. J. Schneider and A. K. Yatsimirsky, *Chemical Society Reviews*, 2008, **37**, 263-277.
16. J. W. Steed, D. R. Turner and K. J. Wallace, *Core concepts in supramolecular chemistry and nanotechnology*, John Wiley and Sons, 2007.
17. J. Rebek, *Journal of the American Chemical Society*, 1980, **102**, 4853-4854.
18. S. Jacobson and R. Pizer, *Journal of the American Chemical Society*, 1993, **115**, 11216-11221.
19. S. J. M. Koskela, T. M. Fyles and T. D. James, *Chemical Communications*, 2005, 945-947.
20. N. F. Curtis and P. O. Whimp, *Journal of the Chemical Society a -Inorganic Physical Theoretical*, 1966, 867-871.
21. P. O. Whimp and N. F. Curtis, *Journal of the Chemical Society a -Inorganic Physical Theoretical*, 1966, 1827-1830.
22. N. F. Curtis, *Journal of the chemical society* 1967, 1979-1980.
23. P. O. Whimp and N. F. Curtis, *Journal of the Chemical Society a -Inorganic Physical Theoretical*, 1968, 188-190.
24. P. O. Whimp, N. F. Curtis and M. F. Bailey, *Journal of the Chemical Society a - Inorganic Physical Theoretical*, 1970, 1956-1963.
25. N. F. Curtis and G. W. Reader, *Journal of the Chemical Society a -Inorganic Physical Theoretical*, 1971, 1771-1777.
26. S. C. Jackels, D. H. Busch, Barefiel.Ek, N. J. Rose and K. Farmery, *Inorganic Chemistry*, 1972, **11**, 2893-2901.
27. S. El Ghachtouli, C. Cadiou, I. Dechamps-Olivier, F. Chuburu, M. Aplincourt, V. Patinec, M. Le Baccon, H. Handel and T. Roisnel, *New Journal of Chemistry*, 2006, **30**, 392-398.
28. C. Bazzicalupi, A. Bencini, A. Bianchi, A. Danesi, C. Giorgi, C. Lodeiro, F. Pina, S. Santarelli and B. Valtancoli, *Chemical Communications*, 2005, 2630-2632.
29. C. Bazzicalupi, S. Biagini, A. Bencini, E. Faggi, C. Giorgi, I. Matera and B. Valtancoli, *Chemical Communications*, 2006, 4087-4089.
30. C. Bazzicalupi, A. Bencini, A. Bianchi, S. Del Piero, P. Fornasari, C. Giorgi, A. Melchior, R. Portanova, M. Tolazzi and B. Valtancoli, *New Journal of Chemistry*, 2005, **29**, 805-811.

31. C. Bazzicalupi, A. Bencini, A. Bianchi, L. Borsari, A. Danesi, C. Giorgi, C. Lodeiro, P. Mariani, F. Pina, S. Santarelli, A. Tamayo and B. Valtancoli, *Dalton Transactions*, 2006, 4000-4010.
32. C. Bazzicalupi, A. Bencini, A. Bianchi, A. Danesi, C. Giorgi, M. A. M. Lorente and B. Valtancoli, *New Journal of Chemistry*, 2006, **30**, 959-965.
33. C. Bazzicalupi, A. Bencini, E. Faggi, A. Garau, C. Giorgi, V. Lippolis, A. Perra and B. Valtancoli, *Dalton Transactions*, 2006, 1409-1418.
34. C. Bazzicalupi, A. Bencini, L. Bussotti, E. Berni, S. Biagini, E. Faggi, P. Foggi, C. Giorgi, A. Lapini, A. Marcelli and B. Valtancoli, *Chemical Communications*, 2007, **12**, 1230 - 1232.
35. J. M. Lehn, *Journal of the American Chemical Society*, 1978, **100**, 4914-4916.
36. D. J. Cram, *Science*, 1988, **240**, 760-767.
37. J. M. Lehn, *Supramolecular Chemistry: Concepts and perspectives*, VCH, Weinheim, 1995.
38. K. K. Sadhu, S. Banerjee, A. Datta and P. K. Bharadwaj, *Chemical Communications*, 2009, 4982-4984.
39. J. B. Coldwell, C. E. Felton, L. P. Harding, R. Moon, S. J. A. Pope and C. R. Rice, *Chemical Communications*, 2006, 5048-5050.
40. M. H. V. Werts, R. H. Woudenberg, P. G. Emmerink, R. B. Gassel, J. W. Hofstraat and J. W. Verhoeven, *Angewandte Chemie-International Edition*, 2000, **39**, 4542-4544.
41. L. Kovbasyuk and R. Kramer, *Chemical Reviews*, 2004, **104**, 3161-3187.
42. Y. Kobuke and Y. Satoh, *Journal of the American Chemical Society*, 1992, **114**, 789-790.
43. T. Nabeshima, Y. Yoshihira, T. Saiki, S. Akine and E. Horn, *Journal of the American Chemical Society*, 2002, **125**, 28-29.
44. Y. Kobuke, K. Kokubo and M. Munakata, *Journal of the American Chemical Society*, 1995, **117**, 12751-12758.
45. J. Monod, J. P. Changeux and F. Jacob, *Journal of Molecular Biology*, 1963, **6**, 306-&.
46. B. Kobe and B. E. Kemp, *Nature*, 1999, **402**, 373-376.
47. J. Rebek, T. Costello and R. Wattlely, *Journal of the American Chemical Society*, 1985, **107**, 7487-7493.
48. J. Rebek, *Accounts of Chemical Research*, 1984, **17**, 258-264.
49. J. Rebek, J. E. Trend, R. V. Wattlely and S. Chakravorti, *Journal of the American Chemical Society*, 1979, **101**, 4333-4337.
50. D. E. Koshland, *Proceedings of the National Academy of Sciences of the United States of America*, 1958, **44**, 98 -104.
51. R. W. Cattrall, *Chemical Sensors*, Oxford University Press, Oxford, 1997.
52. B. R. Eggins, *Chemical Sensors and Biosensors*, John Wiley and Sons, Colchester, 2002.
53. E. M. Nolan, J. Jaworski, M. E. Racine, M. Sheng and S. J. Lippard, *Inorganic Chemistry*, 2006, **45**, 9748-9757.
54. E. M. Nolan and S. J. Lippard, *Inorganic Chemistry*, 2004, **43**, 8310-8317.
55. S. C. Burdette, G. K. Walkup, B. Spingler, R. Y. Tsien and S. J. Lippard, *Journal of the American Chemical Society*, 2001, **123**, 7831-7841.
56. A. E. Dennis and R. C. Smith, *Chemical Communications*, 2007, 4641-4643.
57. S. J. A. Pope and R. H. Laye, *Dalton Transactions*, 2006, 3108-3113.
58. T. Gunnlaugsson and J. P. Leonard, *Dalton Transactions*, 2005, 3204-3212.
59. M. Taki, J. L. Wolford and T. V. O'Halloran, *Journal of the American Chemical Society*, 2004, **126**, 712-713.
60. M. Taki, M. Desaki, A. Ojida, S. Iyoshi, T. Hirayama, I. Hamachi and Y. Yamamoto, *Journal of the American Chemical Society*, 2008, **130**, 12564-+.
61. C. J. Frederickson and A. I. Bush, *Biometals*, 2001, **14**, 353-366.

62. S. C. Burdette and S. J. Lippard, *Proceedings of the National Academy of Sciences of the United States of America*, 2003, **100**, 3605-3610.
63. E. L. Que, D. W. Domaille and C. J. Chang, *Chemical Reviews*, 2008, **108**, 4328-4328.
64. J.-Y. Lee, T. B. Cole, R. D. Palmiter, S. W. Suh and J.-Y. Koh, *Proceedings of the National Academy of Sciences of the United States of America*, 2002, **99**, 7705-7710.
65. G. K. Walkup, S. C. Burdette, S. J. Lippard and R. Y. Tsien, *Journal of the American Chemical Society*, 2000, **122**, 5644-5645.
66. K. Hanaoka, K. Kikuchi, H. Kojima, Y. Urano and T. Nagano, *Angewandte Chemie-International Edition*, 2003, **42**, 2996-2999.
67. C. J. Chang, J. Jaworski, E. M. Nolan, M. Sheng and S. J. Lippard, *Proceedings of the National Academy of Sciences of the United States of America*, 2004, **101**, 1129-1134.
68. F. Qian, C. L. Zhang, Y. M. Zhang, W. J. He, X. Gao, P. Hu and Z. J. Guo, *Journal of the American Chemical Society*, 2009, **131**, 1460-1468.
69. E. C. Constable and A. M. W. Cargill Thompsons, *Journal of the Chemical society, Dalton transactions*, 1994, 1409-1414-1418.
70. E. C. Constable, in *Progress in Inorganic Chemistry*, ed. K. D. Karlin, Wiley Interscience, Editon edn., 1994, vol. 42.
71. J. M. Lehn, *Chemical Society Reviews*, 2007, **36**, 151-160.
72. M. Fujita, *Chemical Society Reviews*, 1998, **27**, 417-425.
73. P. N. Remya, S. Biju, M. L. P. Reddy, A. H. Cowley and M. Findlater, *Inorganic Chemistry*, 2008, **47**, 7396-7404.
74. A. R. Stefankiewicz, G. Rogez, J. Harrowfield, M. Drillon and J. M. Lehn, *Dalton Transactions*, 2009, 5787.
75. L. N. Dawe and L. K. Thompson, *Dalton Transactions*, 2008, 3610-3618.
76. Y. S. Moroz, K. Kulon, M. Haukka, E. Gumienna-Kontecka, H. Kozlowski, F. Meyer and I. O. Frtsky, *Inorganic Chemistry*, 2008, **47**, 5656-5665.
77. J. I. Van Der Vlugt, S. Demeshko, S. Dechert and F. Meyer, *Inorganic Chemistry*, 2008, **47**, 1576-1585.
78. S. R. Parsons, L. K. Thompson, S. K. Dey, C. Wilson and J. A. K. Howard, *Inorganic Chemistry*, 2006, **45**, 8832-8834.
79. J. R. Price, N. G. White, A. Perez-Velasco, G. B. Jameson, C. A. Hunter and S. Brooker, *Inorganic Chemistry*, 2008, **47**, 10729-10738.
80. J. R. Price, Y. Lan and S. Brooker, *Dalton Transactions*, 2007, 1807-1820.
81. L. Hou, D. Li, W.-J. Shi, Y.-G. Yin and S.-W. Ng, *Inorganic Chemistry*, 2005, **44**, 7825-7832.
82. S. Leininger, B. Olenyuk and P. J. Stang, *Chemical Reviews*, 2000, **100**, 853-908.
83. M. Fujita, S. Nagao and K. Ogura, *Journal of the American Chemical Society*, 1995, **117**, 1649-1650.
84. S. P. Argent, H. Adams, T. Riis-Johannessen, J. C. Jeffery, L. P. Harding and M. D. Ward, *Journal of the American Chemical Society*, 2006, **128**, 72-73.
85. N. K. Al-Rasbi, I. S. Tidmarsh, S. P. Argent, H. Adams, L. P. Harding and M. D. Ward, *Journal of the American Chemical Society*, 2008, **130**, 11641-11649.
86. S. P. Argent, H. Adams, T. Riis-Johannessen, J. C. Jeffery, L. P. Harding, O. Mamula and M. D. Ward, *Inorganic Chemistry*, 2006, **45**, 3905-3919.
87. I. S. Tidmarsh, T. B. Faust, H. Adams, L. P. Harding, L. Russo, W. Clegg and M. D. Ward, *Journal of the American Chemical Society*, 2008, **130**, 15167-15175.
88. M. D. Ward, *Chemical Communications*, 2009, 4487-4499.
89. R. L. Paul, A. J. Amoroso, P. L. Jones, S. M. Couchman, Z. R. Reeves, L. H. Rees, J. C. Jeffery, J. A. McCleverty and M. D. Ward, *Dalton Transactions*, 1999, 1563-1568.
90. M. Albrecht, *Chemical Reviews*, 2001, **101**, 3457-3497.

91. J. M. Lehn, A. Rigault, J. Siegel, J. Harrowfield, B. Chevrier and D. Moras, *Proceedings of the National Academy of Sciences of the United States of America*, 1987, **84**, 2565-2569.
92. L. P. Harding, J. C. Jeffery, T. Riis-Johannessen, C. R. Rice and Z. T. Zeng, *Dalton Transactions*, 2004, 2396-2397.
93. M. Barley, E. C. Constable, S. A. Corr, R. C. S. McQueen, J. C. Nutkins, M. D. Ward and M. G. B. Drew, *Journal of the Chemical Society-Dalton Transactions*, 1988, 2655-2662.
94. C. S. Tsang, H. L. Yeung, W. T. Wong and H. L. Kwong, *Chemical Communications*, 2009, 1999-2001.
95. C. J. Baylies, L. P. Harding, J. C. Jeffery, T. Riis-Johannessen and C. R. Rice, *Angewandte Chemie-International Edition*, 2004, **43**, 4515-4518.
96. C. J. Baylies, T. Riis-Johannessen, L. P. Harding, J. C. Jeffery, R. Moon, C. R. Rice and M. Whitehead, *Angewandte Chemie-International Edition*, 2005, **44**, 6909-6912.
97. G. Bokolinis, T. Riis-Johannessen, L. P. Harding, J. C. Jeffery, N. McLaya and C. R. Rice, *Chemical Communications*, 2006, 1980-1982.
98. H. J. Clayton, L. P. Harding, J. P. Irvine, J. C. Jeffery, T. Riis-Johannessen, A. P. Laws, C. R. Rice and M. Whitehead, *Chemical Communications*, 2008, 108-110.
99. T. Riis-Johannessen, L. P. Harding, J. C. Jeffery, R. Moon and C. R. Rice, *Dalton Transactions*, 2007, 1577-1587.
100. C. J. Baylies, J. C. Jeffery, T. A. Miller, R. Moon, C. R. Rice and T. R. Riis-Johannessen, *Chemical Communications*, 2005, 4158-4160.
101. V. Armendola, Y. D. Fernandez, C. Mangano, M. Montalti, P. Pallavicini, L. Prodi, N. Zaccheroni and M. Zema, *Dalton Transactions*, 2003, 4340.
102. T. Riis-Johannessen, L. P. Harding, J. C. Jeffery, A. P. Robson, C. R. Rice, *Inorg. Chim. Acta*, 2005, **358**, 2781-2798
103. J. C. Jeffery, T. Riis-Johannessen, C. J. Anderson, C. J. Adams, A. Robinson, S. P. Argent, M. D. Ward, C. R. Rice, *Inorg. Chem.*, 2007, **46**, 2417
104. H. S. Jung, P. S. Kwon, J. W. Lee, J. I. Kim, C. S. Hong, J. W. Kim, S. Yan, J. Y. Lee, J. H. Lee, T. Joo, J. S. Kim, *J. Am. Chem. Soc.*, 2009, **131**, 2008
105. C. R. Rice, S. Onions, N. Vidal, J. D. Wallis, M.C. Senna, M. Pilkington, H. Stoeckli-Evans, *Eur. J. Inorg. Chem.* 2002, 1985.
106. Prepared from 2-bromo-3-methoxypyridine see: Clayton, H. J., 2008, Synthesis and coordination chemistry of ligands for supramolecular chemistry and sensing applications, Thesis (PhD) University of Huddersfield

Copyright Declaration

- i. The author of this thesis (including any appendices and/or schedules to this thesis) owns any copyright in it (the "Copyright") and s/he has given The University of Huddersfield the right to use such Copyright for any administrative, promotional, educational and/or teaching purposes.
- ii. Copies of this thesis, either in full or in extracts, may be made only in accordance with the regulations of the University Library. Details of these regulations may be obtained from the Librarian. This page must form part of any such copies made.
- iii. The ownership of any patents, designs, trade marks and any and all other intellectual property rights except for the Copyright (the "Intellectual Property Rights") and any reproductions of copyright works, for example graphs and tables ("Reproductions"), which may be described in this thesis, may not be owned by the author and may be owned by third parties. Such Intellectual Property Rights and Reproductions cannot and must not be made available for use without the prior written permission of the owner(s) of the relevant Intellectual Property Rights and/or Reproductions.

Appendix 1: Crystal Data Tables

Table 1 – Aza crown ligand crystallographic data ^a

Compound	L ₁
Formula	C ₁₆ H ₂₂ N ₆
M (g mol ⁻¹)	298.39
System, space group	Monoclinic, <i>P</i> 2 ₁
<i>a</i> /Å	9.0171(8)
<i>b</i> /Å	10.4120(9)
<i>c</i> /Å	16.4432(15)
<i>α</i> /°	90
<i>β</i> /°	92.592(2)
<i>γ</i> /°	90
<i>V</i> /Å ³	1542.2(2)
<i>Z</i>	4
<i>μ</i> /mm ⁻¹	0.082
Reflections collected: Total, independent, <i>R</i> _{int}	15305, 3806, 0.0284
Final <i>R</i> ₁ , <i>wR</i> ₂ ^{b,c}	0.0986, 0.0384

^a Bruker APEX-II-CCD area detector diffractometer using Mo-K α ₁ radiation; temperature of data collection 100 K.

^b Structure was refined on F_o^2 using all data; the value of *R*₁ is given for comparison with older refinements based on F_o with a typical threshold of $F \geq 4\sigma(F)$.

^c $wR_2 = [\sum[w(F_o^2 - F_c^2)^2] / \sum w(F_o^2)^2]^{1/2}$ where $w^{-1} = \sigma^2(F_o^2) + (aP)^2 + (bP)$ and $P = [\max(F_o^2, 0) + 2F_c^2]/3$

Table 2 – [Cu(L₁)]²⁺ Crystallographic data

Compound	[Cu(L ₁)Cl][Cl] MeCN·0.5MeCO ₂ Et
Formula	C ₁₈ H ₂₆ Cl ₂ CuN ₆ O
M (g mol ⁻¹)	476.89
System, space group	Monoclinic C2/c
a/Å	18.9791(5)
b/Å	15.7030(4)
c/Å	16.1009(5)
α/°	90
β/°	103.9230(10)
γ/°	90
V/Å ³	4657.6(2)
Z	8
μ/mm ⁻¹	3.595
Reflections collected: Total, independent, R _{int}	17740, 4348, 0.0456
Final R ₁ , wR ₂ ^{b,c}	0.1052, 0.0399

^a Bruker rotating anode Proteum-CCD area detector diffractometer using Cu-Kα₁ radiation; temperature of data collection 100 K.

^b Structure was refined on F_o^2 using all data; the value of R₁ is given for comparison with older refinements based on F_o with a typical threshold of $F \geq 4\sigma(F)$.

^c $wR_2 = [\sum[w(F_o^2 - F_c^2)^2] / \sum w(F_o^2)^2]^{1/2}$ where $w^{-1} = \sigma^2(F_o^2) + (aP)^2 + (bP)$ and $P = [\max(F_o^2, 0) + 2F_c^2]/3$

Table 3 – [Cu₂(L₁)]⁴⁺ Crystallographic data

Compound	{[Cu ₂ (L ₁)Cl ₄]·1.5MeOH·0.5H ₂ O}
Formula	C ₃₅ H ₅₈ Cl ₈ Cu ₄ N ₁₂ O ₄
M (g mol ⁻¹)	1246.68
System, space group	Monoclinic C2/c
a/Å	33.163(4)
b/Å	11.0684(16)
c/Å	14.2704(18)
α/°	90
β/°	102.902(6)
γ/°	90
V/Å ³	5105.9(12)
Z	4
μ/mm ⁻¹	2.111
Reflections collected: Total, independent, R _{int}	20143, 20143
Final R ₁ , wR ₂ ^{b,c}	0.1538, 0.0600

^a Bruker rotating anode Proteum-CCD area detector diffractometer using Mo-Kα₁ radiation; temperature of data collection 100 K.

^b Structure was refined on F_o^2 using all data; the value of R₁ is given for comparison with older refinements based on F_o with a typical threshold of $F \geq 4\sigma(F)$.

^c $wR_2 = [\sum[w(F_o^2 - F_c^2)^2] / \sum w(F_o^2)^2]^{1/2}$ where $w^{-1} = \sigma^2(F_o^2) + (aP)^2 + (bP)$ and $P = [\max(F_o^2, 0) + 2F_c^2]/3$

Table 4 – Diamino-functionalised cryptate crystallographic data ^a

Compound	[L ² NH ₄] ⁺ I ⁻ ·4CHCl ₄
Formula	C ₂₈ H ₄₄ Cl ₁₂ I ₁₂ N ₇ O ₄
M (g mol ⁻¹)	1095.00
System, space group	Monoclinic C2/c
a/Å	21.472(2)
b/Å	19.1956(19)
c/Å	24.047(3)
α/°	90
β/°	114.006(2)
γ/°	90
V/Å ³	9053.9(18)
Z	8
μ/mm ⁻¹	1.456
Reflections collected: Total, independent, R _{int}	60788, 7675, 0.0363
Final R ₁ , wR ₂ ^{b,c}	0.0479, 0.0883

^a Bruker Apex II Duo-CCD area detector using Mo-Kα₁ radiation; temperature of data collection 100 K.

^b Structure was refined on F_o^2 using all data; the value of R₁ is given for comparison with older refinements based on F_o with a typical threshold of $F \geq 4\sigma(F)$.

^c $wR_2 = [\sum[w(F_o^2 - F_c^2)^2] / \sum w(F_o^2)^2]^{1/2}$ where $w^{-1} = \sigma^2(F_o^2) + (aP)^2 + (bP)$ and $P = [\max(F_o^2, 0) + 2F_c^2]/3$

Table 5 – Diamino-functionalised Barium cyclised cryptate crystallographic data ^a

Compound	[L ² Ba][ClO ₄] ₂
Formula	C ₂₈ H ₄₂ BaCl ₂ N ₆ O ₁₂
M (g mol ⁻¹)	1095.00
System, space group	Triclinic P ₁
a/Å	11.9010(4)
b/Å	12.8430(5)
c/Å	14.1790(5)
α/°	112.394(2)
β/°	94.887(2)
γ/°	113.231(2)
V/Å ³	1769.16
Z	2
μ/mm ⁻¹	1.341
Reflections collected: Total, independent, R _{int}	7946, 5561, 1.039
Final R ₁ , wR ₂ ^{b,c}	0.1152, 0.1998

^a Nonius Kappa-CCD area detector diffractometer using Mo-Kα₁ radiation; temperature of data collection 150 K.

^b Structure was refined on F_o^2 using all data; the value of R₁ is given for comparison with older refinements based on F_o with a typical threshold of $F \geq 4\sigma(F)$.

^c $wR_2 = [\sum[w(F_o^2 - F_c^2)^2] / \sum w(F_o^2)^2]^{1/2}$ where $w^{-1} = \sigma^2(F_o^2) + (aP)^2 + (bP)$ and $P = [\max(F_o^2, 0) + 2F_c^2]/3$

Table 6 – Helicate crystallographic data ^a

Compound	[Cu ₂ L ₃] ₂ (ClO ₄) ₄ ·4MeNO ₂
Formula	C ₇₆ H ₆₆ Cl ₄ Cu ₂ N ₁₂ O ₃₆ S ₄
M (g mol ⁻¹)	2128.46
System, space group	Monoclinic <i>P2_{1/n}</i>
<i>a</i> /Å	16.5727(8)
<i>b</i> /Å	26.2699(12)
<i>c</i> /Å	19.3291(9)
<i>α</i> /°	90
<i>β</i> /°	97.4190(10)
<i>γ</i> /°	90
<i>V</i> /Å ³	8344.7(7)
<i>Z</i>	4
<i>μ</i> /mm ⁻¹	0.71073
Reflections collected: Total, independent, <i>R</i> _{int}	43033, 10512, 0.0381
Final <i>R</i> ₁ , <i>wR</i> ₂ ^{b,c}	0.1148, 0.0445

^a Bruker Apex II Duo-CCD area detector diffractometer using Mo-K α_1 radiation; temperature of data collection 100 K.

^b Structure was refined on F_o^2 using all data; the value of *R*₁ is given for comparison with older refinements based on F_o with a typical threshold of $F \geq 4\sigma(F)$.

^c $wR_2 = [\sum[w(F_o^2 - F_c^2)^2] / \sum w(F_o^2)^2]^{1/2}$ where $w^{-1} = \sigma^2(F_o^2) + (aP)^2 + (bP)$ and $P = [\max(F_o^2, 0) + 2F_c^2]/3$

Appendix 2: Publications